INTERNATIONAL JOURNAL OF
IJCOE
COASTAL OFF SHORE AND ENVIRONMENTAL ENGINEERING

Volume 10 Tssue 1| Feb 2025

International Journal of Coastal, Offshore and Environmental Engineering (IJCOE) Vol.10/Issue 1/ Feb 2025

International Journal of Coastal, Offshore & Environmental Engineering
Since 2015
ISSN: 2980-4752 (online)

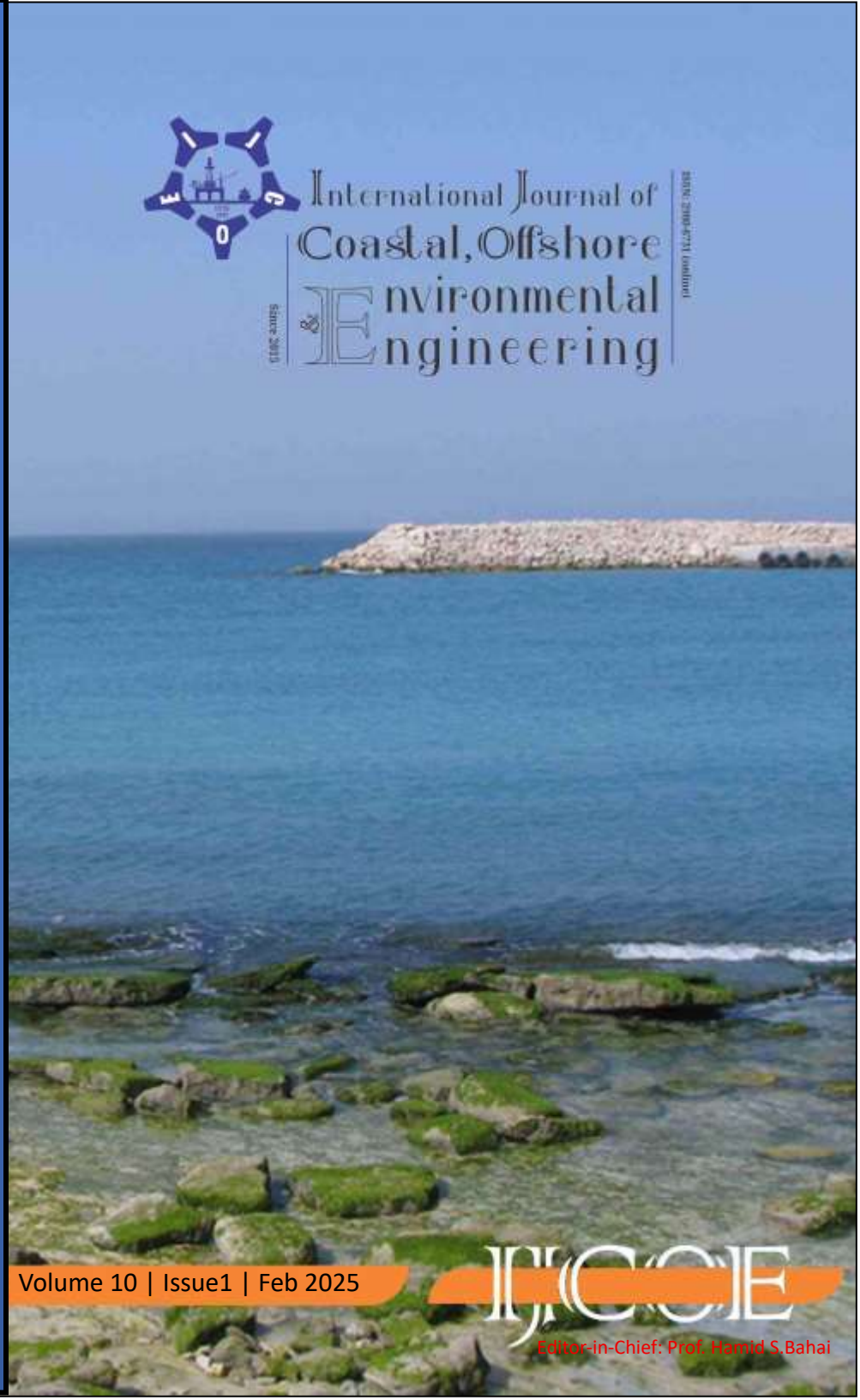

Volume 10 | Issue1 | Feb 2025
IJCOE
Editor-in-Chief: Prof. Hamid S.Bahai

International Journal of Coastal, Offshore & Environmental Engineering
Since 2015
ISSN: 2980-8721 (online)

In The Name of God

Message from the Editor-in-Chief

The IJCOE journal office was established in 2015,and its first issue was published in 2016. TheIJCOE covers a wide range of research in thefields of oceanography & ocean technology, aswell as marine industries & marine engineering.The editorial board of IJCOE consists of nearly130 of the greatest scientists and researchersfrom over 30 countries worldwide, and thejournal's review board comprises 1,000 membersfrom all five continents. The membership andapplication process for joining the editorial andreview boards of this journal is ongoing. IJCOE isa research-academic quarterly journal that haspublication and distribution permissions fromthe Press Organization and permission topublish scientific-research articles from theMinistry of Science, Research, and Technology(MSRT) with an "A" rating. It also holds a "Q1"rating from the ISC institute with an impactfactor (IF) of approximately 0.43 and isconsidered a "core journal" (prestigious andoutstanding journal). IJCOE is an open-accessjournal and allows the download and receipt ofaccepted articles in full text for free. It respectsand adheres to copyright and COPE regulations.The journal's office operates 24/7, providingservices to researchers. In addition to publishinga regular quarterly journal, IJCOE has 16 specialissues on specific topics in preparation. It alsoprovides conditions for publishing specializedbooks, references, and handbooks. Moreover, itis ready to cooperate with the secretariats ofreputable international conferences to publishtheir selected and outstanding articles. IJCOEevaluates, appraises, and publishes books,articles, and the scientific achievements andfindings of esteemed researchers and scientistsworldwide who are innovating and conductingin-depth research in the "important and strategicfield of the maritime technology & Oceanengineering." It welcomes any form of jointcooperation with universities, research institutes,and related research centers at the national,regional, and international levels, and extends ahand for collaboration.

Classification of Editorial Board in IJCOE

Editor-in-Chief

Director-in-Chief

Deputy Editor

Executive Managers

English Text Editor

Technical Editor

International Editorial Board

National Editorial Board

Editorial Board Associate

Editorial Board Assistant

Guest Editorial Board

Advisory Board

Administrative Coordinator

Honorary Board Member

Methodology Advisor

Author Benefits

- Open Access
- Rapid Publication
- Thorough Peer-Review
- No Copyright Constraints
- Coverage by Leading Indexing Services
- Discounts On Article Processing Charges (APC)
- No Space Constraints, No restriction on the maximum length of the papers, number of figures or colors

INTERNATIONAL JOURNAL OF IJCOE COASTAL, OFFSHORE & ENVIRONMENTAL ENGINEERING

Aims of IJCOE

Hydrodynamics

Marine equipment

Structural mechanics

Ocean environmental predictions

Stochastic calculations Experimental

Automatic Control of Marine Systems

Scope of IJCOE

Marine Hazards

Ocean Acoustics

Naval Architecture

Ocean Engineering

Coastal Engineering

Marine Meteorology

Marine Earth Sciences

Underwater Technology

Marine Renewable Energy

Polar & Arctic Engineering

Marine Renewable Energy

Marine Geography & Geodesy

Marine Environmental Engineering

Automatic Control of Marine Systems

Hydro Physics & Physical Oceanography

Type of papers

- Case Studies
- Book Reviews
- Review Article
- Letters to the Editor
- Methodology Papers
- Editorials and Commentaries
- Response or Rejoinder Papers
- Perspective or Opinion Papers
- Conceptual or Theoretical Papers
- Meta-Analysis and Systematic Reviews
- Short Communications or Brief Reports
- Research Articles (Original Research Papers)

Scientific Research Journal

Ministry of Science, Research And Technology (MSRT)

Jurnal Ranking 2023: A

Ministry Of Science, Research And Technology (ISC)

Citation Impact 2022: 0.429

Quartile 2022 : Q1

Core Collection

IJCOE is a Member of

Cantact Us

Office 1 | Research Institute of Meteorology and Atmospheric Science

Address | Tehran, Shahid Kharrazi Highway, Pajoohesh Blvd, Research Institute of Meteorology and Atmospheric Science, Sand and Dust Storm International Research Center (SDS-IRC), No. 13, 1st floor.

Phone | +982144787652

Postal code | 13611-14977

website | www.rimac.ac.ir

Office 2 | Iranian National Institute for Oceanography and Atmospheric Science

Address | Tehran, Dr. Fatemi Gharbi St., Shahid Etemadzade St., No. 3, third floor.

Phone | +982166944873

Postal code | 13389 – 14118

website | www.inio.ac.ir

Email | Info@ijcoe.org

Website | www.ijcoe.org

Follow Us

Volume & Issue:

Volume 10, Issue 1, Feb 2025

Number of Articles: 6

Content

IJCOE
COASTAL, OFFSHORE & ENVIRONMENTAL ENGINEERING

INTERNATIONAL JOURNAL OF
COASTAL, OFFSHORE & ENVIRONMENTAL ENGINEERING IJCOE Vol.10/No. 1/Winter 2025 (1-19)

Available online at: www. Ijcoe.org

The impact of recycled plastic fibers on bending behavior of green RC beams in the sea conditions

Hamed Safayenikoo[1]*, Hamid Shahrabadi[2]

[1] Civil Engineering Department, Marine Engineering School, Chabahar Maritime University, Chabahar, Iran; hamed.safayenikoo@gmail.com*
[2] Civil Engineering Department, Marine Engineering School, Chabahar Maritime University, Chabahar, Iran; hamid.shahrabadi@gmail.com

ARTICLE INFO

Article History:
Received: 1 Oct 2024
Accepted: 11 Jun 2025

Keywords:
Disposable Glasses Fiber
Garbage Bag Fiber
Green Reinforced Concrete
Metakaolin and Zeolite
Flexural and Cracking Behavior

ABSTRACT

Marine concrete structures, due to proper mechanical behavior and high durability for the world population, which are directly or indirectly related to marine infrastructure and various industries seem essential. On the other hand, concrete production and other related industries in marine environments are the main agents of production of pollution and waste and excessive consumption of the earth's natural resources and energy. Therefore, it seems that the simultaneous use of cement replacements to reduce the generation of greenhouse gases derived from cement production and plastic waste as fiber can decrease environmental pollution and improve concrete mechanical behavior. This study investigates the impact of incorporating 0.5 and 1% strip disposable glass fibers (GF) and strip garbage bag fibers (BF) on the flexural and cracking characteristics of reinforced concrete (RC) beams containing 10% metakaolin/zeolite. The investigation is conducted over 28 and 180 days in the tidal environment of the Oman Sea. Considering the results, by adding GF and BF to the green RC beams the flexural toughness (T) increased up to 47 and 27%, respectively. Furthermore, the cracking load (P_{cr}) of glass fibers RC (GC) and bags fibers RC (BC) beams was lower than RC up to 32 and 21%, respectively. Moreover, the incorporation of GF and BF resulted in an increase of up to 28% and 16% in the maximum load capacity (P_{max}) of RC beams, respectively. In addition, the P_{max} and T of GC beams were higher than BC. Besides, it was observed that metakaolin GC and BC beams exhibited a greater value of P_{max} and T compared with zeolite beams.).

1. Introduction

The importance of the sea and its related industries, and sustainable human access to food, industrial, and energy resources, has caused an increase in maritime regions' human population [1], [2]. Therefore, there is a greater human demand for building coastal and offshore infrastructure. Hence, concrete, which is a mixture of readily available and cheap raw materials, can be the best choice for the construction of marine structures [3], [4], [5], [6]. Furthermore, based on the environmental conditions of sea, concrete with high durability and suitable strength can increase the service life of marine structures. However, excessive consumption of irreversible primary resources, generation of air and marine pollution (produce less than 1 ton of CO_2 greenhouse gas per 1 ton of cement), low tensile force, and ductility are the most important weaknesses of concrete [1], [3], [7], [8], [9]. The supplementary cementitious materials (SCMs) like metakaolin and zeolite can be used to reduce the generation of environmental pollution and energy consumption [1], [3].

Metakaolin is a material characterized by its smaller particle size compared to cement and its significant pozzolanic reactivity. It is produced through the process of calcination, wherein kaolin is heated to temperatures ranging from 600 to 900 °C, without producing CO_2, in a specified time. Moreover, the mechanical and durability characteristics of mixes by substitution of cement with metakaolin are improved [10], [11], [12], [13]. Kavitha et al. found that substituting cement with metakaolin in self-

compacting concrete (SCC) mixes enhanced the compressive (f'_c) and tensile (T_c) strengths [14]. Furthermore, Punitha et al. demonstrated that the substitution of 10% of cement with metakaolin in concrete incorporating high-density polyethylene plastic waste resulted in an increase in the f'_c, T_c, and flexural strength of the concrete [15].

On the other hand, zeolite is a material with a regular crystalline structure, porous, and high specific surface area, which has high pozzolanic activity [2], [3], [16]. By using zeolite as an SCM in concrete mixture, the quality of microstructures improved, the mechanical strength increased, and the porosity and permeability of concrete decreased [3], [16], [17], [18]. Najimi et al. reported that the use of zeolite enhanced water and chloride ion penetration while decreasing f'_c and workability [5]. Tran et al. presented that the f'_c and T_c, water permeability, and capillary absorption of concrete mixtures by use of zeolite, were decreased over a long time [7].

As a result, metakaolin and zeolite as SCMs improved concrete mixes' mechanical properties and environmental impact [3], [8], [10], [14], [19], [20], [21]. On the other hand, fine particles and high specific surface area in SCMs increase chemical activities, produce more heat, and finally, cause cracking in the mixtures. Cracks' appearance in concrete structures, especially in marine environments are the main cause of chemical ions attacking and deterioration [22], [23]. Therefore, using different types of fibers can prevent and reduce cracking and limit crack propagation. Moreover, the incorporation of fibers into concrete mixes has the potential to enhance resistance parameters, including flexural behavior and ductility [8], [22], [23], [24], [25]. On the other hand, by recycling, incorporating waste fibers into concrete mixes, and generating green concrete, environmental pollution from landfilling and incineration will be reduced [26], [27]. Green concrete is an environmentally friendly concrete that uses waste, residual or recycled materials or requires less energy consumption due to SCMs use in concrete. Based on environmental conditions and the application type of concrete structure, different types of fibers, like synthetic and recycled synthetic fiber in concrete are utilized [27], [28], [29], [30].

Alabduljabbar et al. concluded that green concrete using recycled polypropylene fibers and palm oil fuel ash (POFA) showed greater flexural strengths and T than control specimens while having less drying shrinkage and workability [29]. Song et al. found that the incorporation of nylon and polypropylene fibers in concrete resulted in increased values of f'_c, T_c, modulus of rupture, and impact resistance compared to plain concrete [9]. In addition, Yap et al. reported that the flexural strengths, T_c, and f'_c of the concrete by adding polypropylene, nylon, and oil palm shells fibers will be increased [27].

Kim et al. discovered that by using beverage container fibers in concrete mixes, the flexural behavior and ductility increased while the f'_c, modulus of elasticity, and drying shrinkage were reduced [26]. Also, according to Alani et al. strip fibers from PET bottle waste and POFA enhanced the f'_c, porosity, and chloride permeability of ultra-high-performance green concrete [30]. In another study, Ahdal et al. showed that the f'_c of green concrete samples containing 10% zeolite and 1% PET fibers increased than plain concrete [28].

According to this background and little research has been done, it seems that fibers and SCMs in green concrete mixes may reduce pollutants and improve maritime concrete structures' mechanical properties, ductility, and durability. Thus, in current research, the impact of various types and amounts of GF and BF on flexural capacity, T, cracking behavior, and microstructure of green RC beams that incorporate metakaolin and zeolite in Oman Sea conditions, will be investigated.

2. Experimental Program

2.1 Materials

Portland cement (Type II), metakaolin or zeolite, aggregate (fine and coarse), water, superplasticizer, and GF and BF were used. The concrete mixtures were made with Kerman industrial cement. In all concrete mixtures, metakaolin or zeolite replaced 10% of the cement weight (Figure 1). Cementitious materials' chemical and physical properties are shown in Tables 1 and 2 [31].

Metakaolin Zeolite Cement (Type II)

Figure 1. The binders

Table 1. Binder's physical properties [31]

	Cement	Metakaolin	Zeolite
Specific gravity	3.15	2.45	2.18
Surface area (m^2/kg)	310	1200	320

Table 2. Binder's chemical composition [31]

Combination (%)	Cement	Metakaolin	Zeolite
Calcium oxide	63.52	1.34	7.38
Silica dioxide	21.50	81.29	58.15
Aluminum oxide	4.95	11.32	8.18
Iron oxide	3.97	0.56	1.54
Magnesium oxide	1.75	0.59	3.92
Potassium oxide	0	0.82	0.82
Sodium oxide	0	1.04	1.11

Titanium oxide	0	0.107	0.175
Manganese oxide	0	0.003	0.019

The Chabahar mines were utilized to prepare fine and coarse aggregates with maximum diameters of 4.75 and 19 mm, respectively. Figure 2 showed the sieve analysis of aggregates as per the guidelines of ASTM C136 [32].

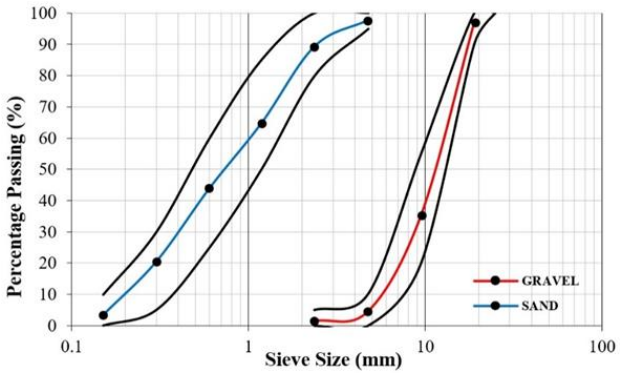

Figure 2. The sieve analysis of aggregates [32]

Table 3. The aggregates' characteristics [31]

Aggregate	Water absorption (%)	Specific gravity
Sand	2.92	2.64
Gravel	1.84	2.42

In the laboratory, potable water was utilized for the preparing and curing (in primary ages) of all concrete mixes. Conversely, the utilization of both SCMs and fibers in concrete mixtures has led to the use of Farco Plast, a modified polycarboxylate-based superplasticizer, for regulating the concrete's workability. In Table 4, the main characteristics of Farco Plast are shown.

Table 4. The Farco Plast superplasticizer properties [31]

Physical state	Color	Specific gravity
Liquid	Light Brown	1.09 (kg/Lit)

Figure 3. Drinking water curing tanks [31]

The recycled strip fibers used in mixtures (hereafter named strip fibers) were prepared by cutting polyethylene disposable glasses and garbage bags. The V_f of fibers utilized in the production of blends was determined to be 0.5 and 1%. Furthermore, for fibers with a rectangular section, the fiber aspect ratio (A.R.) formula was:

$$\lambda = \frac{l}{d_e} = \frac{l}{2 \times \sqrt{\frac{A}{\pi}}} = \frac{l}{2 \times \sqrt{\frac{b \times c}{\pi}}} \quad (1)$$

Where λ is A.R., l is fiber length (mm), d_e is equivalent diameter (mm), A is fiber cross-section area (mm^2), b is fiber width (mm) and c is fiber thickness (mm) [33]. For desired strength performance of mixtures, an A.R. of fiber more than 20 is required [34].

Table 5. The fiber properties [31]

Strip Fibers	No	Width (mm)	Thickness (mm)	Length (mm)	Aspect Ratio	Density (kg/m^3)	Tensile Strength (MPa)
Disposable Glasses (G)	G1	10	0.03	25	≈ 40	≈ 680	≈ 570
	G2			50	≈ 80		
Garbage Bags (B)	B1	10	0.03	25	≈ 40	≈ 570	≈ 52
	B2			50	≈ 80		

A B

Figure 4. Strip fiber types: A) GF [31]**, B) BF**

2.2. Concrete Mixtures

In this study, 18 green RC mixtures were prepared. Throughout all concrete mixes, the W/B was always kept at 0.5. There were 410 kg/m^3 of binders in all concrete mixtures. Moreover, the Farco plast superplasticizer was used at up to 2% of cement weight to control and improve concrete workability. Table 6 illustrates the concrete composition [31].

2.3. Preparation of samples

Following the preparation and measurement of the materials, a rotary mixer was employed to blend them. After the completion of the task, the diverse varieties of fibers were incorporated into the homogeneous mixture of concrete and blended for a short time. Subsequently, concrete mixes, based on the type of test, were cast in the relevant molds. Following 24 hours, the molds were extracted and the samples were transferred to tanks containing potable water for a curing duration of three days. Finally, the specimens were transferred to the Oman Sea's tidal zone and left to acclimate for a duration ranging from 28 to 180 days. The number of cubes (150 mm for f'_c) and beams (150×150×650 mm for four-point bending tests) was 54 and 72, respectively. On the other hand, for concrete microstructure analyses, 52 cubes (70 mm) were prepared.

Table 6. The concrete composition [31]

Mix		Sand (kg/m^3)	Gravel (kg/m^3)	Water (kg/m^3)	Binders (kg/m^3)			Strip Fibers (kg/m^3)			
					Cement (C)	Metakaolin (Mk)	Zeolite (Ze)	Garbage Bag		Disposable Glass	
								B1	B2	G1	G2
1	NF1	664	1054	205	369	41	- - -	- - -		- - -	
2	NF2					- - -	41	- - -		- - -	
3	B1					41	- - -	2.85	- - -	- - -	
4	B2					41	- - -	- - -	2.85	- - -	
5	B3					- - -	41	2.85	- - -	- - -	
6	B4					- - -	41	- - -	2.85	- - -	
7	B5					41	- - -	5.7	- - -	- - -	
8	B6					41	- - -	- - -	5.7	- - -	
9	B7					- - -	41	5.7	- - -	- - -	
10	B8					- - -	41	- - -	5.7	- - -	
11	G1					41	- - -	- - -		3.4	- - -
12	G2					41	- - -	- - -		- - -	3.4
13	G3					- - -	41	- - -		3.4	- - -
14	G4					- - -	41	- - -		- - -	3.4
15	G5					41	- - -	- - -		6.8	- - -
16	G6					41	- - -	- - -		- - -	6.8
17	G7					- - -	41	- - -		6.8	- - -
18	G8					- - -	41	- - -		- - -	6.8

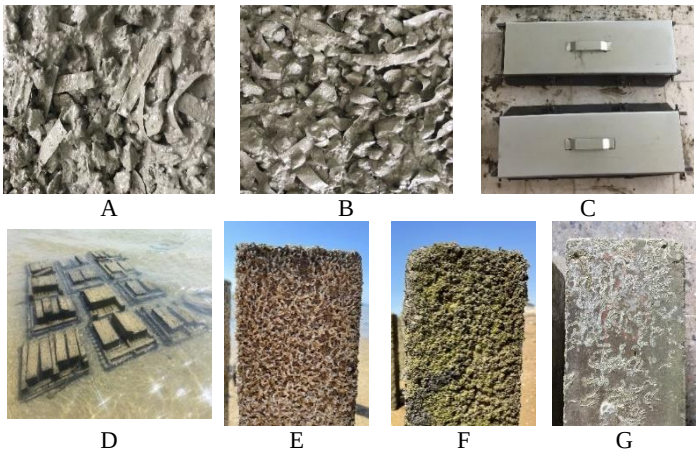

Figure 5. A) The GC, B) The BC, C) Specimen's molds, D) Samples in the coastal zone, E and F) Samples collected from the Oman Sea, G) Samples after preparing for tests [31]

The GC/BC beams were made utilizing steel bars (f_y=400 MPa and f_u=600 MPa) with diameters of 8 mm and 6 mm for the longitudinal reinforcements and stirrups. Figure 6 illustrated the specifics of GC/BC beams [31].

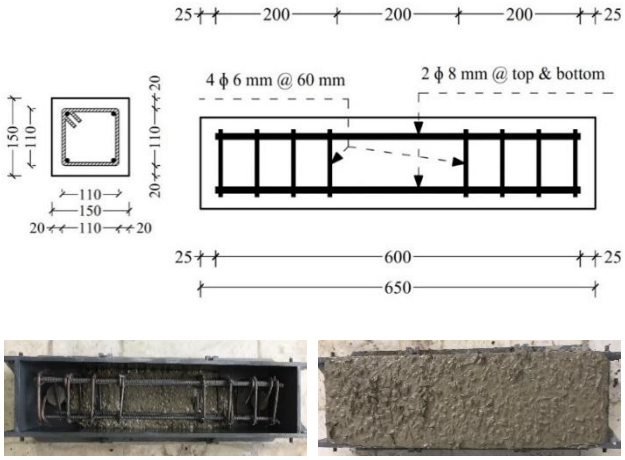

Figure 6. The GC/BC beam [31]

2.4. Exposure conditions

In this research, due to consider the most destructive effects of sea environment on concrete structures, the specimens were exposed to a 180-day exposure period in the Oman Sea's tidal zone. Figure 5 demonstrated the state of the concrete samples located on the shoreline of the Oman Sea. Also, Table 7 presents the chemical characteristics of both laboratory and Oman seawater [31].

Table 7. The chemical properties of water (gr/Lit) [31]

	PH	Hardness	Alkalinity	SO_4^{2-}	NO_2^-	NO_3^-	Cl^-	Ca	Mg	NH_3	Zn	Al	Cu	Mn	Fe
Lab-water	6.70	45	20	102	0.010	2.820	5	4	≈0	≈0	≈0	0.32	0.02	0.004	≈0
Seawater	7.97	225	120	≈0	0.007	0.222	5	68	95	1.29	0.22	0.32	0.02	≈ 0	0.04

3. Testing methods

3.1 Compressive strength (f'_c)

The BS EN12390-3 standard measured the f'_c value by exposing three 150×150×150 mm cubic specimens for 28 days in the Oman Sea's tidal zone. By averaging three specimens, the concrete mixture's f'_c was computed [35].

3.2 Flexural behavior

The ASTM C78 standard's four-point bending test was used to evaluate the flexural behavior of concrete beams. A universal testing machine was used, with a constant rate of 100 N/s [36]. During the loading process, the deformation of the beams was recorded by a mobile camera and computer. Based on the recorded information, the behavior and characteristics of beam cracks were investigated. Moreover, the maximum deflection of mid-span for beams was terminated to 20 mm [31].

In the following, the load-deflection curve for various types of GC/BC beams was drawn and then some characteristics of flexural behavior of beams such as P_{cr}, P_{max}, and T were calculated. Moreover, flexural toughness was calculated by integrating the load-deflection curve.

4. Results and Discussions

4.1. Specific gravity (γ)

The γ of green concrete, both with and without fibers, is presented in Figure 7. Also, Table 8 compares the influence of fiber types on the γ of concrete samples.

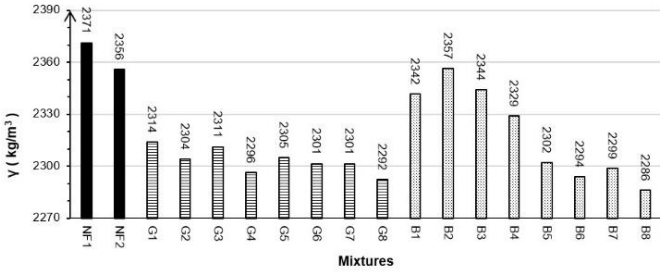

Figure 7. The green concrete's specific gravity (γ)

Table 8. Comparison of specific gravity (γ) at 28 days

Mix	γ	Mix	γ	Mix	γ	Mix	γ
NF1	**1**	**NF2**	**1**	**NF1**	**1**	**NF2**	**1**
G1	0.976	**G3**	0.981	**B1**	0.988	**B3**	0.992
G2	0.972	**G4**	0.975	**B2**	0.984	**B4**	0.989
G5	0.972	**G7**	0.977	**B5**	0.971	**B7**	0.976
G6	0.970	**G8**	0.973	**B6**	0.967	**B8**	0.970

The results show that fibers in green concrete mixes reduce the γ of concrete. Moreover, by increasing the V_f of fibers in mixes, the γ decreased more. At 28 days, the γ of concrete with 0.5% GF was observed to be higher than that of concrete with 0.5% BF. However, increasing the V_f of fibers up to 1% resulted in equal γ for both types of fibers. It seems that adding fibers and augmentation of V_f within mixes resulted in an increase in the volume of pore space and porosity, while concurrently leading to a decrease in γ [2], [28], [37], [38], [39], [40], [41], [42], [43].

4.2. Compressive strength

In Figure 8 and Table 9, the results of f'_c in different mixtures containing various types of strip fibers and SCMs are shown at 28 days.

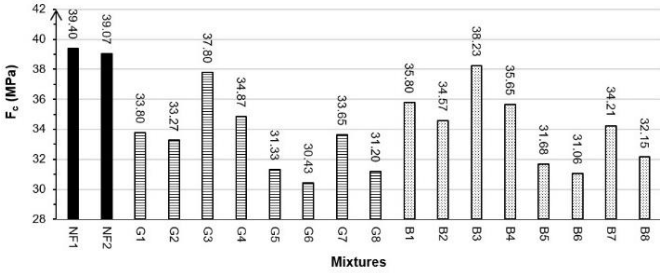

Figure 8. The f'_c of specimens

Table 9. Comparison of f'_c

Mix	f_c'	Mix	f_c'	Mix	f_c'	Mix	f_c'
NF1	**1**	**NF2**	**1**	**NF1**	**1**	**NF2**	**1**
G1	0.86	**G3**	0.97	**B1**	0.91	**B3**	0.98
G2	0.84	**G4**	0.89	**B2**	0.88	**B4**	0.91
G5	0.80	**G7**	0.86	**B5**	0.80	**B7**	0.88
G6	0.77	**G8**	0.80	**B6**	0.79	**B8**	0.82

By comparing the results, it is evident that the combining of fibers and augmentation of the V_f in green concrete led to a rise in the volume of pore space, thereby causing a reduction in the density, adhesion between fibers and cement paste, integrity, and f'_c. Similarly, through the augmentation A.R. and dimensions of fibers in mixtures, porosity increased but adhesion and f'_c decreased [44], [45], [46], [47], [48], [49], [50], [51], [52]. Adding 0.5 and 1% GF resulted in a reduction of up to 16 and 23% in the f'_c of the green concrete specimens, respectively. While concrete samples containing 0.5 and 1% BF had lower f'_c than simple ones about 12 and 21%, respectively.

In contrast, it was noted that the f'_c of concrete samples with 0.5% BF was greater than that of those containing 0.5% GF. However, the addition of 1% BF or GF fibers to plain concrete resulted in equivalent f'_c values among the specimens.

The enhanced flexibility of BF in comparison to GF has improved the homogeneity and integrity of the concrete. Conversely, GF mixtures exhibited higher porosity, leading to reduced fiber-cement paste adhesion, ultimately resulting in a lower f'_c [9], [23], [27], [44], [49], [50], [51], [53], [54], [55].

Furthermore, at 28 days, in mixtures with an equal amount of fiber, f'_c of metakaolin concrete specimens had up to 12% lower than zeolite ones. The hydrophilic structure of zeolite appears to result in heightened water absorption and reduced workability, decreasing concrete porosity and increasing f'_c [7], [22], [25], [56], [57].

4.3. Flexural behavior

After four-point bending test on RC and fiber RC beams at 28 and 180 days, flexural properties consisting of P_{cr}, P_{max}, T, and cracking behavior were examined. The flexural properties are demonstrated in Tables 10-12.

Table 10. Four-point bending test results

Mixes	P_{cr} * (kN)		Δ_{Pmax} (mm)		P_{max} ** (kN)		T ■■ (kN.m)	
	28	180	28	180	28	180	28	180
N1	28.40	37.20	4.04	4.53	80.15	90.5	1133.41	1250.62
N2	27.10	36.20	3.86	4.36	71.9	84.2	1035.07	1210.24
G1	22.10	28.87	6.18	6.48	89.6	104.2	1432.09	1594.07
G2	24.40	30.88	7.64	7.76	97.8	115.6	1601.39	1785.50
G3	21.41	29.83	5.86	6.16	80.4	96.6	1261.13	1493.18
G4	22.17	32.29	6.46	6.72	88.7	107.6	1425.28	1707.09
G5	20.16	25.37	6.78	7.02	84.9	99.0	1499.22	1671.75
G6	21.07	27.08	8.32	8.48	94.3	108.9	1648.13	1842.20
G7	18.67	26.06	6.08	6.38	76.3	90.8	1326.87	1568.42
G8	19.35	27.87	7.12	7.32	83.5	101.7	1460.39	1745.28
B1	25.21	34.32	4.96	5.56	82.6	95.1	1223.72	1358.53
B2	26.56	36.42	5.94	6.64	87.6	100.4	1303.67	1450.88
B3	23.88	33.98	4.74	5.32	76.4	92.2	1114.17	1323.39
B4	25.17	35.78	5.16	5.78	80.8	97.2	1202.41	1413.93
B5	23.02	29.51	5.36	6.00	80.6	92.8	1304.35	1475.84
B6	23.87	31.02	6.42	7.16	84.6	96.8	1426.25	1581.67
B7	21.07	30.44	4.88	5.48	73.4	88.6	1188.51	1393.77
B8	22.01	32.01	5.60	6.26	78.8	94.6	1287.14	1508.75

Δ_{Pmax}: Mid-span deflection of beams at P_{max}

Table 11. Comparison of P_{cr} for beams

Age	Mix	P_{cr}	Mix	P_{cr}	Mix	P_{cr}	Mix	P_{cr}
28	**NF1**	**1**	**NF2**	**1**	**NF1**	**1**	**NF2**	**1**
	G1	0.778	**G3**	0.790	**B1**	0.888	**B3**	0.881
	G2	0.859	**G4**	0.818	**B2**	0.935	**B4**	0.929
	G5	0.710	**G7**	0.689	**B5**	0.811	**B7**	0.777
	G6	0.742	**G8**	0.714	**B6**	0.841	**B8**	0.812
180	**NF1**	**1**	**NF2**	**1**	**NF1**	**1**	**NF2**	**1**
	G1	0.776	**G3**	0.824	**B1**	0.923	**B3**	0.939
	G2	0.830	**G4**	0.892	**B2**	0.979	**B4**	0.988
	G5	0.682	**G7**	0.720	**B5**	0.793	**B7**	0.841
	G6	0.728	**G8**	0.770	**B6**	0.834	**B8**	0.884

4.3.1. The GC beams' load-deflection behavior

Figures 9–12 illustrate the load-deflection curves for GC and RC beams incorporating metakaolin or zeolite.

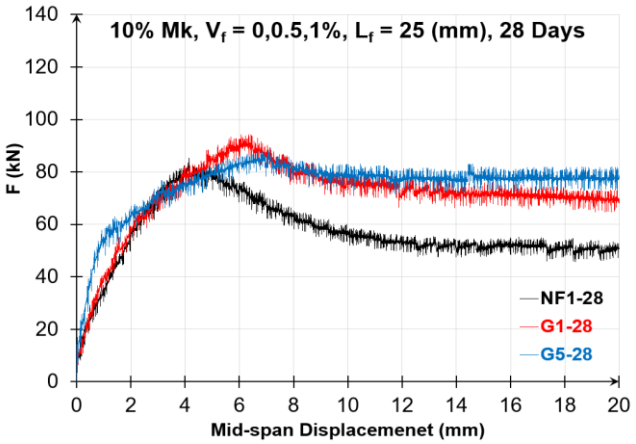

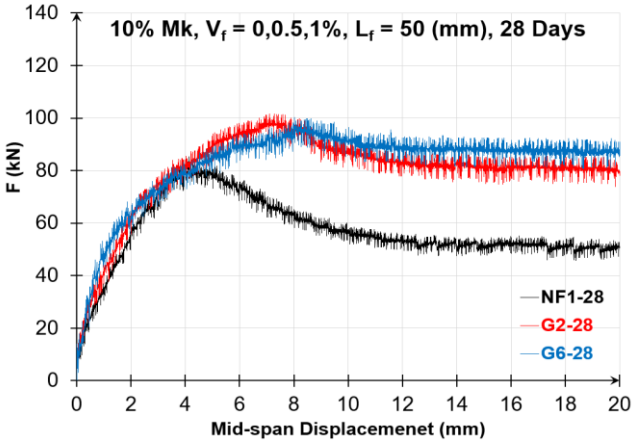

Figure 9. Metakaolin GC beam load-deflection curve

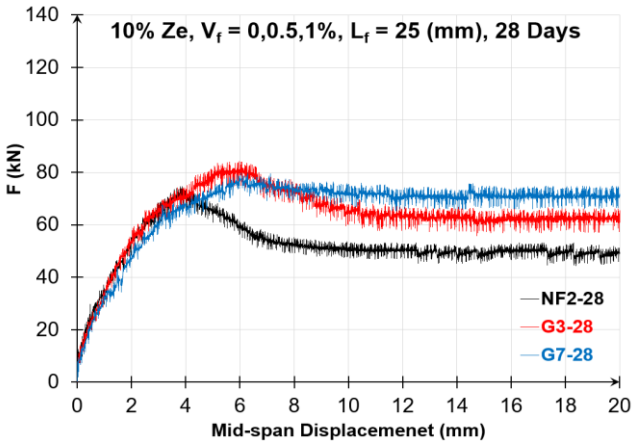

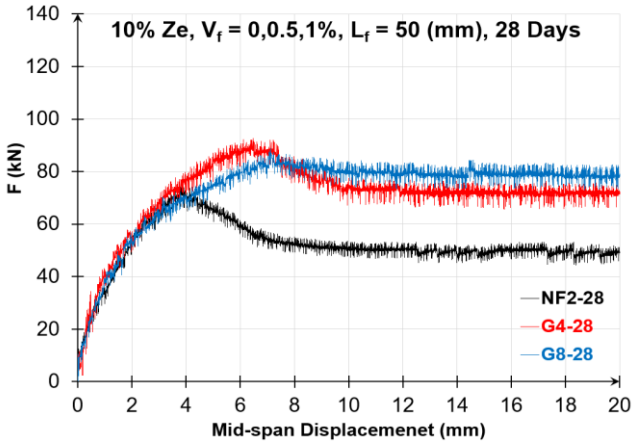

Figure 10. Zeolite GC beam load-deflection curve

Table 12. Comparison of P_{max} and T of RC beams

Age	Mix	P_{max}	T	Mix	P_{max}	T	Mix	P_{max}	T	Mix	P_{max}	T
28	**NF1**	**1**	**1**	**NF2**	**1**	**1**	**NF1**	**1**	**1**	**NF2**	**1**	**1**
	G1	1.118	1.264	**G3**	1.118	1.218	**B1**	1.031	1.080	**B3**	1.063	1.076
	G2	1.231	1.413	**G4**	1.234	1.377	**B2**	1.093	1.150	**B4**	1.124	1.162
	G5	1.059	1.323	**G7**	1.061	1.282	**B5**	1.007	1.151	**B7**	1.021	1.148
	G6	1.177	1.454	**G8**	1.161	1.411	**B6**	1.056	1.258	**B8**	1.096	1.244
180	**NF1**	**1**	**1**	**NF2**	**1**	**1**	**NF1**	**1**	**1**	**NF2**	**1**	**1**
	G1	1.151	1.275	**G3**	1.147	1.234	**B1**	1.051	1.086	**B3**	1.095	1.093
	G2	1.277	1.428	**G4**	1.278	1.411	**B2**	1.109	1.160	**B4**	1.154	1.168
	G5	1.094	1.337	**G7**	1.078	1.296	**B5**	1.025	1.180	**B7**	1.052	1.152
	G6	1.203	1.473	**G8**	1.208	1.442	**B6**	1.070	1.265	**B8**	1.124	1.247

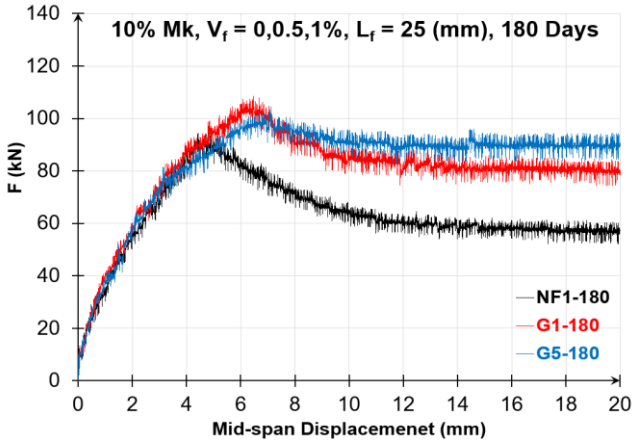

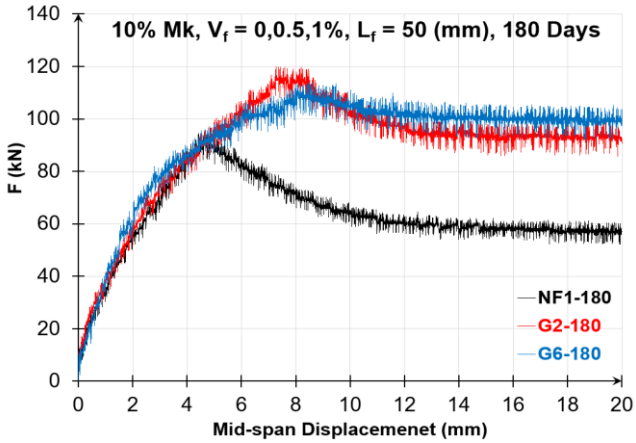

Figure 11. Metakaolin GC beam load-deflection curve

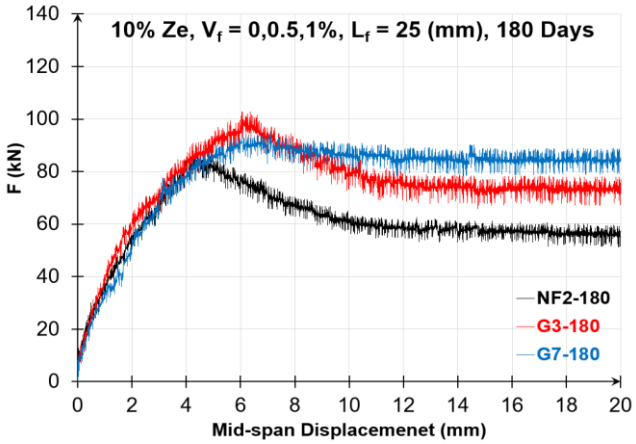

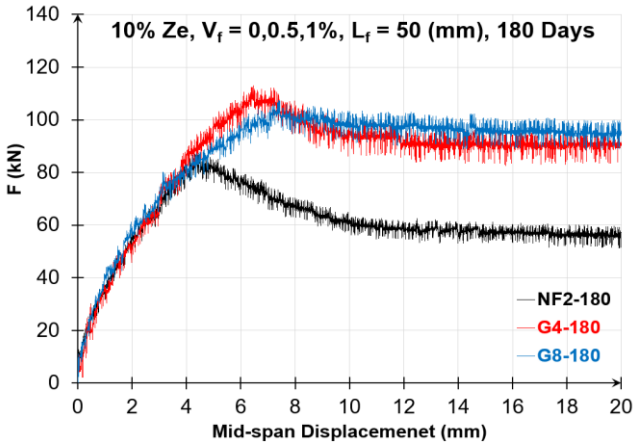

Figure 12. Zeolite GC beam load-deflection curve

4.3.1.1. The GC beam cracking load

In Tables 10-11 and Figure 13, the P_{cr} of GC beams are presented and compared at 28 and 180 days.

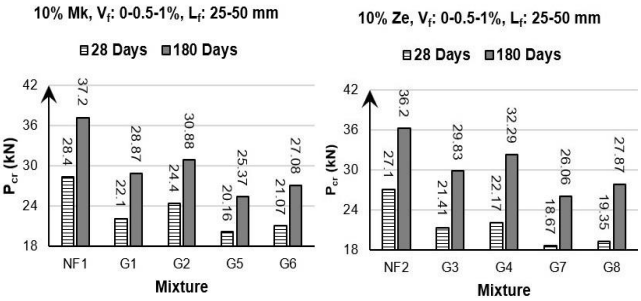

Figure 13. The Cracking load

Based on the result, the P_{cr} was reduced when 0.5 and 1% GF were added to metakaolin/zeolite RC beams at all ages. By combining 0.5 and 1% GF to metakaolin RC beams after 28 days, the P_{cr} dropped by 22 or 29%, respectively. Moreover, depending on whether the beams included 0.5 or 1% GF, the P_{cr} of the metakaolin GC beams after 180 days was 24 and 32% lower than RC beams. Besides, the P_{cr} of the zeolite GC beams was 21 and 31% lower than RC beams at 28 days, respectively, based on that the beams included 0.5 or 1% GF. At 180 days, the P_{cr} was reduced by either 0.5 or 1% GF when added to RC beams, respectively. According to the results, it seems that by adding GF to RC beams, pores in cement matrixes and porosity are increased which may lead to

a decrease in cohesion and the P_{cr} [15], [26], [55], [58], [59], [60], [61].

Conversely, the GC beams P_{cr} was enhanced by augmentation of the GF A.R. For instance, in 10% metakaolin/zeolite GC beams and 0.5 and 1% GF, the P_{cr} demonstrated an increase, reaching a maximum of 6 and 9% for A.R. of 40 and 80, respectively. The enhancement of adhesion and bonding length in the cement matrix can be achieved by increasing the A.R. of fibers. As a result, it is feasible to enhance the fiber's resistance to extraction and the occurrence of cracks in beams [33], [48], [62].

Results and Figures 9-12 reveal that the P_{cr} of GC beams including metakaolin was approximately 10% greater than those of zeolite, after a curing period of 28 days. Also, the P_{cr} of Zeolite GC beams exhibited a similar trend to that of the Metakaolin at long time [8], [16], [31], [60].

4.3.1.2. The GC beams peak load

Based on the data displayed in Table 12 and Figure 14, it is evident that an increase in the V_f of GF in the metakaolin/zeolite GC beams resulted in a decrease in P_{max} at all days.

The P_{max} of GC beams was greater than that of RC beams, nevertheless. For instance, the addition of 0.5 and 1% GF to the RC beams resulted in a significant increase in P_{max} by 23 and 18%, respectively, within a brief period. Moreover, GC beams with 0.5 and 1% GF had P_{max} 28 and 21% greater than RC beams after 180 days. Focusing on the obtained findings, it can be concluded that by increasing porosity and reducing the integrity of concrete, which occurs due to the increase of volume fraction in the mixtures, the P_{max} decreases [23], [30], [53], [59], [62], [63].

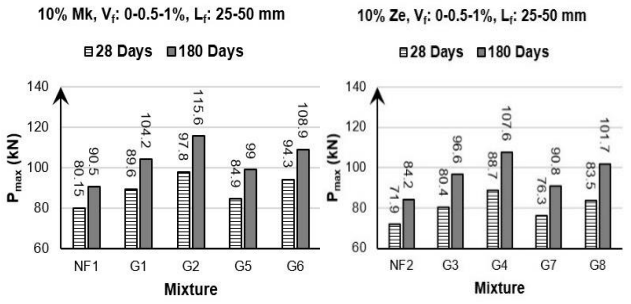

Figure 14. P_{max} of the GC beams

On the other hand, it was observed that the P_{max} of the GC beams enhanced on all days as the A.R. of the GF was increased. For example, the P_{max} values of G2/G8 beams having an A.R. of 80 were 11% greater than those of G1/G7 beams having an A.R. of 40, across all observed days. The length and aspect ratio of GF seems to increase fiber resistance to pull out, slip, and P_{max} [33], [48], [49], [62].

Besides, Table 10 demonstrated that at 28 days, the P_{max} of metakaolin GC beams exceeded that of zeolite GC beams by up to 13%. However, at 180 days, there was a reduction in the disparity between the P_{max} values of GC beams including metakaolin, and those of zeolite, amounting to approximately 8%.

4.3.1.3. The GC beams flexural toughness

Considering Figures 9-12, 15, and Table 10, obvious that the incorporation of GF into the RC beams resulted in a notable increase in T.

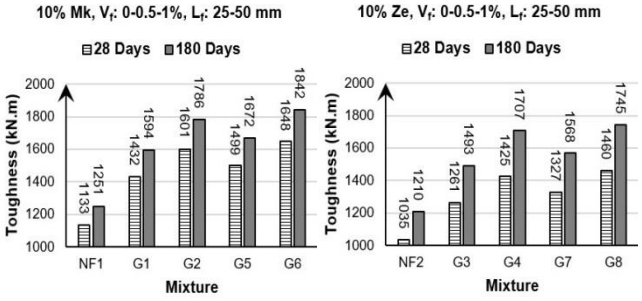

Figure 15. T of the GC beams

The GC beams, which were composed of 0.5 and 1% GF, exhibited significantly higher T values of up to 41% and 45%, respectively, compared to the RC beams after 28 days. While a combination of 0.5 and 1% GF to the RC beams resulted in a respective increase of 43 and 47% for T after 180 days. The bridging phenomenon of GF on the surface and edges of cracks is evidently responsible for the dispersion of the applied loads and constrains the propagation of the initial cracks. Moreover, the V_f of GF in the mixes increased the interfacial bonding between fibers and cement matrix, toughness, and ductility of GC beams [42], [45], [46], [54], [64], [65], [66], [67], [68], [69].

Also, in Figure 16, the crack bridging of GF in bending tests of the GC beams has been presented.

Figure 16. Crack bridging of GF in the GC beams

Based on Table 12, it can be observed that the GC beams with an A.R. of 80 exhibited a higher T value in comparison to those with an A.R. of 40. At 28 days, the T value of the 0.5% GC beams with A.R. of 40 and 80 demonstrated an increase of 27 and 41%, respectively, in comparison to the RC beams. Also, the incorporation of 0.5% GF with A.R. of 40 and 80 resulted in a significant enhancement of the T of RC beams, with an increase of up to 32 and 46% at 180 days, respectively. Furthermore, it was observed that in GC beams with an 80 A.R. and 1% GF content, the highest rise in T, as compared to the 40 A.R., was approximately 11%. The augmentation of length and aspect ratio amplifies both the contact surface and the developmental length of GF. The T of GC beams can be increased by enhancing the adhesion and pull-out

resistance of the cement matrix [28], [43], [45], [47], [54], [58].

On the other hand, it was observed that metakaolin GC beams overtook zeolite ones in T. However, in the long term, zeolite's unique pozzolanic properties reduce the T difference between metakaolin and zeolite in GC beams. The pozzolanic reactivity and finer particles of metakaolin are more effective than that of zeolite, resulting in increased speed of the hydration process. This, in turn, enhances the adhesion between fibers and cement paste, ultimately leading to higher T values at 28 days. However, after 180 days, zeolite outperforms metakaolin due to its ability to produce C-S-H secondary gels, which improve the microstructure of the concrete and accelerate the rate of T growth [8], [10], [13], [16], [22], [25], [31], [38], [60].

4.3.2. The BC beams' load-deflection behavior

Figures 17-20 present the load-deflection curves of the metakaolin or zeolite BC and RC beams.

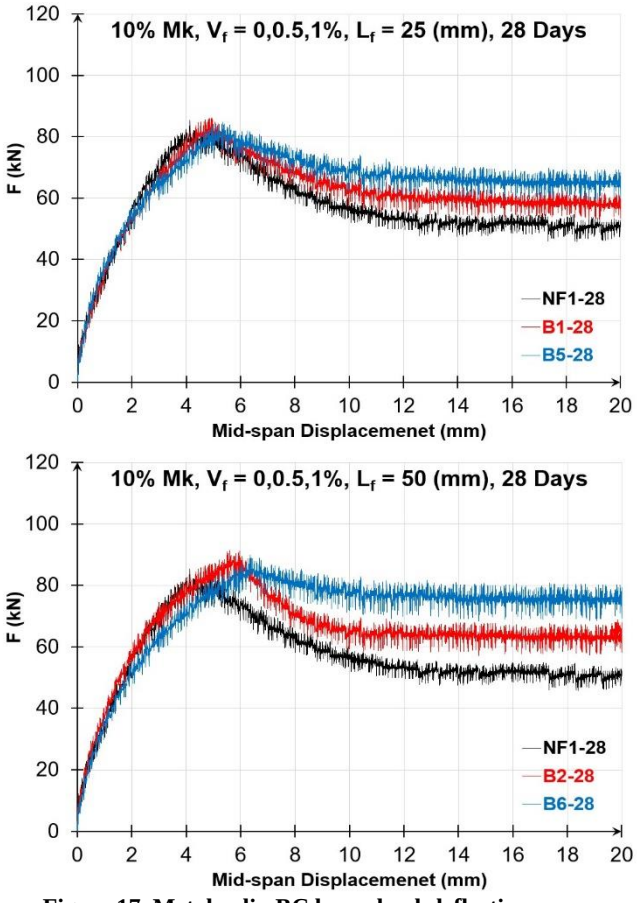

Figure 17. Metakaolin BC beam load-deflection curve

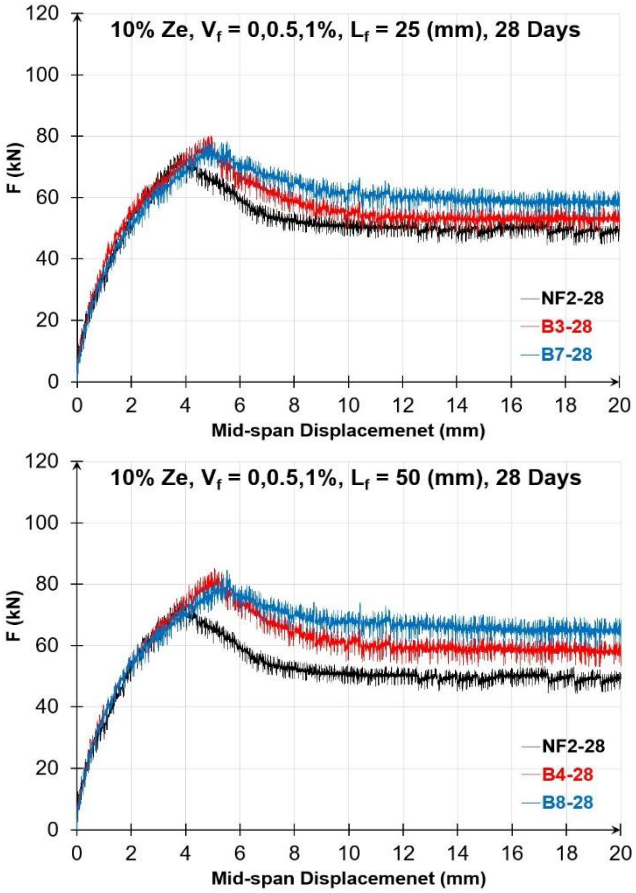

Figure 18. Zeolite BC beam load-deflection curve

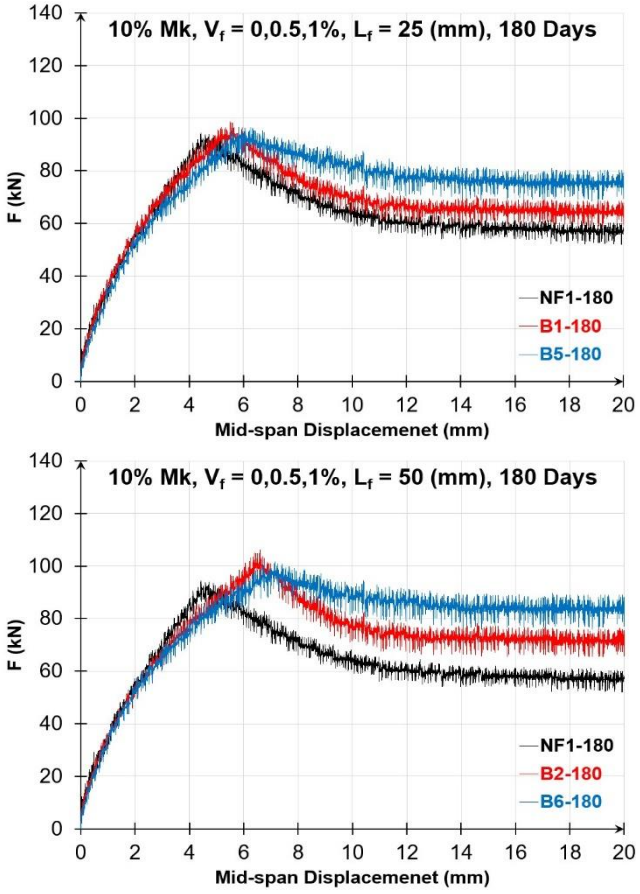

Figure 19. Metakaolin BC beam load-deflection curve

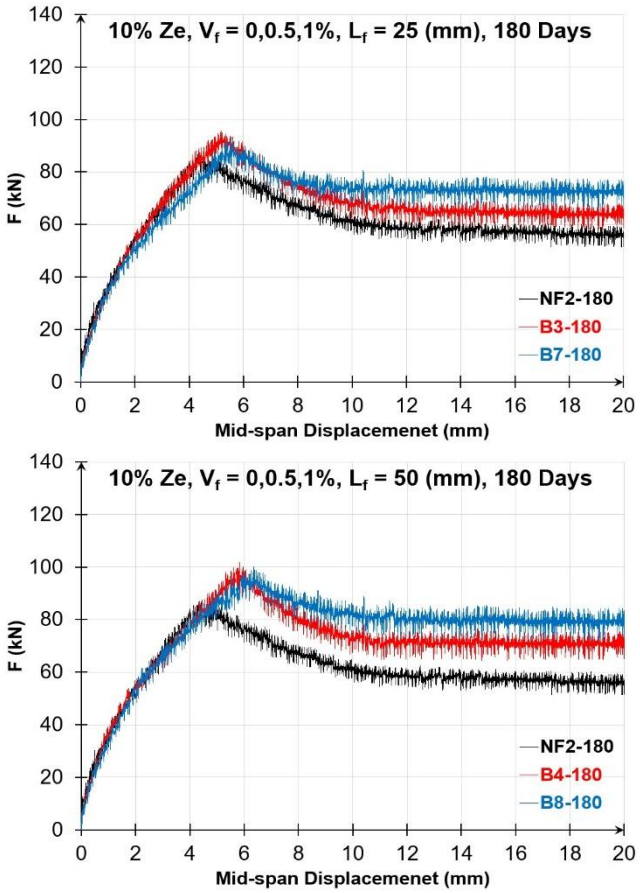

Figure 20. Zeolite BC beam load-deflection curve

4.3.2.1. The BC beams cracking load

In Tables 10-11 and Figure 21, the P_{cr} of the BC beams at 28 and 180 days are shown.

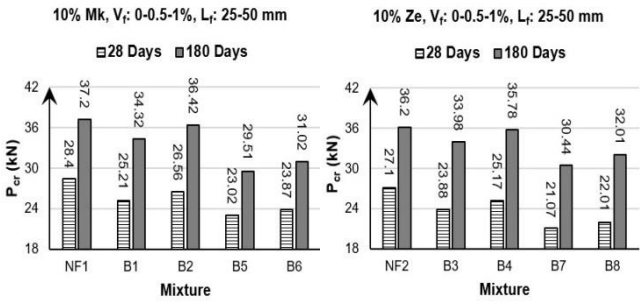

Figure 21. The Cracking load

The P_{cr} of RC beams by adding 0.5 or 1% BF decreased. Furthermore, the P_{cr} of the BC beams was reduced significantly due to the increase in the V_f of BF in the concrete mixtures.

Results revealed that the P_{cr} of the BC beams, which contained 0.5 and 1% BF, exhibited a reduction of up to 11 and 19% as compared to the RC beams, respectively, after 28 days. While the addition of 0.5 and 1% BF resulted in a reduction of P_{cr} in RC beams by 8 and 21%, respectively, at 180 days. In addition, the inclusion of 0.5 and 1% BF in the zeolite RC beams resulted in a reduction of P_{cr} by 12 and 22%, respectively, after 28 days. At 180 days, the P_{cr} of the 0.5 and 1% BC beams exhibited a respective increase of 6 and 16% compared to the RC beams. The inclusion of BF in mixtures has been observed to result in an augmentation of void space and porosity, ultimately leading to a reduction in the integrity and P_{cr} of specimens [9], [27], [49], [50], [51].

Furthermore, the increase in the A.R. of the BF resulted in a rise in the P_{cr} of BC beams. The increase of P_{cr} for 80 A.R. metakaolin/zeolite BC beams was about 7% more than 40 A.R. ones, at 180 days.

The higher A.R. of BF led to increased bonding length within the cement matrix and greater adhesion compared to the 40 A.R. Consequently, the P_{cr} of the 80 A.R. BC beams was higher than that of the 40 A.R. [9], [27], [33], [49], [50], [51].

Based on the obtained results, the findings suggest that, after 28 days, the P_{cr} of metakaolin BC beams was greater than that of zeolite BC beams. However, at 180 days, the same results were obtained for zeolite and metakaolin mixtures [8], [16], [60]. For instance, at 28 days, metakaolin BC beams with 0.5 and 1% BF exhibited P_{cr} up to 6 and 10% greater than zeolite ones.

4.3.2.2. The BC beams peak load

Table 12 and Figure 22 illustrate the impact of fibers and SCMs, such as metakaolin or zeolite, on the P_{max}.

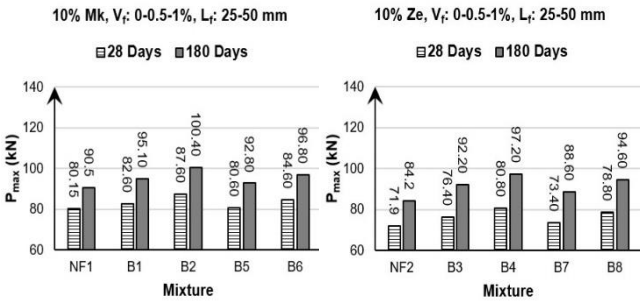

Figure 22. P_{max} of the BC beams

The findings indicated that the P_{max} of the metakaolin/zeolite BC beams was higher than the RC ones. While the GRFC beams containing 1% BF had lower P_{max} than 0.5% BF. The beams containing 0.5 and 1% BF exhibited greater P_{max} at 28 days, with increases of up to 13 and 10% compared to those of RC. Furthermore, at 180 days, the P_{max} increased up to 16 and 13% by adding 0.5 and 1% BF to the metakaolin/zeolite RC beams, respectively. According to extracted results, as the V_f of BF in the mixes increases, there is a parallel rise in hole volume and porosity, while the integrity and P_{max} of RC decrease [9], [27], [49], [50], [51], [54], [61].

Besides, the augmentation of the BF A.R. led to a rise in the P_{max} of the BC beams. The BC beams with an A.R. of 80 exhibited a P_{max} that was approximately 8% greater than that of the beams with an A.R. of 40, at all days. Through the enhancement of BF's length and A.R., cement paste-fiber adhesion, as well as the development length of fibers, and P_{max}, are enhanced [9], [27], [33], [49], [50], [51], [54], [62].

Moreover, considering the results presented in Tables 10 and 12, it is evident that the P_{max} of the metakaolin BC beams surpassed that of the zeolite ones by up to 10 and 5% at 28 and 180 days, respectively.
The results reveal that metakaolin BC beams with finer particle size and higher pozzolanic activity exhibit a greater P_{max} than their zeolite ones at 28 days. However, at 180 days, the completion of the hydration process and the enhancement of microstructure and bond strength lead to a reduction in the disparity between the P_{max} values of metakaolin/zeolite BC beams [8], [16], [60].

4.3.2.3. The BC beams flexural toughness

The T value of RC beams was observed to increase upon the use of BF, as evidenced by the data presented in Figures 17-20 and 23, as well as Tables 10 and 12.

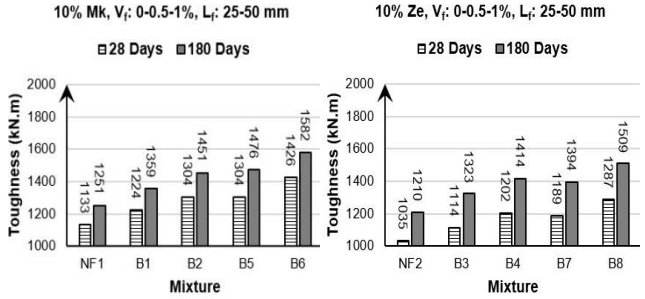

Figure 23. T of the BC beams

Furthermore, by increasing the V_f of BF in BC beams from 0.5 to 1%, the T rose. For instance, the combination of 0.5 and 1% BF to RC beams resulted in an increase in T to 17 and 27% at early and long times, respectively. Also, the 1% BC beams had higher T up to 9% than the 0.5% BC ones. Despite the higher strength of GF compared to BF, the BF has a role in helping to control and distribute loads through the crack bridging. Therefore, the increase of the T will be expected [45], [46], [48], [49], [54], [61], [67], [68], [69].

Figure 24. The BC beams crack bridging

Crack bridging is a fiber performance to delay and prevent from distribution of cracks in the concrete beams. The T and ductility of beams are enhanced by strengthening fiber bridging. Therefore, by augmenting the V_f, more fibers can bear the applied load, so the effectiveness of crack bridging and the T of beams will be risen [23], [48], [49], [53], [70]. The crack bridging of fibers in BC beams has been illustrated in Figure 24.
According to Table 12 and Figure 23, by changing the A.R. of BF from 40 to 80, the T of the BC beams rose about 10%. It will be expected that the T of BC beams will be enhanced when the A.R. of BF, length, developmental length, adhesion, and fiber pull out resistance from the cement paste is enhanced [9], [27], [49], [50], [51], [54].
After comparing the findings, it was observed that the T of BC beams containing metakaolin surpassed that of BC beams containing zeolite. However, for a long time, it was found that the T of BF beams and metakaolin/zeolite were identical. After 28 days, the T of BC beams with metakaolin exhibited an increase of up to 11% in comparison to the zeolite ones. However, after 180 days, the T of metakaolin BC beams including 0.5% BF was found to be similar to that of the zeolite beams [8], [13], [16], [60].

4.3.3. Comparison of the GC and BC beams

Figures 26-28 demonstrate the P_{cr}, P_{max}, and T of the GC and BC beams with zeolite or metakaolin as SCM, after 180 days.

Figure 25. The cross-section of GC and BC beams

According to the findings displayed in Figure 26 and Table 10, it is apparent that the BC beams' P_{cr} was higher than the GC beams. However, it is notable that the disparity in P_{cr} between the types of beams exhibited an upward trend over time.

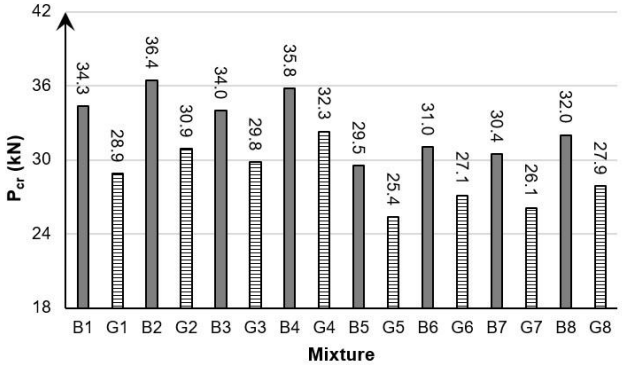

Figure 26. P_{cr} of GC and BC beams (180 days)

To illustrate, at 28 and 180 days, the P_{cr} of BC beams were about 14 and 19% higher than GC beams, respectively. It can be concluded that the greater hardness and inflexibility of GF compared to BF

causes to increase in porosity and decrease the density, integrity, and P_{cr} of GC beams [9], [23], [27], [29], [33], [46], [48], [49], [50], [51], [53], [54], [58], [62].

Furthermore, according to the results of Table 10 and Figures 27-28, it can be determined that in comparison to BC beams, the GC beams had higher P_{max} and T.

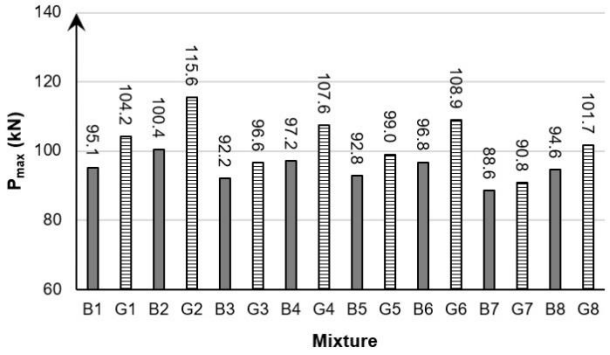

Figure 27. P_{max} of GC and BC beams (180 days)

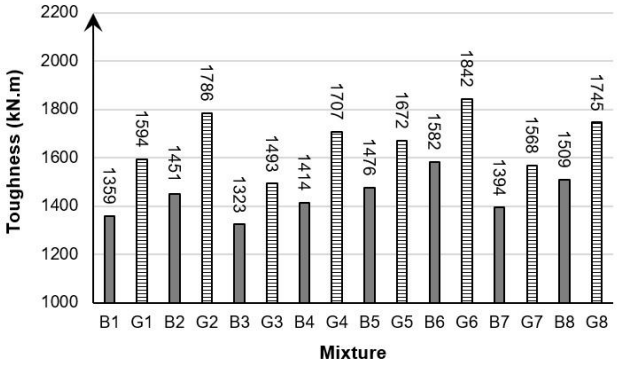

Figure 28. T of GC and BC beams (180 days)

For example, the P_{max} of the GC beams with 0.5 and 1% GF was more than the BC beams up to 16 and 13% at 28 days. Moreover, the T of the 0.5 and 1% GC beams exhibited an increase of up to 23 and 17%, in comparison to the BC beams after 180 days, respectively. It seems that although the flexibility of GF is lower than BF but its higher tensile strength (about 11 times) helps to better control cracking, prevent crack development, better distribute loads, and finally, increase the P_{max} and T of the GC beams [9], [23], [27], [33], [48], [49], [50], [51], [54], [58].

4.4. The scanning electron microscope (SEM)

Figure 29 illustrates the SEM analysis of concrete mixes that incorporate metakaolin/zeolite, providing a precise investigation and evaluation of their microstructural characteristics. The samples were prepared by taking small pieces of fiber concrete from cubic specimens (70×70×70 mm) which were coated with thin gold sheets to improve the image quality.

Figure 30 displays the SEMs of the area located between the cement paste and fiber. Furthermore, in Figure 31, the cement hydration products including ettringite, HC, and C-S-H gels are displayed. Also, the micro/macro pore and cracks in cement paste are demonstrated in Figure 32.

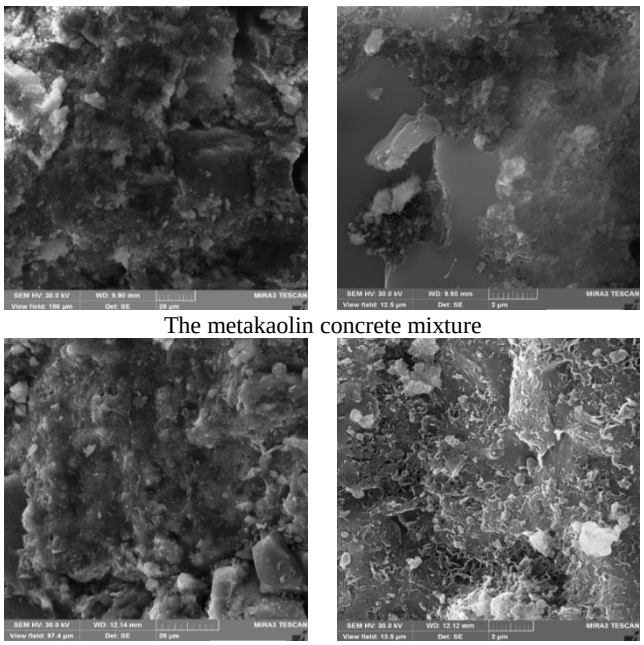

The metakaolin concrete mixture

The zeolite concrete mixture

Figure 29. The microstructural properties of concrete mixtures

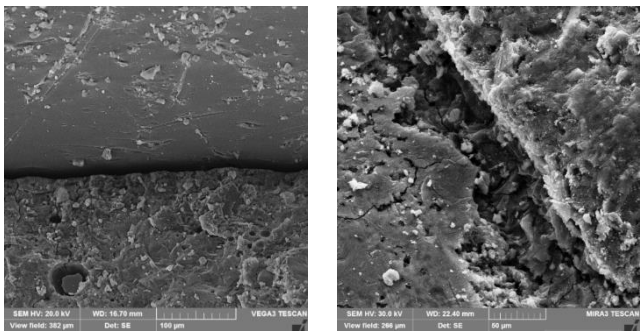

Figure 30. Fiber and cement paste contact zone

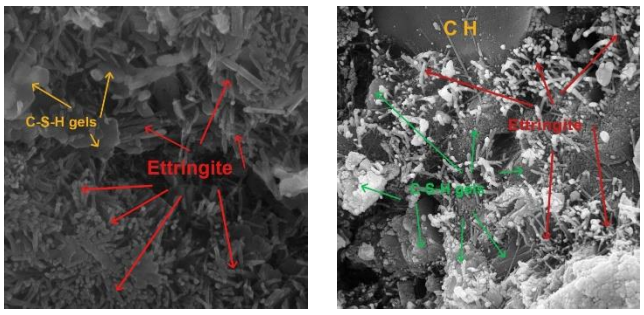

Figure 31. The cement hydration products

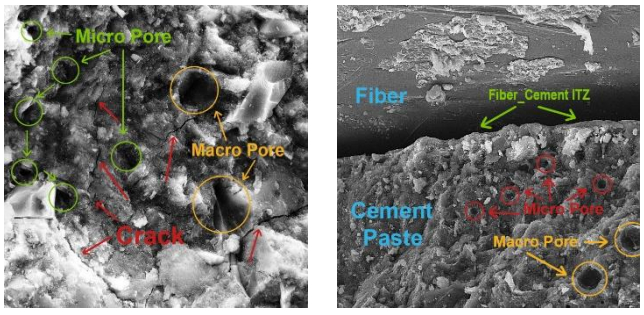

Figure 32. The micro/macro pore and cracks in cement paste

4.5. Cracking behavior

The four-point bending test is utilized for both RC and FRC beams, wherein a load protocol that increases monotonically is applied to the beams. Typically, the first crack in a beam occurs in the tensile zone, specifically on the bottom face. Subsequently, by raising the load, flexural fractures developed from the beams' bottom faces upward. In continuation and with an increase in the load, flexural cracks emerged and extended toward the compressive zone. The initial cracks exhibited greater depth and width. The majority of the flexural cracks manifested in the vicinity of the mid-span beams. The improvement of crack propagation resistance can be achieved by augmenting RC beams with fibers and enhancing the V_f of fibers [31], [71], [72].

The findings suggest a direct correlation between the quantity and attributes of flexural cracks and the fiber type and amount in the concrete mixes. The combination of fibers into the RC beams led to an increase in both primary and secondary cracking. The dimension of cracks like breadth and spacing were also reduced. For instance, according to Figure 30, by adding 1% GF/BF fibers to the RC beams, the number of major and minor cracks were increased. Furthermore, fiber RC beams containing 1% GF/BF fibers had cracks with less width and distance than RC beams.

Figure 33. Measurement of the crack dimensions

Furthermore, elevating the A.R. of GF/BF fibers from 40 to 80 resulted in heightened adhesion of fibers in the cement paste, thereby augmenting the pull-out resistance of fibers. This, in turn, reinforced crack bridging, restricted the distribution of cracks, and reduced the number and width of cracks[26], [63], [67], [73].

For more examination of the crack behavior of RC beams without/with fiber, in Figure 34, the cracking patterns are shown.

As a result, the concurrent utilization of recycled strip fibers (GF/BF) and SCMs such as metakaolin and zeolite, has the potential to mitigate air and marine pollution, restrict crack development, and enhance the ductility of RC beams.

5. Conclusion

The current research aims to evaluate the compressive strength, flexural toughness, flexural behavior, and cracking behavior of RC, GC, and BC beams that incorporated SCM like metakaolin and zeolite. The evaluation was conducted at 28 and 180 days in the Oman Sea's tidal zone. The primary findings are:

1- The incorporation of GF/BF into the concrete mixes led to a reduction of approximately 22% in the f'_c of the concrete specimens. Moreover, it was discovered that the f'_c of concrete containing zeolite was greater than that of metakaolin concrete at an early age.

2- The P_{cr} of fiber RC beams containing GF/BF fibers was up to 32 and 23% lower than RC beams, respectively. In a short time, the fiber RC beams containing metakaolin exhibited a greater P_{cr} by up to 10% compared to those containing zeolite. However, at long term, the P_{cr} of zeolite fiber RC beams was found to be nearly equivalent to that of metakaolin fiber RC beams.

3- The P_{max} of RC beams by adding 0.5% GF and BF decreased by 28 and 16%, at 180 days, respectively, but RC beams containing 1% GF and BF had higher P_{max} than RC beams up to 21 and 13%, respectively.

4- At 28 and 180 days, the GC beams, which were composed of 0.5 and 1% GF, exhibited a greater P_{max} of up to 16 and 13% compared to the BC beams, respectively.

5- The P_{max} of FRC beams containing metakaolin was found to be 13 and 9% greater than those containing zeolite after 28 and 180 days, respectively.

6- The combination of 0.5 or 1% GF in RC beams resulted in an increase in the toughness of the beams up to 43 and 48%, respectively. Moreover, it was observed that the toughness of beams made with BC containing 0.5 or 1% BF was 17 and 27% higher, respectively, compared to RC beams.

7- The toughness of fiber RC beams with 0.5 or 1% GF exhibited an increase of 23 and 17%, respectively, compared to those with BF.

8- The toughness of metakaolin FRC beams was observed to be higher than that of zeolite FRC beams. However, as time goes on, the disparity in their toughness reduced.

9- The propagation of cracks in RC beams was found to be mitigated through the incorporation of GF/BF, as well as an increase in both the V_f and A.R. of fibers. Additionally, it was discovered that there were more cracks than before.

Figure 34. Cracking patterns of GC/BC beams (180 days)

6. References

[1] M. Valipour, M. Shekarchi, and M. Arezoumandi, 'Chlorine diffusion resistivity of sustainable green concrete in harsh marine environments', *J Clean Prod*, vol. 142, pp. 4092–4100, Jan. 2017, doi: 10.1016/j.jclepro.2016.10.015.

[2] A. Azad, A. Saeedian, S.-F. Mousavi, H. Karami, S. Farzin, and V. P. Singh, 'Effect of zeolite and pumice powders on the environmental and physical characteristics of green concrete filters', *Constr Build Mater*, vol. 240, p. 117931, Apr. 2020, doi: 10.1016/j.conbuildmat.2019.117931.

[3] M. Valipour, M. Yekkalar, M. Shekarchi, and S. Panahi, 'Environmental assessment of green concrete containing natural zeolite on the global warming index in marine environments', *J Clean Prod*, vol. 65, pp. 418–423, Feb. 2014, doi: 10.1016/j.jclepro.2013.07.055.

[4] H. Shahrabadi and D. Vafaei, 'Effect of kerosene impacted sand on compressive strength of concrete in different exposure conditions', *Journal of Materials and Environmental Science*, vol. 6, no. 9, 2015.

[5] M. Najimi, J. Sobhani, B. Ahmadi, and M. Shekarchi, 'An experimental study on durability properties of concrete containing zeolite as a highly reactive natural pozzolan', *Constr Build Mater*, vol. 35, pp. 1023–1033, Oct. 2012, doi: 10.1016/j.conbuildmat.2012.04.038.

[6] H. Shahrabadi, S. Sayareh, and H. Sarkardeh, 'Effect of silica fume on compressive strength of oil-polluted concrete in different marine environments', *China Ocean Engineering*, vol. 31, no. 6, 2017, doi: 10.1007/s13344-017-0082-6.

[7] Y. T. Tran, J. Lee, P. Kumar, K.-H. Kim, and S. S. Lee, 'Natural zeolite and its application in concrete composite production', *Compos B Eng*, vol. 165, pp. 354–364, May 2019, doi: 10.1016/j.compositesb.2018.12.084.

[8] P. Rashiddadash, A. A. Ramezanianpour, and M. Mahdikhani, 'Experimental investigation on flexural toughness of hybrid fiber reinforced concrete (HFRC) containing metakaolin and pumice', *Constr Build Mater*, vol. 51, pp. 313–320, Jan. 2014, doi: 10.1016/j.conbuildmat.2013.10.087.

[9] P. S. Song, S. Hwang, and B. C. Sheu, 'Strength properties of nylon- and polypropylene-fiber-reinforced concretes', *Cem Concr Res*, vol. 35, no. 8, pp. 1546–1550, Aug. 2005, doi: 10.1016/j.cemconres.2004.06.033.

[10] D. K. Panesar and R. Zhang, 'Performance comparison of cement replacing materials in concrete: Limestone fillers and supplementary cementing materials – A review', *Constr Build Mater*, vol. 251, p. 118866, Aug. 2020, doi: 10.1016/j.conbuildmat.2020.118866.

[11] A. M. Rashad, 'Metakaolin as cementitious material: History, scours, production and composition – A comprehensive overview', *Constr Build Mater*, vol. 41, pp. 303–318, Apr. 2013, doi: 10.1016/j.conbuildmat.2012.12.001.

[12] X. Qian and Z. Li, 'The relationships between stress and strain for high-performance concrete with metakaolin', *Cem Concr Res*, vol. 31, no. 11, pp. 1607–1611, Nov. 2001, doi: 10.1016/S0008-8846(01)00612-3.

[13] R. Siddique and J. Klaus, 'Influence of metakaolin on the properties of mortar and concrete: A review', *Appl Clay Sci*, vol. 43, no. 3–4, pp. 392–400, Mar. 2009, doi: 10.1016/j.clay.2008.11.007.

[14] O. R. Kavitha, V. M. Shanthi, G. Prince Arulraj, and P. Sivakumar, 'Fresh, micro- and macrolevel studies of metakaolin blended self-compacting concrete', *Appl Clay Sci*, vol. 114, pp. 370–374, Sep. 2015, doi: 10.1016/j.clay.2015.06.024.

[15] V. Punitha, N. Sakthieswaran, and O. Ganesh Babu, 'Experimental investigation of concrete incorporating HDPE plastic waste and metakaolin', *Mater Today Proc*, no. xxxx, Jul. 2020, doi: 10.1016/j.matpr.2020.06.288.

[16] F. A. Sabet, N. A. Libre, and M. Shekarchi, 'Mechanical and durability properties of self consolidating high performance concrete incorporating natural zeolite, silica fume and fly ash', *Constr Build Mater*, vol. 44, pp. 175–184, Jul. 2013, doi: 10.1016/j.conbuildmat.2013.02.069.

[17] K. Samimi, S. Kamali-Bernard, and A. A. Maghsoudi, 'Durability of self-compacting concrete containing pumice and zeolite against acid attack, carbonation and marine environment', *Constr Build Mater*, vol. 165, pp. 247–263, Mar. 2018, doi: 10.1016/j.conbuildmat.2017.12.235.

[18] H. Shahrabadi, S. Sayareh, and H. Sarkardeh, 'Effect of Natural Zeolite-Pozzolan on Compressive Strength of Oil-Polluted Concrete Marine Structures', *Civil Engineering Journal*, vol. 2, no. 12, p. 623, Feb. 2018, doi: 10.28991/cej-030985.

[19] E. Emam and S. Yehia, 'Performance of concrete containing zeolite as a supplementary cementitious material', *Int. Res. J. Eng. Technol*, vol. 4, no. 12, pp. 1619–

1625, 2017, [Online]. Available: https://www.irjet.net/archives/V4/i12/IRJET-V4I12297.pdf

[20] M. C. G. Juenger and R. Siddique, 'Recent advances in understanding the role of supplementary cementitious materials in concrete', *Cem Concr Res*, vol. 78, pp. 71–80, Dec. 2015, doi: 10.1016/j.cemconres.2015.03.018.

[21] S. Mehdipour *et al.*, 'Mechanical properties, durability and environmental evaluation of rubberized concrete incorporating steel fiber and metakaolin at elevated temperatures', *J Clean Prod*, vol. 254, p. 120126, May 2020, doi: 10.1016/j.jclepro.2020.120126.

[22] L. Kan, L. Zhang, Y. Zhao, and M. Wu, 'Properties of polyvinyl alcohol fiber reinforced fly ash based Engineered Geopolymer Composites with zeolite replacement', *Constr Build Mater*, vol. 231, p. 117161, Jan. 2020, doi: 10.1016/j.conbuildmat.2019.117161.

[23] D. Foti, 'Preliminary analysis of concrete reinforced with waste bottles PET fibers', *Constr Build Mater*, vol. 25, no. 4, pp. 1906–1915, Apr. 2011, doi: 10.1016/j.conbuildmat.2010.11.066.

[24] M. Zaroudi, R. Madandoust, and K. Aghaee, 'Fresh and hardened properties of an eco-friendly fiber reinforced self-consolidated concrete composed of polyolefin fiber and natural zeolite', *Constr Build Mater*, vol. 241, p. 118064, Apr. 2020, doi: 10.1016/j.conbuildmat.2020.118064.

[25] O. B. Ozger *et al.*, 'Effect of nylon fibres on mechanical and thermal properties of hardened concrete for energy storage systems', *Mater Des*, vol. 51, pp. 989–997, Oct. 2013, doi: 10.1016/j.matdes.2013.04.085.

[26] S. B. Kim, N. H. Yi, H. Y. Kim, J.-H. J. Kim, and Y.-C. Song, 'Material and structural performance evaluation of recycled PET fiber reinforced concrete', *Cem Concr Compos*, vol. 32, no. 3, pp. 232–240, Mar. 2010, doi: 10.1016/j.cemconcomp.2009.11.002.

[27] S. P. Yap, U. J. Alengaram, and M. Z. Jumaat, 'Enhancement of mechanical properties in polypropylene– and nylon–fibre reinforced oil palm shell concrete', *Mater Des*, vol. 49, pp. 1034–1041, Aug. 2013, doi: 10.1016/j.matdes.2013.02.070.

[28] A. Q. Ahdal *et al.*, 'Mechanical performance and feasibility analysis of green concrete prepared with local natural zeolite and waste PET plastic fibers as cement replacements', *Case Studies in Construction Materials*, vol. 17, no. June, p. e01256, Dec. 2022, doi: 10.1016/j.cscm.2022.e01256.

[29] H. Alabduljabbar, H. Mohammadhosseini, M. Md. Tahir, and R. Alyousef, 'Green and sustainable concrete production using carpet fibers waste and palm oil fuel ash', *Mater Today Proc*, vol. 39, pp. 929–934, 2021, doi: 10.1016/j.matpr.2020.04.047.

[30] A. H. Alani, N. M. Bunnori, A. T. Noaman, and T. A. Majid, 'Durability performance of a novel ultra-high-performance PET green concrete (UHPPGC)', *Constr Build Mater*, vol. 209, pp. 395–405, Jun. 2019, doi: 10.1016/j.conbuildmat.2019.03.088.

[31] M. Shayanfar and H. Shahrabadi, 'Flexural behavior of green RC beams with disposable glasses fibers in a marine environment', *Case Studies in Construction Materials*, vol. 18, p. e01972, Jul. 2023, doi: 10.1016/j.cscm.2023.e01972.

[32] ASTM International, 'ASTM C136, Standard Test Method forSieve Analysis of Fine and Coarse Aggregates.', West Conshohocken, PA, 2001. doi: 10.1520/C0136_C0136M-19.

[33] A. Meza and S. Siddique, 'Effect of aspect ratio and dosage on the flexural response of FRC with recycled fiber', *Constr Build Mater*, vol. 213, pp. 286–291, Jul. 2019, doi: 10.1016/j.conbuildmat.2019.04.081.

[34] ACI, 'ACI 360R-10, Guide to Design of Slabs-on-Ground', 2010.

[35] British Standard, 'British Standard BS-EN-12390-3-2009 Testing Hardened Concrete Part 3: Compressive Strength of Test Specimens', London, England, 2009. [Online]. Available: https://shop.bsigroup.com/ProductDetail/?pid=000000000030253049

[36] ASTM International, 'ASTM C78-08, Standard Test Method for Flexural Strength of Concrete (Using Simple Beam with Third-Point Loading)', West Conshohocken, PA, 2008. doi: 10.1520/C0078-08.

[37] G. Rojo-López, B. González-Fonteboa, F. Martínez-Abella, and I. González-Taboada, 'Rheology, durability, and mechanical performance of sustainable self-compacting concrete with metakaolin and limestone filler', *Case Studies in Construction Materials*, vol. 17, no. May, p. e01143, Dec. 2022, doi: 10.1016/j.cscm.2022.e01143.

[38] M. Amran *et al.*, 'Properties and performance of polypropylene fibered high-strength concrete with an improved composite binders', *Case Studies in Construction Materials*, vol. 17, no. August, p. e01621, Dec. 2022, doi: 10.1016/j.cscm.2022.e01621.

[39] J. J. Chen, L. G. Li, P. L. Ng, and A. K. H. Kwan, 'Effects of superfine zeolite on strength, flowability and cohesiveness of cementitious paste', *Cem Concr Compos*, vol.

83, pp. 101–110, Oct. 2017, doi: 10.1016/j.cemconcomp.2017.06.010.

[40] M. Abdellatief, S. M. AL-Tam, W. E. Elemam, H. Alanazi, G. M. Elgendy, and A. M. Tahwia, 'Development of ultra-high-performance concrete with low environmental impact integrated with metakaolin and industrial wastes', *Case Studies in Construction Materials*, vol. 18, no. August 2022, p. e01724, Jul. 2023, doi: 10.1016/j.cscm.2022.e01724.

[41] N. Saboo, S. Shivhare, K. K. Kori, and A. K. Chandrappa, 'Effect of fly ash and metakaolin on pervious concrete properties', *Constr Build Mater*, vol. 223, pp. 322–328, Oct. 2019, doi: 10.1016/j.conbuildmat.2019.06.185.

[42] L. Gu and T. Ozbakkaloglu, 'Use of recycled plastics in concrete: A critical review', *Waste Management*, vol. 51, pp. 19–42, May 2016, doi: 10.1016/j.wasman.2016.03.005.

[43] F. Fraternali, S. Spadea, and V. P. Berardi, 'Effects of recycled PET fibres on the mechanical properties and seawater curing of Portland cement-based concretes', *Constr Build Mater*, vol. 61, pp. 293–302, Jun. 2014, doi: 10.1016/j.conbuildmat.2014.03.019.

[44] R. Merli, M. Preziosi, A. Acampora, M. C. Lucchetti, and E. Petrucci, 'Recycled fibers in reinforced concrete: A systematic literature review', *J Clean Prod*, vol. 248, p. 119207, Mar. 2020, doi: 10.1016/j.jclepro.2019.119207.

[45] H. Safayenikoo, 'Metalized Plastic Waste Fiber Effects on Green Concrete Beams Mechanical Performance', *Shock and Vibration*, vol. 2022, pp. 1–15, May 2022, doi: 10.1155/2022/3113841.

[46] A. Meena, A. Surendranath, and P. V. Ramana, 'Assessment of mechanical properties and workability for polyethylene terephthalate fiber reinforced concrete', *Mater Today Proc*, vol. 50, pp. 2307–2314, 2022, doi: 10.1016/j.matpr.2021.10.054.

[47] Z. Z. Ismail and E. A. AL-Hashmi, 'Use of waste plastic in concrete mixture as aggregate replacement', *Waste Management*, vol. 28, no. 11, pp. 2041–2047, Nov. 2008, doi: 10.1016/j.wasman.2007.08.023.

[48] R. Sharma and P. P. Bansal, 'Use of different forms of waste plastic in concrete – a review', *J Clean Prod*, vol. 112, pp. 473–482, Jan. 2016, doi: 10.1016/j.jclepro.2015.08.042.

[49] Y. Ghernouti, B. Rabehi, T. Bouziani, H. Ghezraoui, and A. Makhloufi, 'Fresh and hardened properties of self-compacting concrete containing plastic bag waste fibers (WFSCC)', *Constr Build Mater*, vol. 82, pp. 89–100, May 2015, doi: 10.1016/j.conbuildmat.2015.02.059.

[50] A. Zia and M. Ali, 'Behavior of fiber reinforced concrete for controlling the rate of cracking in canal-lining', *Constr Build Mater*, vol. 155, pp. 726–739, Nov. 2017, doi: 10.1016/j.conbuildmat.2017.08.078.

[51] Y. Qin, X. Zhang, and J. Chai, 'Damage performance and compressive behavior of early-age green concrete with recycled nylon fiber fabric under an axial load', *Constr Build Mater*, vol. 209, pp. 105–114, Jun. 2019, doi: 10.1016/j.conbuildmat.2019.03.094.

[52] B. Ali, M. Fahad, A. S. Mohammed, H. Ahmed, A. B. Elhag, and M. Azab, 'Improving the performance of recycled aggregate concrete using nylon waste fibers', *Case Studies in Construction Materials*, vol. 17, no. July, p. e01468, Dec. 2022, doi: 10.1016/j.cscm.2022.e01468.

[53] S. Ullah Khan and T. Ayub, 'Flexure and shear behaviour of self-compacting reinforced concrete beams with polyethylene terephthalate fibres and strips', *Structures*, vol. 25, no. December 2019, pp. 200–211, Jun. 2020, doi: 10.1016/j.istruc.2020.02.023.

[54] M. Kumaresan, S. Sindhu Nachiar, and S. Anandh, 'Implementation of waste recycled fibers in concrete: a review', *Mater Today Proc*, vol. 68, pp. 1988–1994, 2022, doi: 10.1016/j.matpr.2022.08.228.

[55] N. K. Bui, T. Satomi, and H. Takahashi, 'Recycling woven plastic sack waste and PET bottle waste as fiber in recycled aggregate concrete: An experimental study', *Waste Management*, vol. 78, pp. 79–93, Aug. 2018, doi: 10.1016/j.wasman.2018.05.035.

[56] H. K. Shehab El-Din, A. S. Eisa, B. H. Abdel Aziz, and A. Ibrahim, 'Mechanical performance of high strength concrete made from high volume of Metakaolin and hybrid fibers', *Constr Build Mater*, vol. 140, pp. 203–209, Jun. 2017, doi: 10.1016/j.conbuildmat.2017.02.118.

[57] M. Valipour, F. Pargar, M. Shekarchi, and S. Khani, 'Comparing a natural pozzolan, zeolite, to metakaolin and silica fume in terms of their effect on the durability characteristics of concrete: A laboratory study', *Constr Build Mater*, vol. 41, pp. 879–888, Apr. 2013, doi: 10.1016/j.conbuildmat.2012.11.054.

[58] F. S. Khalid, J. M. Irwan, M. H. W. Ibrahim, N. Othman, and S. Shahidan, 'Performance of plastic wastes in fiber-reinforced concrete beams', *Constr Build Mater*, vol. 183, pp. 451–464, Sep. 2018, doi: 10.1016/j.conbuildmat.2018.06.122.

[59] H. M. Adnan and A. O. Dawood, 'Strength behavior of reinforced concrete beam using re-cycle of PET wastes as synthetic fibers', *Case Studies in Construction Materials*, vol.

13, p. e00367, Dec. 2020, doi: 10.1016/j.cscm.2020.e00367.

[60] A. Jain, N. Sharma, R. Choudhary, R. Gupta, and S. Chaudhary, 'Utilization of non-metalized plastic bag fibers along with fly ash in concrete', *Constr Build Mater*, vol. 291, p. 123329, Jul. 2021, doi: 10.1016/j.conbuildmat.2021.123329.

[61] S. Spadea, I. Farina, A. Carrafiello, and F. Fraternali, 'Recycled nylon fibers as cement mortar reinforcement', *Constr Build Mater*, vol. 80, pp. 200–209, Apr. 2015, doi: 10.1016/j.conbuildmat.2015.01.075.

[62] R. Alyousef, H. Mohammadhosseini, M. Md. Tahir, and H. Alabduljabbar, 'Green concrete composites production comprising metalized plastic waste fibers and palm oil fuel ash', *Mater Today Proc*, no. xxxx, Apr. 2020, doi: 10.1016/j.matpr.2020.04.023.

[63] A. C. Bhogayata and N. K. Arora, 'Fresh and strength properties of concrete reinforced with metalized plastic waste fibers', *Constr Build Mater*, vol. 146, pp. 455–463, Aug. 2017, doi: 10.1016/j.conbuildmat.2017.04.095.

[64] M. A. Farooq, M. Fahad, B. Ali, S. Ullah, M. H. El Ouni, and A. B. Elhag, 'Influence of nylon fibers recycled from the scrap brushes on the properties of concrete: Valorization of plastic waste in concrete', *Case Studies in Construction Materials*, vol. 16, no. March, p. e01089, Jun. 2022, doi: 10.1016/j.cscm.2022.e01089.

[65] I. H. Alfahdawi, S. A. Osman, R. Hamid, and A. I. AL-Hadithi, 'Influence of PET wastes on the environment and high strength concrete properties exposed to high temperatures', *Constr Build Mater*, vol. 225, pp. 358–370, Nov. 2019, doi: 10.1016/j.conbuildmat.2019.07.214.

[66] R. H. Faraj, H. F. Hama Ali, A. F. H. Sherwani, B. R. Hassan, and H. Karim, 'Use of recycled plastic in self-compacting concrete: A comprehensive review on fresh and mechanical properties', *Journal of Building Engineering*, vol. 30, p. 101283, Jul. 2020, doi: 10.1016/j.jobe.2020.101283.

[67] F. Pacheco-Torgal, Y. Ding, and S. Jalali, 'Properties and durability of concrete containing polymeric wastes (tyre rubber and polyethylene terephthalate bottles): An overview', *Constr Build Mater*, vol. 30, pp. 714–724, May 2012, doi: 10.1016/j.conbuildmat.2011.11.047.

[68] A. H. Alani, M. Azmi Megat Johari, A. Tareq Noaman, N. Muhamad Bunnori, and T. A. Majid, 'Effect of the incorporation of PET fiber and ternary blended binder on the flexural and tensile behaviour of ultra-high performance green concrete', *Constr Build Mater*, vol. 331, no. August 2021, p. 127306, May 2022, doi: 10.1016/j.conbuildmat.2022.127306.

[69] N. Z. Nkomo, L. M. Masu, and P. K. Nziu, 'Optimisation of mechanical properties of polyethylene terephthalate fibre/fly ash hybrid concrete composite', *Case Studies in Construction Materials*, vol. 17, no. July, p. e01395, Dec. 2022, doi: 10.1016/j.cscm.2022.e01395.

[70] F. S. Khalid, J. M. Irwan, M. H. Wan Ibrahim, N. Othman, and S. Shahidan, 'Splitting tensile and pullout behavior of synthetic wastes as fiber-reinforced concrete', *Constr Build Mater*, vol. 171, pp. 54–64, May 2018, doi: 10.1016/j.conbuildmat.2018.03.122.

[71] W. Alnahhal and O. Aljidda, 'Flexural behavior of basalt fiber reinforced concrete beams with recycled concrete coarse aggregates', *Constr Build Mater*, vol. 169, pp. 165–178, 2018, doi: 10.1016/j.conbuildmat.2018.02.135.

[72] H. C. Mertol, E. Baran, and H. J. Bello, 'Flexural behavior of lightly and heavily reinforced steel fiber concrete beams', *Constr Build Mater*, vol. 98, pp. 185–193, Nov. 2015, doi: 10.1016/j.conbuildmat.2015.08.032.

[73] S. Y. Al-Darzi, 'The effect of using shredded plastic on the behavior of reinforced concrete slab', *Case Studies in Construction Materials*, vol. 17, no. November, p. e01681, Dec. 2022, doi: 10.1016/j.cscm.2022.e01681.

INTERNATIONAL JOURNAL OF
COASTAL & OFFSHORE ENGINEERING
IJCOE Vol.10/No. 1/Winter 2025 (20-34)

Available online at: www. Ijcoe.org

Investigating the Impact of Distance between Diffusers in Wastewater discharge system for Marine Environmental Protection by Numerical Method

Amirreza Afifeh[1], Mehdi Nezhadnaderi[2]*, Babak Pordel Maragheh[3], Babak Fazli Malidareh[4], Ali Sheykhbahaei[5] and Seyed Mohammad Mousavi[6]

[1)] Department of Civil Engineering, Tonekabon Branch, Islamic Azad University, Tonekabon, Iran. amirrezaafife@gmail.com
*[*2)] Department of Civil Engineering, Tonekabon Branch, Islamic Azad University, Tonekabon, Iran. (Corresponding Author). mehdi2930@yahoo.com.*
[3)] Department of Civil Engineering, Ardabil Branch, Islamic Azad University, Ardabil, Iran. civil_babak2005@yahoo.com
[4)] Department of Civil Engineering, Babol Branch, Islamic Azad University, Babol, Iran. Fazli.babak@babolia.ac.ir
[5)] PhD Candidate in Physical Oceanography at university of Hormozgan/ Iranian National Institute for Oceanography and Atomospheric science, Ali.sheykhbahaei@inio.ac.ir
[6)] Department of Civil Engineering, Tonekabon Branch, Islamic Azad University, Tonekabon, Iran. Mosavi.622@gmail.com

ARTICLE INFO

Article History:
Received: 15 Nov 2024
Accepted: 25 Jan 2025

Keywords:
wastewater discharge site
leachate, mixing area
primary development
angular spreader

ABSTRACT

The rate of initial development and its characteristics play an important role in the design of wastewater discharge into the sea. It is very common to use mixing zone models to estimate the initial gradient. Considering that salty sea water causes environmental damage due to mixing with wastewater discharged from the desalination site into the sea on the coasts, it was determined by modeling the angled channels that distribute the wastewater on the sea floor that the wastewater from the water site The sweetener enters the sea through the angled channels of the spreader and is pulled towards the shore due to the velocity of the current. The lowest density is in the areas between the spreaders, which shows that the promotion system works well and prevents the sedimentation of the effluent on the sea floor and has reduced the density of the effluent. Also, the lowest velocity is in the areas between the spreaders, which shows that the promotion system works well and prevents the sewage from settling on the sea floor.

[1, 5)] MSc
[2)] Associate Professor
[3 to 6)] Assistant Professor

1. Introduction

Multi-port diffusers are often used to dilute industrial effluents to receiving waters characterized by shallow water depth. Examples of these effluents include heated water from power plants located near the ocean or the coast of Great Lakes, sewage effluent from treatment plants discharged into a river or lake, and saltwater runoff from desalination plants. the ocean Concentrated brine from desalination plants is sometimes mixed with lighter heated water from an on-site power plant or treated wastewater from a sewage treatment plant for energy recovery using pressurized delayed osmosis (PRO) or reverse electrodialysis. (RED) Akram et al. 2013; Weiner et al., 2015)
(Shrivastava and Adam, 2019 studied the mixing of tee diffusers in shallow water with cross flow. This paper analyzes the mixing of a tee diffuser discharging into shallow water with the flow. Experiments are performed for tee diffusers of various designs discharging in a crossflow. Dilution measurements are reported and analyzed along with results obtained by previous studies to investigate the effects of various outlet and environmental parameters on dilution. The effect of ambient flow velocity, diffuser length, port distance, port angle with respect to horizontal, ambient depth, distance near the shore and effluent buoyancy on dilution is investigated. Previous investigations have shown different effects of the ambient flow on the dilution of the three-way diffuser, which is characterized by the ratio of the ambient momentum to the discharge momentum. This apparent confusion is resolved by showing that many of the differences can be attributed to the different range of parameters used in the different studies. While most studies have focused on minimum dilution inside the column, dilution measurements at the edge of a regulatory mixing zone are considered in this paper because they are important to meet regulatory requirements. Measurements of centerline and mean flux dilution at the edge of a mixing zone are reported. Recommendations are given for the design of tee diffusers in shallow receiving waters with cross-flow.

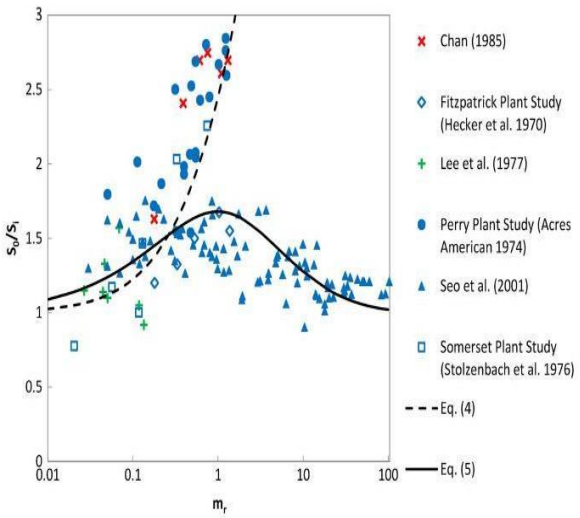

Figure 1- Progressive measurements in areas S1, S2, and S3 for a T-shaped spreader(Shrivastava and Adam, 2019).

Reference	S_0	θ_0 (degrees)	m_r	L/H	l/H	ϕ	Γ
Perry plant study (Acres American 1974)	4–9	0	0.05–1.26	15–75	1–6	0.1–0.3	0
Fitzpatrick plant study (Hecker et al. 1970)	14.9	0	0.18–1.37	30.3	2.5	0.64	1/50
Lee et al. (1977)	7–10	0	0.04–0.14	19–40	0.5–2.5	0–0.2	0
Seo et al. (2001)	10–30	22.5	0.03–104	4–15	0–1	0.1–1.2	0
Somerset plant study (Stolzenbach et al. 1976)	6–15	0	0–0.75	6–34	2	0.2–0.5	1/73.5
Chan (1985)	7.2	0	0.17–1.31	25.4,33.9	0.85	0	0

Figure 2-The parameters used by the previous researchers in the advanced calculation(Shrivastava and Adam, 2019).

Set	Run	L (m)	N	Q_0 (m^3/s)	u_a (m/s)	S_0	m_r	L/H	l/H	ϕ	n	S_3	S_{ave}	L_r
1	1	240	24	25.3	0.07	15.6	0.08	24	1	0.17	2	13.2	—	272
	2	240	24	25.3	0.22	15.6	0.92	24	1	0.17	6	10.6	17.3	272
	3	240	24	25.3	0.52	15.6	4.94	24	1	0.17	2	12.4	23.8	272
	4	240	24	25.3	1.13	15.6	23.29	24	1	0.17	2	15.7	27.6	272
2	5	240	48	25.3	0.06	15.6	0.07	24	0.5	0.17	1	11.2	—	225
	6	240	48	25.3	0.21	15.6	0.81	24	0.5	0.17	1	9.0	—	225
	7	240	48	25.3	0.48	15.6	4.27	24	0.5	0.17	1	10.2	19.6	225
	8	240	48	25.3	0.63	15.6	7.26	24	0.5	0.17	1	11.1	—	225
	9	240	48	25.3	1.05	15.6	20.16	24	0.5	0.17	1	12.9	21.8	225
3	10	240	12	25.3	0.07	15.6	0.08	24	2	0.17	2	14.2	—	267
	11	240	12	25.3	0.22	15.6	0.92	24	2	0.17	2	11.1	—	267
	12	240	12	25.3	0.52	15.6	4.94	24	2	0.17	2	11.2	—	267
	13	240	12	25.3	1.13	15.6	23.29	24	2	0.17	2	15.5	—	267
4	14	240	6	25.3	0.07	15.6	0.08	24	4	0.17	4	13.0	—	242
	15	240	6	25.3	0.22	15.6	0.92	24	4	0.17	3	9.5	—	242
	16	240	6	25.3	0.52	15.6	4.94	24	4	0.17	3	8.7	—	242
	17	240	6	25.3	1.13	15.6	23.29	24	4	0.17	2	11.6	—	242
5	18	300	30	25.3	0.07	17.4	0.10	30	1	0.18	2	14.1	—	245
	19	300	30	25.3	0.22	17.4	1.16	30	1	0.18	2	9.9	—	245
	20	300	30	25.3	0.52	17.4	6.15	30	1	0.18	4	10.1	17.7	245
	21	300	30	25.3	1.13	17.4	29.13	30	1	0.18	2	13.8	24.7	245
6	22	160	16	25.3	0.07	13.1	0.06	16	1	0.15	2	13.3	—	273
	23	160	16	25.3	0.22	13.1	0.59	16	1	0.15	2	10.4	—	273
	24	160	16	25.3	0.52	13.1	3.29	16	1	0.15	2	10.5	—	273
	25	160	16	25.3	1.13	13.1	15.53	16	1	0.15	2	15.0	—	273

Figure 3- Parameters used in advanced calculation (Shrivastava and Adam, 2019).

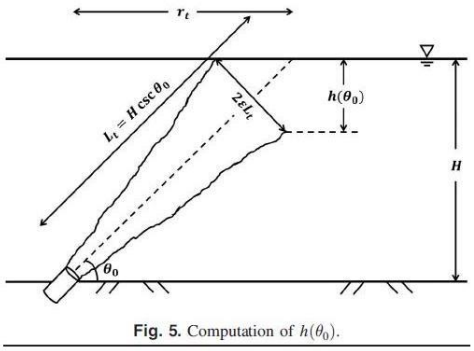

Fig. 5. Computation of $h(\theta_0)$.

Figure 4- Parameters used in advanced calculation (Shrivastava and Adam, 2019).

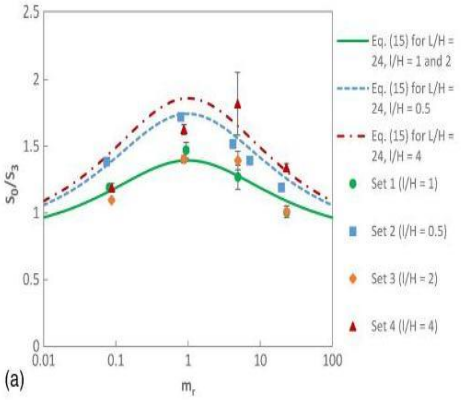

Figure 5- The parameters used in the progress calculation for 6 plans for different *l*/(H) (Shrivastava and Adam, 2019).

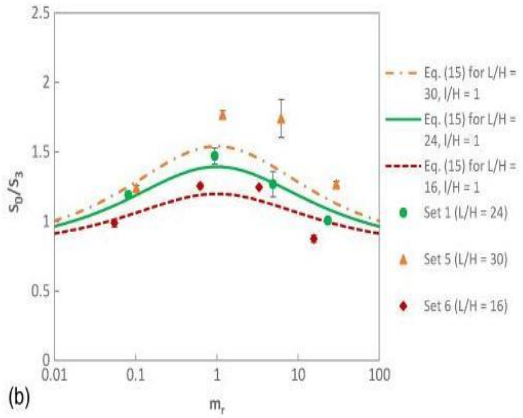

Figure 6- The parameters used in the progress calculation for 6 designs for different L/(H) (Shrivastava and Adam, 2019).

ε ≈ 0.1 is the expansion rate of the half-width jet (Lee and Chu, 2003). h(θ_0) is less than water depth for θ_0 > 11.3 degrees. Therefore, the dilution ratio for a diffuser with horizontal ports relative to ports inclined at an angle θ_0 for θ_0 > 11.3) is as follows:

$$\frac{S(0^{\circ})}{S(\theta_0)} = \sqrt{\frac{A(0^{\circ})}{A(\theta_0)}} = \sqrt{\frac{HL}{lh(\theta_0)}} = \frac{1}{\sqrt{2\varepsilon cot\theta_0}}$$

S1 = ratio of flow induced from behind the diffuser to the
discharge flow rate for a tee diffuser in crossflow;
S2 = minimum dilution within the plume for a tee diffuser in
crossflow;
S3 = minimum dilution at the edge of a mixing zone for a tee
diffuser in crossflow;
A = cross-sectional area occupied by the diffuser plume;
a0 = individual port area;
B = width of effluent plume as it crosses the mixing zone;
b0 = kinematic buoyancy flux per unit length of discharge
effluent;
cd = empirical drag coefficient for tee diffuser in crossflow;
D0 = port diameter;
F0 = densimetric Froude number;
g = acceleration due to gravity;
g00 = reduced gravity of effluent discharging from the outfall;
H = ambient water depth;
hθ0 = water depth occupied by the plume when it hits the
water surface;
L = length of diffuser;
Lm = characteristic length scale for the diffuser;
Lr = ratio of length in the prototype to length in the model;
Lt = length of trajectory till the plume hits the water surface;
l = spacing between ports;
ma = kinematic momentum flux per unit length of the ambient crossflow;
mr = momentum ratio, a nondimensional parameter characterizing the effect of ambient current;
m0 = kinematic momentum flux per unit length of discharge effluent;
N = number of ports;
n = number of replicates for each experimental run;
Q = flow induced by the discharge;
Q0 = flow rate of discharge effluent;
R = jet Reynolds number;
rt = horizontal distance of the point of surface impact from the jet;
S = diffuser dilution;
S ave = flux-averaged dilution at the edge of a mixing zone for atee diffuser in crossflow;
S0 = theoretical dilution of a tee diffuser in quiescent ambient;
ua = ambient current speed;
ud = speed of the plume perpendicular to the mixing zone boundary;
ue = average velocity of the flow being entrained into the diffuser plume;
uf = average velocity of the induced flow in front of the diffuser;
u0 = exit velocity through a port;
xs = distance of the diffuser from the nearshore;
Γ = bottom slope in the offshore direction;
Δρ = density difference between discharge effluent and ambient water;
ε = rate of increase of the jet half-width;
θ = local value of plume inclination relative to horizontal;
θ0 = angle of port inclination with horizontal;
ν = kinematic viscosity of water;
ρa = density of ambient water;
ρ0 = density of discharge effluent;
σ = contraction in the width of the plume discharged from a
tee diffuser; and
ϕ = nondimensional shallowness parameter.

$$\frac{S_t}{S_0} = 1 - C_d m_r$$

$$m_r = \frac{{U_a}^2 H}{{U_0}^2 B}$$

$$B = \frac{A}{l}$$

$$S_0 = \sqrt{\frac{H cos\theta_0}{2B}}$$

$$\frac{S_t}{S_0} = (1 + 5m_r)^{-1/2}$$

In 2017, Absi investigated how to discharge wastewater through angular ducts with the help of laboratory models. There have been extensive reports of dense gradient jets typical of brackish water discharge into shallow water. Experiments were performed with nozzles at 30, 45, and 60 degrees to the horizontal direction, and the spatial changes of restoration concentrations were measured by three-dimensional laser fluorescence (3DLIF). Three flow regimes are known: deep water, surface contact and shallow water. The regimes depend on the value of dF/H, where d is the nozzle diameter, F is the dense mass number of the jet, and H is the water depth; Criteria for transitioning between them are provided. Flow images showed three-dimensional interactions with the free surface, especially for steep nozzle angles in shallow water. The drop in critical points and their locations were measured. For deep water, all results followed those previously reported for fully submerged jets. As the depth (or increase in dF/H) decreases to surface contact, dilutions begin to decrease. Tracer concentration profiles are reduced at the water surface and resemble semi-Gaussian profiles similar to wall jets in shallow water. The jets can stick to the water surface, although the impact point locations and near-field length are not significantly affected by the water surface. In deep water-surface contact regimes, the impact point and near-field dilutions are higher for 60° nozzles. However, the depth decreases, but the dilution is almost equal for the three nozzle angles, until for shallow water, the 30° nozzle leads to a slightly higher dilution. A 30° discontinuity may be preferred for this case because the interaction surface is lower and therefore has less visual effect than the water surface. The previous recommendations that dense jets are located underwater, so that the height of the upper boundary to the jet is less than 75% of the water depth to avoid surface effects seems to be too conservative and the current results show which increase can be up to 90% of water depth for all angles without detrimental effect on dilution.

In 2017, Alden designed the wastewater discharge facility for the Huntington Beach desalination site. Suggested publisher goals (Alden 2017) are to maintain a underground sewers that do not tolerate water table and reduce low amounts of ocean salinity water, requiring discharge shall not exceed a daily maximum of 2.0 ppt above natural sodium not more than 100 meters horizontally from any point of discharge.

The ports are spaced to ensure proper flow between the jets and deliver a horizontal vertical motion of the bay to the dump.

Segregation analysis of this design published by Poseidon was performed using CORMIX (Jenkins, 2017a). This analysis is discussed below. Four flow scenarios are considered: worst case #1 and worst case #2 with temperature difference between effluent and seawater at 0°C and +2°C. To illustrate the methods calculated in R2018, we consider here only the worst case number 1 with a temperature difference of 2 °C (here WC1). The conclusion should be similar for other cases.

Donker and Jirka published a manual for using CORMIX software.

In 2017, Jenkins conducted a hydrodynamic study of a 3D designed model of channel spreaders at Huntington Beach.

(Adams, 1982) derived the progressive equation and angular diffuser using Bernoulli's equations and momentum equation for pressure continuity along the axis of the diffuser. In the case of the angled diffuser, the momentum drop that existed due to the stagnation of the surrounding flow in the momentum equation between the back and front section of the diffuser was taken into consideration. Then, by combining the energy equations and the momentum equations, he calculated the rate of promotion in the area near the discharge for angled diffusers.

The present invention relates to a multiport submerged cooling water discharge diffuser and, in particular, to a diffuser in which the direction of the cooling water discharge is variable as a function of the position of the water discharge relative to the longitudinal center of the diffuser as well as half the length of the diffuser.

When the wastewater is discharged into the sea, the initial mixing of an area with a radius of about 100 meters is done after the wastewater is discharged into the environment through the spreader, which is called the near field. It moves and is spread by the turbulence of this environment, which is called the far field. becomes

For brines, because it has a higher density than sea water and there is a possibility of settling on the bed. Therefore, the discharge of brine should be in such a way that it creates a jet state in the water at the beginning of the discharge so that it can move in the surrounding water and by creating more disturbance in the environment, it causes the mixing of the brine

with the surrounding water to accelerate the progress of the brine and before it drops. The speed and settling of that concentration should be reduced to such an extent that it cannot be separated from the surrounding environment. It should be noted that based on the standards provided by the US Environmental Agency, this process should be carried out within a maximum radius of 200 meters from the sewage discharge location (Moshirpanahei et al., 2019).

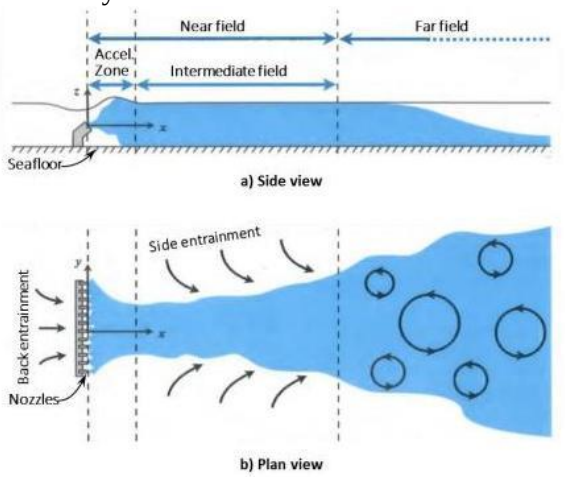

Figure 8- The output flow from the diffuser in the side views and plan modeled in Cormix software (Robert, 2018).

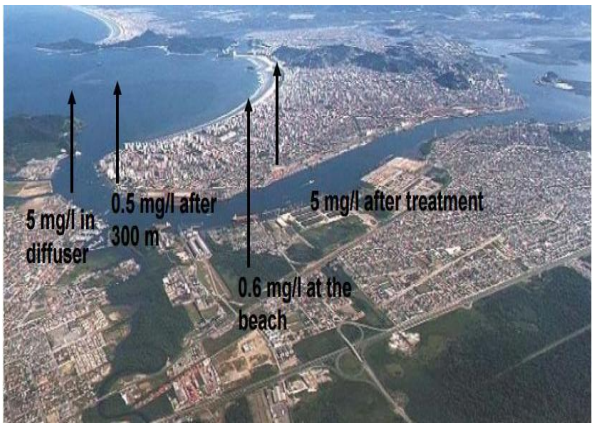

Figure 9- Areas investigated for the management of water quality protection of the effluent discharge environment (Jirka, 2003 and 2004).

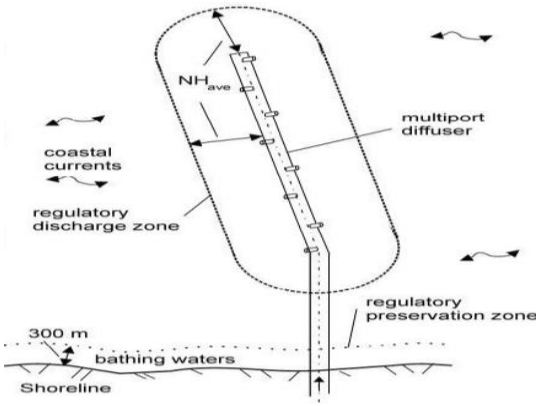

Figure 10- Proposed plan to improve the condition of the investigated areas for the management of water quality protection of the effluent discharge environment (Jirka, 2003 and 2004).

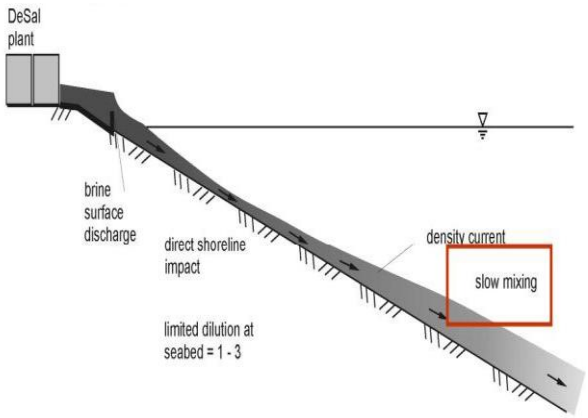

Figure 11- The effect of the output density of wastewater discharge from the RO desalination system (Jirka, 2003 and 2004).

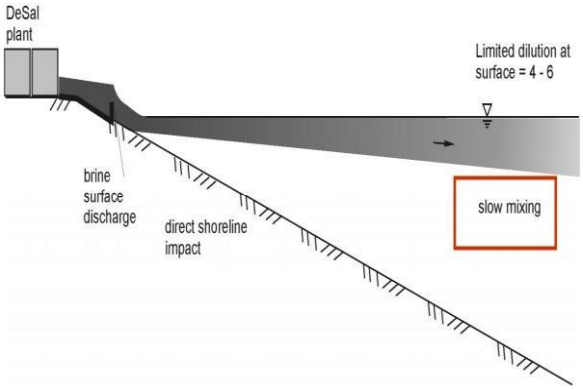

.

Figure 12- The effect of the temperature of the effluent from the thermal desalination system (Jirka, 2003 and 2004).

Figure 13- Effluent from the discharge of effluents from the surface desalination system in Ashkelon (Jirka, 2003 and 2004).

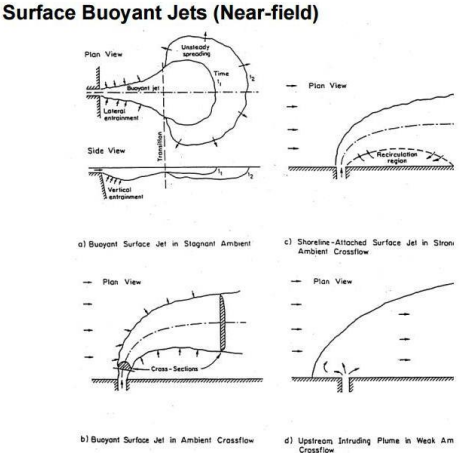

Figure 14- Effluent from the discharge of wastewater from the desalination system in the form of jet flow (Jirka, 2003 and 2004).

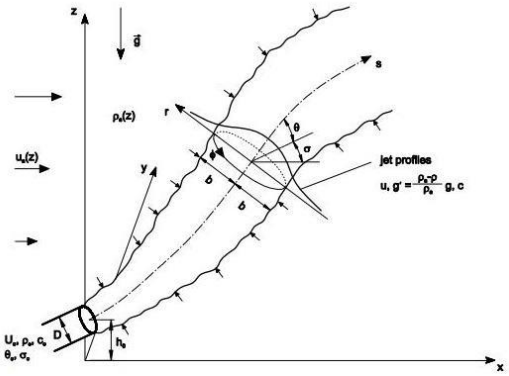

Figure 15- Effluent from the discharge of wastewater from the desalination system in the form of jet flow (Jirka, 2003 and 2004).

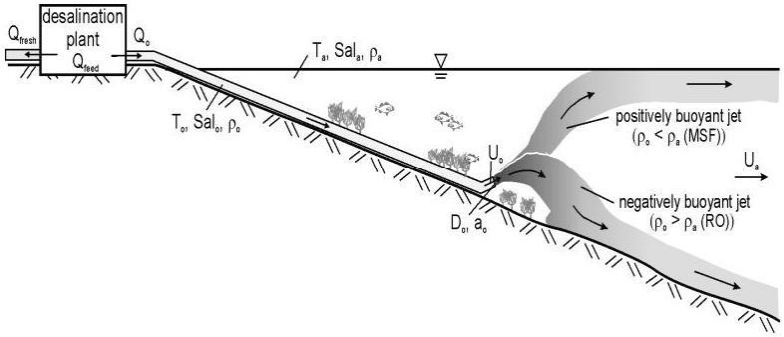

Figure 16- Effluent from the discharge of wastewater from the desalination system in the form of jet flow (Jirka, 2003 and 2004).

Figure 16- Effluent from surface water desalination system in Kuwait (Jirka, 2003 and 2004).

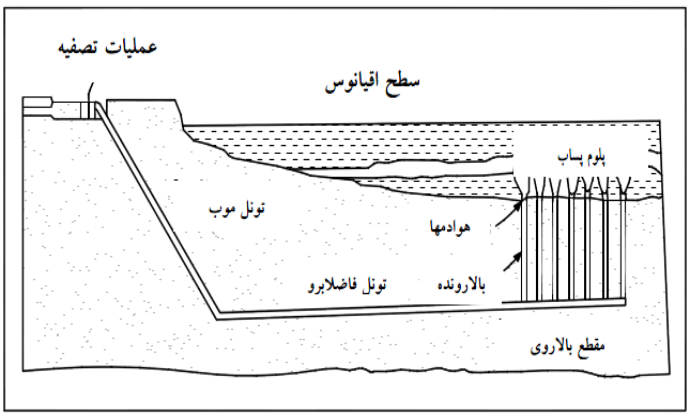

Figure 17- A type of sewage on a tunnel to discharge sewage into sea water (Takdestan et al., 2015).

(Adams, 2014) obtained the progressive equation and angular diffuser using Bernoulli's equations and momentum equation for pressure continuity along the axis of the diffuser.

S_t/S_O=1-$C_d\ M_r$ (۱)

where S_t is the minimum surface elevation for angled diffusers, C_d is the coefficient related to the influence of the stillness of the surrounding flow and M_r is the ratio of the momentum of the surrounding flow to the discharge momentum, which is calculated as follows:

$$M_r = \frac{(U_a)^2 H}{(U_O)^2 D} \quad (2)$$

In this formula, H is the discharge depth, D is the diameter of the discharge channel, Ua is the surrounding flow velocity, and Uo is the discharge velocity. So is the rate of advancement in the surrounding flow at rest, which is presented as follows by (Adams, 2014):

$$S_0 = \sqrt{\frac{H\cos\theta_0}{2B}} \quad (۳)$$

θ_0 is the angle between the channel and the sea floor, which is usually chosen less than 45 degrees.

(Subramania and Puri, 1984) proposed an exponential function based on three-dimensional experiments of a jet in a transverse flow.

(Van Su et al., 2012) obtained the constant coefficients related to the equation by fitting the experimental data as follows:

$$\frac{S_t}{S_o} = \frac{1}{1-[60\exp(-5{M_r}^{0.2})]M_r} \quad (4)$$

By replacing equation (3) in equation (4), we will have:

$$S_t = [1 - [60\exp(-5{M_r}^{0.2})]M_r]\sqrt{\frac{H\cos\theta_0}{2B}} \quad (۵)$$

First, it is necessary to define a parameter for the players. This parameter, which we denote by the letter B, is the ratio of the cross-sectional area of each of the holes of the diffuser to the distance between the holes along the length of the diffuser:

$$B = \frac{A_0}{l} \quad (۶)$$

2. Methods

One of the most important parts of the desalination site is the wastewater disposal system. The importance of this issue is due to both the environmental effects and the economic costs of the project. If the length of the sewage transmission line into the sea is calculated even if it is a few tens of meters extra, considering that the implementation of this transmission line is in the depths of the sea, it will increase the financial burden to the project owner. The rate of initial development and its characteristics play an important role in the design of wastewater disposal into the sea. It is very common to use mixing zone models for initial progressive estimation. In this study, the performance of the distance between diffusers in shallow waters is discussed using hydrodynamic relationships.

Table 1- Environmental parameters of desalinated water

$3\frac{m}{s}$	flow rate
$2\frac{m}{s}$	wind speed
40°C	ambient temperature
0.04	Weissbach Darcy coefficient near the coast
0.13	Weissbach's Darcy coefficient at the point of discharge
4%	Slope near the beach
1.2%	Slope at the discharge site
45000 $\frac{mg}{lit}$	Concentration in the environment

Table 2-The characteristics of the multi-channel desalination device

20cm	Pipe diameter
۹	The number of evacuees

Navier-Stokes equations:

$$\frac{\partial \mathrm{U_i}}{\partial \mathrm{X_i}} = 0 \quad (۷)$$

$$\frac{\partial U_i}{\partial t} + U_j \frac{\partial U_i}{\partial \mathrm{X_j}} = -\frac{1}{\rho_r}\frac{\partial P}{\partial \mathrm{X_i}} + \nu \frac{\partial^2 U_i}{\partial X_j \partial X_j} + g_i \frac{\rho - \rho_r}{\rho_r} \quad (۸)$$

$$\frac{\partial \Phi}{\partial t} + U_i \frac{\partial \Phi}{\partial \mathrm{X_i}} = \lambda \frac{\partial^2 \Phi}{\partial X_i \partial X_i} + S_\Phi \quad (۹)$$

$$\mathrm{U_i}=\overline{\mathrm{U_I}}+u_\mathrm{i} \quad ، \quad \mathrm{P}=\bar{P}+\mathrm{p} \quad ، \quad \Phi = \bar{\Phi} + \varphi \quad (۱۰)$$

$$\overline{U_I} = \frac{1}{t_2-t_1}\int_{t_1}^{t_2} U_i dt \quad , \bar{P} = \frac{1}{t_2-t_1}\int_{t_1}^{t_2} P dt \quad , \quad \bar{\Phi} = \frac{1}{t_2-t_1}\int_{t_1}^{t_2} \Phi dt \tag{1}$$

$$\frac{\partial U_i}{\partial X_i} = 0 \tag{2}$$

$$\frac{\partial U_i}{\partial t} + U_j \frac{\partial U_i}{\partial X_j} = -\frac{1}{\rho_r}\frac{\partial P}{\partial X_i} + \frac{\partial}{\partial X_j}\left(\nu \frac{\partial U_i}{\partial X_j} - \overline{u_i u_j}\right) + g_i \frac{\rho-\rho_r}{\rho_r} \tag{3}$$

$$\frac{\partial \Phi}{\partial t} + U_i \frac{\partial \Phi}{\partial X_i} = \frac{\partial}{\partial X_i}\left(\lambda \frac{\partial \Phi}{\partial X_i} - \overline{\varphi u_i}\right) + S_\Phi \tag{4}$$

$$\frac{\partial(\rho k)}{\partial t} + \mathrm{div}(\rho k U) = \mathrm{div}\left(\frac{\mu_t}{\sigma_k}\,\mathrm{grad}\, k\right) - 2\mu\, E_{ij}.E_{ij} - \rho\varepsilon \tag{5}$$

$$\frac{\partial(\rho\varepsilon)}{\partial t} + \mathrm{div}(\rho\varepsilon U) = \mathrm{div}\left(\frac{\mu_t}{\sigma_\varepsilon}\,\mathrm{grad}\,\varepsilon\right) + C_{1\varepsilon}\frac{\varepsilon}{k}2\mu\, E_{ij}.E_{ij} - C_{2\varepsilon}\,\rho\frac{\varepsilon^2}{k} \tag{6}$$

3. Numerical simulation

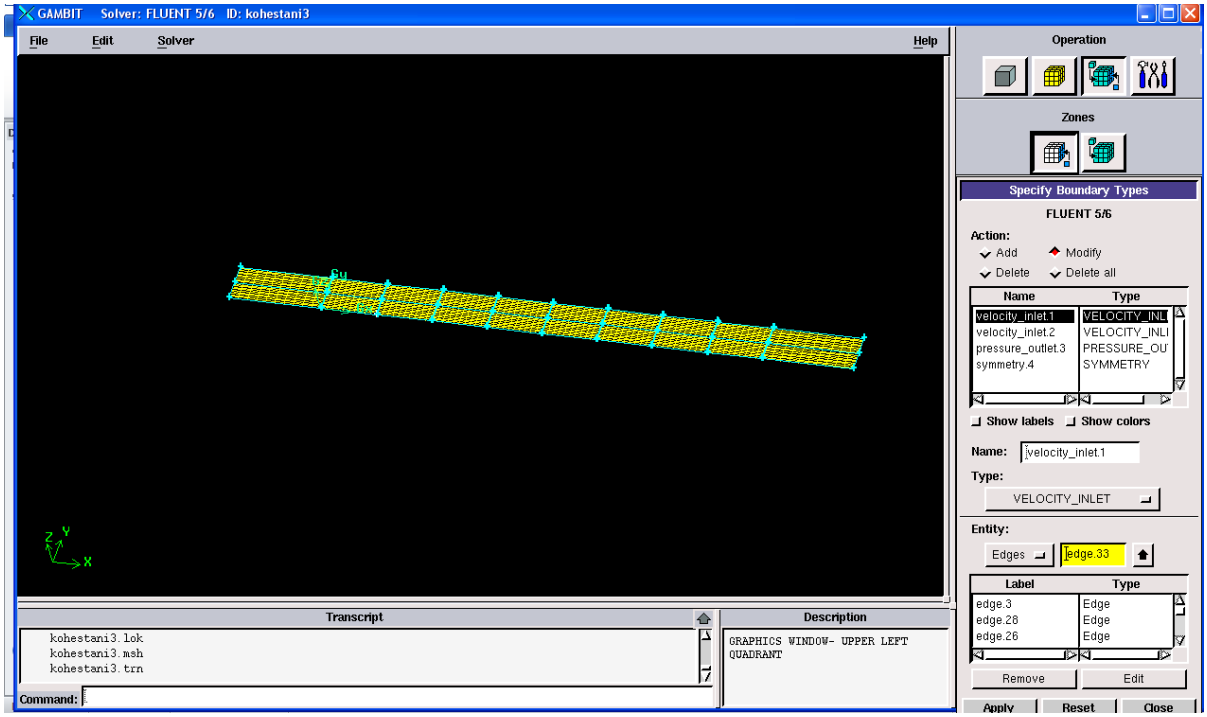

Figure 18- Meshing in Gambit software

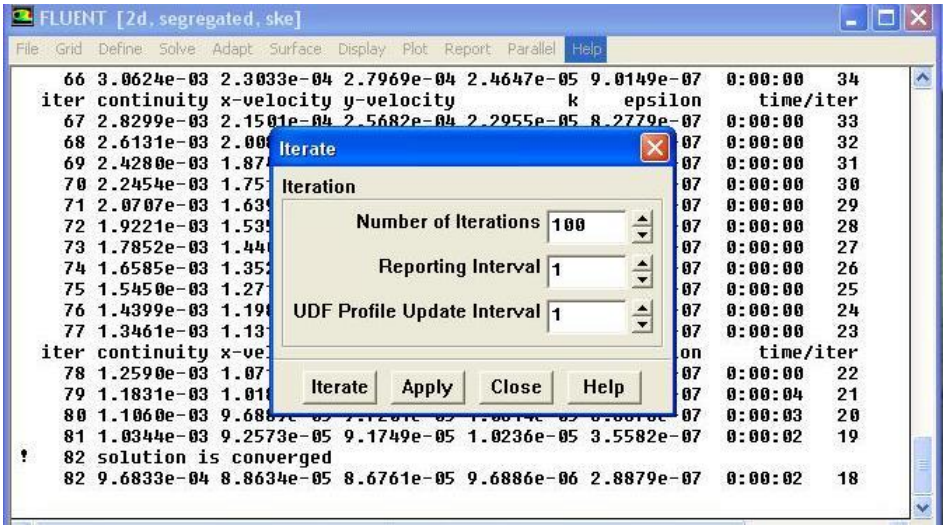

Figure 19- Solving the equations governing the flow in the Fluent environment, which reached convergence after 82 cycles.

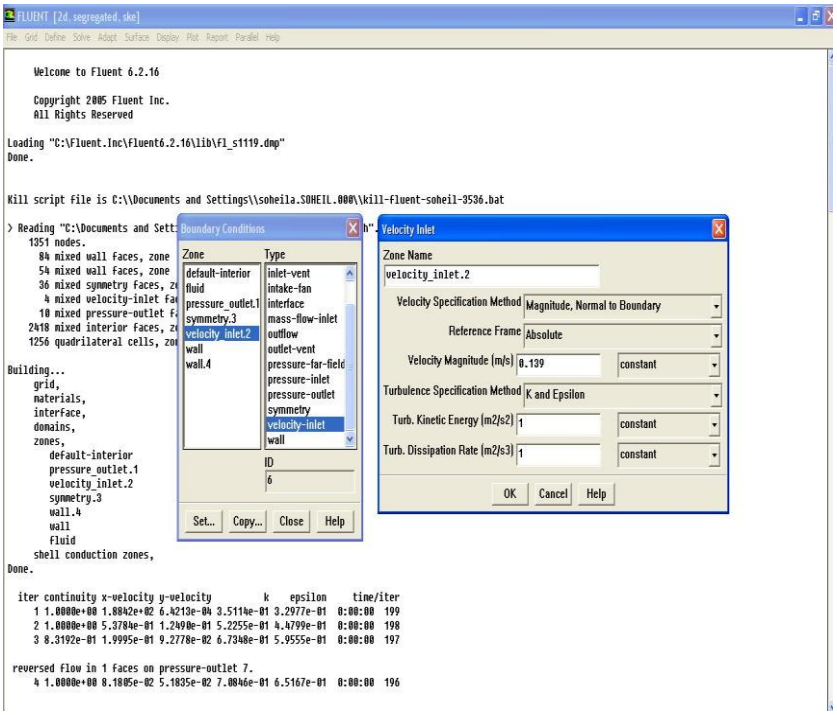

Figure 20- Applying the boundary conditions of the flow velocity in the Fluent environment

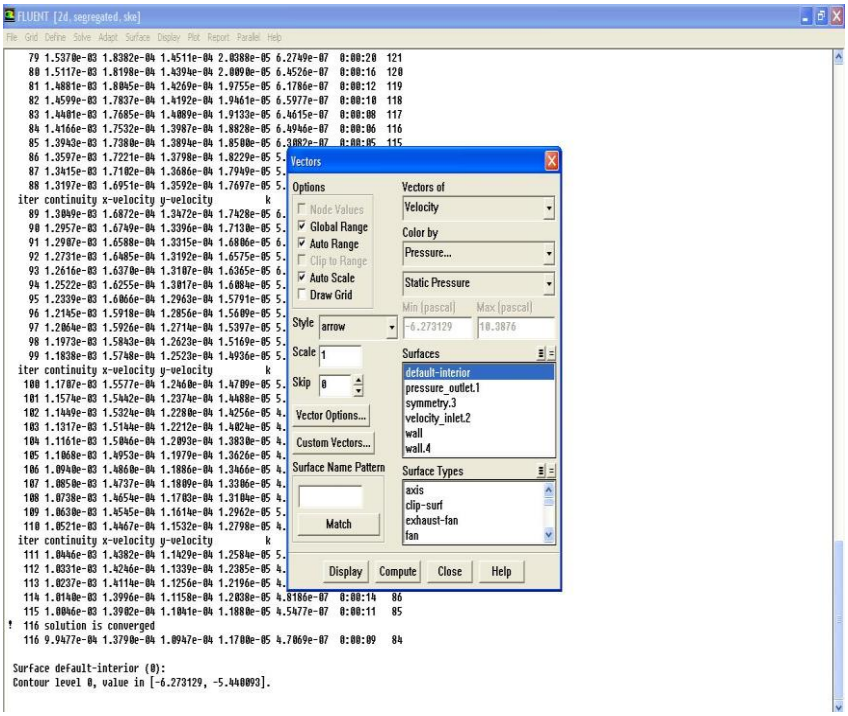

Figure 21-- Reporting the results of solving flow equations in the Fluent environment

According to the information received about the type of water softener system and the introduction of the waste disposal system resulting from it by the multi-duct drainer, considering that the diameter of the ducts is considered to be 20 cm and the distance between the drain holes is 12 meters, the value of B according to the formula (6) is equal to 0.010467. Then, according to the values of H (depth in Table 2-3) and the water velocity in the second column of Table 2-3 and the effluent discharge velocity which is obtained by dividing the effluent flow rate by the outlet cross-sectional area and the outlet diameter, the ratio of the momentum of the surrounding flow to the discharge momentum (M_r) is obtained, also the value of θ_0 is considered equal to 45 degrees. Therefore, the known values are available to find S_t. For the stated scenarios, we obtain S_t.

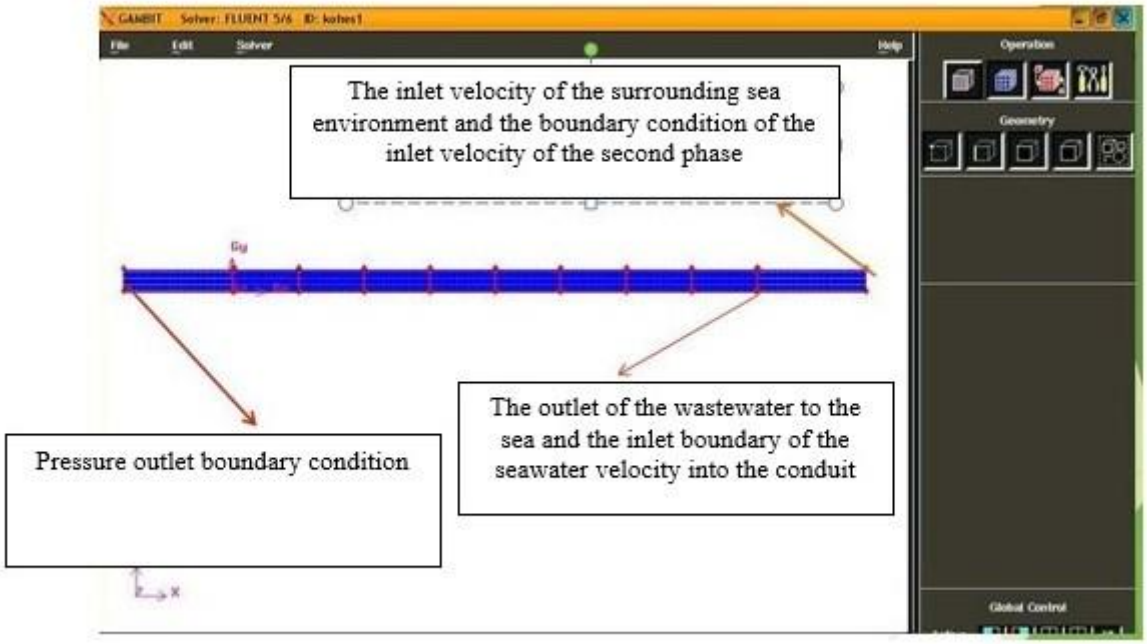

Figure 22- Networking the wastewater flow of the desalination site through the multi-channel system to the sea in Gambit environment

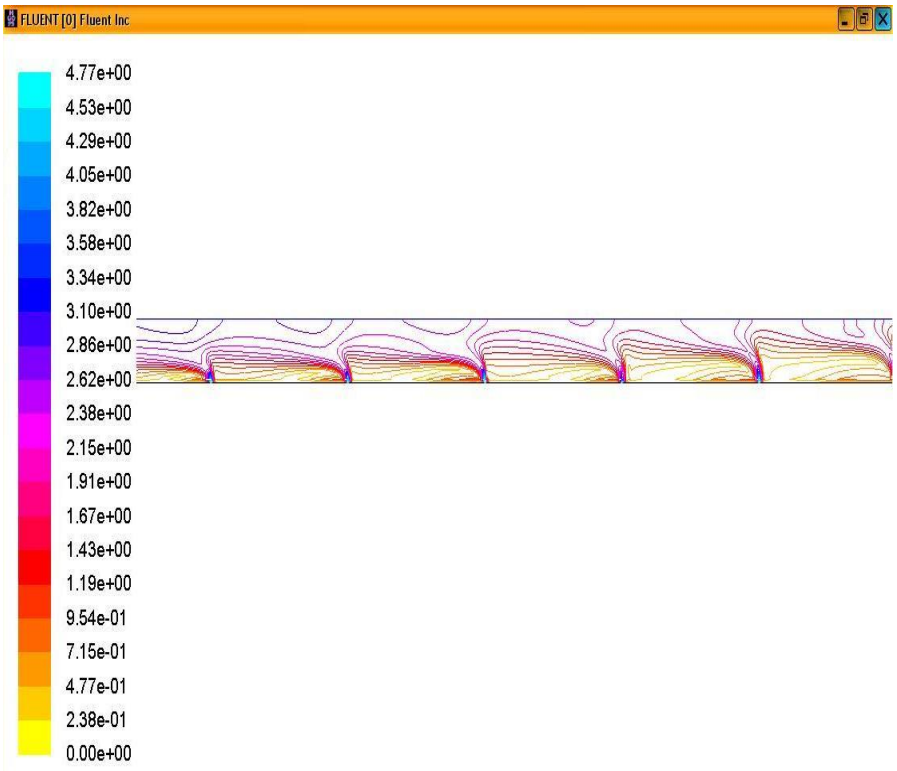

Figure 23- The shape of the iso-velocity curves as a result of the numerical simulation of the effluent flow of the desalination site through the multi-channel system to the sea. The wastewater from the desalination site enters the sea through vertical channels and is dragged to the shore due to the speed of the current. The lowest speed is in the areas between the spreaders, which shows that the promotion system works well and prevents the sewage from settling on the sea floor.

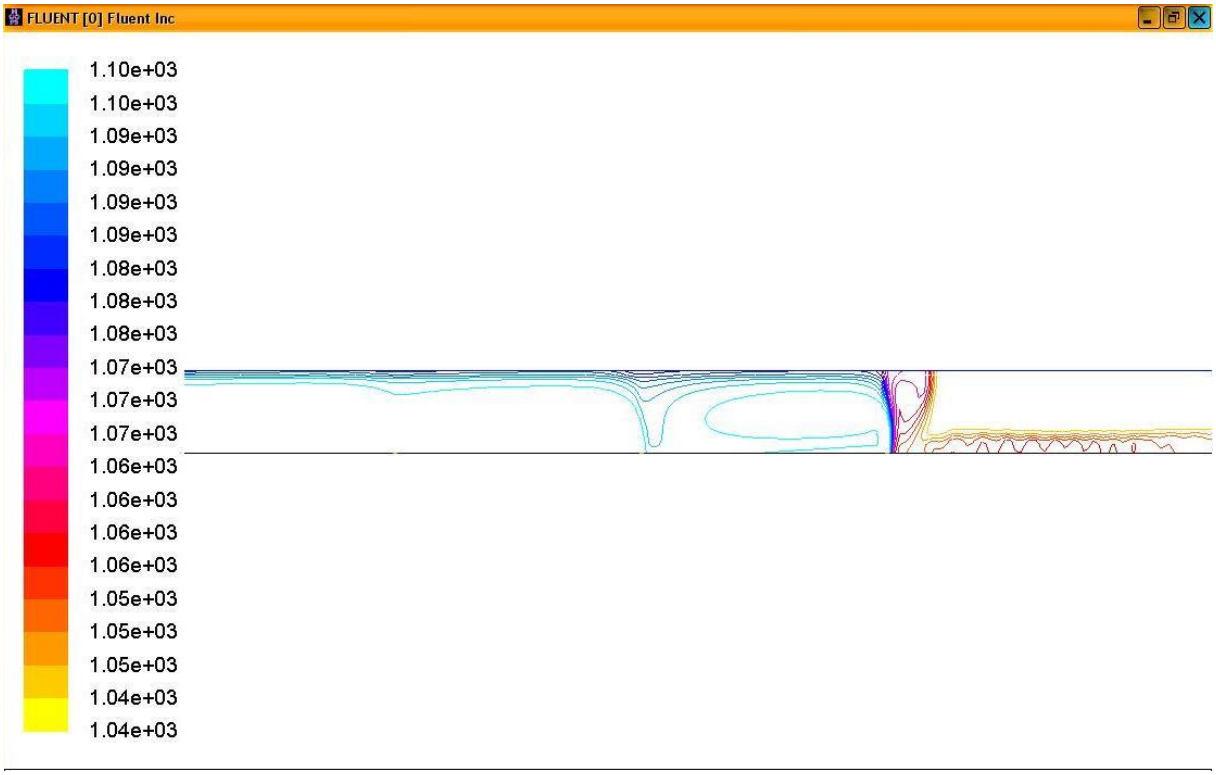

Figure 24- The shape of the density curves as a result of the numerical simulation of the effluent flow of the desalination site through the multi-channel system to the sea. The wastewater from the desalination site enters the sea through vertical channels and is dragged to the shore due to the speed of the current. The lowest density is in the areas between the spreaders, which shows that the promotion system works well and prevents the sewage from settling on the sea floor and has reduced the density of the sewage.

Results

The rate of initial development and its characteristics play an important role in the design of wastewater disposal into the sea. The initial progress depending on the water depth, opening diameter, flow velocity, distance between openings, number of dischargers and ambient water velocity were calculated in this article.

Due to the fact that salty sea water mixed with the wastewater discharged from the desalination site into the sea on the coast causes environmental damage. Using the modeling of the vertical channels for the distribution of wastewater on the sea floor, it was determined that the effluents of the desalination site enter the sea through the angled distribution channels and are drawn towards the shore due to the speed of the current. The lowest density is in the areas between the spreaders, which shows that the promotion system works well and prevents the sewage from settling on the sea floor and has reduced the density of the sewage. Also, the lowest speed is in the areas between the diffusers, which shows that the promotion system works well and prevents the sewage from settling on the sea floor.

References

1. Akram, W., M. H. Sharqawy, and J. H. Lienhard. 2013. “Energy utilization of brine from an MSF desalination plant by pressure retarded osmosis.” In Proc., IDA World Congress on Desalination and Water Reuse. Topsfield, MA: International Desalination Association.

2. Weiner, A. M., R. K. McGovern, and J. H. Lienhard. 2015. “Increasing the power density and reducing the levelized cost of electricity of a reverse electrodialysis stack through blending.” Desalination 369: 140–148.

3. Ishita Shrivastava and E. Eric Adams, M. 2019. Mixing of Tee Diffusers in Shallow Water with Crossflow: A New Look. Journal of Hydraulic Engineering . Volume 145 Issue 4 - April 2019.

4. Lee, J. H. W., and V. H. Chu. 2003. “Turbulent jets and plumes—A Lagrangian approach.” Chap. 2 in Turbulent jets, 36–37.

Dordrecht, Netherlands: Kluwer Academic Publishers.

5. Abessi, O., and Roberts, P. J. W. (2015). "Dense jet discharges in shallow water." J. Hydraul. Eng. 10.1061/(ASCE)HY.1943-7900.0001057.

6. Adams, E. E. (1982). "Dilution Analysis for Unidirectional Diffusers." J. Hydr. Div., ASCE, 108(HY3), 327-342.

7. Alden (2017). "Huntington Beach desalination facility discharge diffuser design." Alden Research Laboratory, Holden, Massachusetts. Memorandum February 23, 2017. H1.pdf.

8. Doneker, R. L. and Jirka, G. H. (2017). "CORMIX User Manual." MixZon, Portland, Oregon. Updated February 2017.

9. Cornell (2014). "Status Report 1 Outfall Redesign Study." SPDES Number NY0244741 Cornell University, Department of Energy & Sustainability, December 22, 2014.

10. Fischer, H. B., List, E. J., Koh, R. C. Y., Imberger, J., and Brooks, N. H. (1979). Mixing in Inland and Coastal Waters, Academic Press, New York.

11. Jenkins, S. A. (2017a). "Alternative Hydrodynamic Model Analysis of the Alden Designed 3-Port Duckbill Diffuser Retrofit at Huntington Beach Desalination Facility (HBDF)- Version 2." Michael Baker International. 29 November 2017. Appendix KKKK3 - Michael Baker Dilution Analysis CORMIX Model Update 2017.11.29 FINAL.pdf

12. Jenkins, S. A. (2017b). "Taylor Micro-Scale Methods for Estimating Injury and Mortality to Marine Organisms Entrained by a Diffuser at Huntington Beach Desalination Facility (HBDF). Michael Baker International. 7 December 2017. Appendix WWWW - Memo - HBDF Turbulence Impact Assessment 2017.12.07 FINAL.pdf

13. Jenkins, S. A. (2018) "Design Evolution of a Diffuser Retrofit at Huntington Beach Desalination Facility (HBDF)." Memorandum submitted to Poseidon Resources, 16 January 2018.

14. Roberts, P. J. W. (2018). "Brine Diffusers and Shear Mortality." Final Report. Prepared for Eastern Research Group, February 2018.

15. Jirka, G. (1982). "Multiport diffusers for heat disposal." J. Hydr. Div., ASCE, 108(HY12), 1425-1468.

16. Jirka, G. H., and Harleman, D. R. F. (1979). "Stability and Mixing of a Vertical Plane Buoyant Jet in Confined Depth." J. Fluid Mech., 94(2), 275-304.

17. Subramanya, K., and Porey, p.d. Trajectory of a turbulent cross. j.hydr.res 2008; Vol(22(5): 343- 345).

18. Won Seo, I.I., Kim, H.S. , Yu, D. and Kim, D.S. Performance of Tee diffusers in shallow water with cross flow. J. of Hydr Eng 2012; Vol(34: 53-61).

19. Lee, J. H., and Jirka, G. H. (1980). "Multiport diffuser as line source of momentum in shallow water." Water Resources Research, 16(4), 695-708.

20. Takdestan, Afshin; Hajizadeh, Nasser and Jafarzadeh, Nematullah. "Sewage discharge into the sea is a favorable option for urban sewage disposal in coastal areas". 7th International Conference on Coasts, Ports and Marine Structures, Ports and Shipping Organization, Tehran. 1385.
21. *Reynolds, O., 1984. On the dynamical theory of incompressible viscous fluids and the determination of the criterion. Phil. Trans. Roy. Soc. London, 123- 161.*
22. *McGurik, J.J. and Rodi, W., 1978. A depth-averaged mathematical model for the near fluid of side discharge into open- channel flow. Journal of Fluid Mechanics, 864, 761-781.*
23. *Keller, R.J. and Rodi, W., 1988. Prediction of flow characteristics in main channel/floodplain flows. Journal of Hydraulic Research, IAHR, 26(4), 425-441.*
24. *Biglari, B. and Sturm, T.W., 1998. Numerical modeling of flow around bridge abutments in compound channel. Journal of Hydraulic Engineering, ASCE, 124(2), 156-163.*
25. *Gibson, M.M. and Launder, B.E., 1978. Ground effects on pressure fluctuations in the atmospheric boundary layers. Journal of Fluid Mechanics, 86, 491-511.*
26. *Rastogi A. K. and Rodi, W., 1978. Prediction of heat and mass transfer in open channels. Journal of Hydraulics Division, ASCE, 104(3), 397- 420.*
27. *Yakhot V., Orszag S.A., Thangam, S., Gatski, T.B. and speziale, C.G., 1992. Development of turbulence models for shear flows by a double expansion technique. Physics of Fluids A, Vol. 4, No. 7, pp1510-1520.*
28. *Wilcox D.C., 1988. Re-assessment of the scale-determining equation for advanced turbulence models. AIAA Journal, vol. 26, pp. 1414- 1421.*
29. *Versteeg, H.K. and Malalasekera, W., 2007. An Introduction to Computational Fluid Dynamics: The Finite Volume Method, Prentice Hall, Feb 16, 503 pages.*
30. *Soltani, M.V. and Rahimi Asl, R., 2003. Computational fluid dynamics by Fluent software, Tehran, Tarrah issues.*
31. Fluent 6.2 User's Guide, Janurary 2005.
32. Gambit 2.2 User's Guide, September 2004.

INTERNATIONAL JOURNAL OF
COASTAL & OFFSHORE ENGINEERING
IJCOE Vol.10/No. 1/Winter 2025 (35-39)

Available online at: www. Ijcoe.org

The prediction of wind-induced waves in Hormuz Strait using the SWAN numerical model

Mahmud Reza Abbasi[1], Ali Sheykhbahaei[2] *

[1] *Faculty of Basic Sciences, Imam Khamenei University of Marine Sciences, P.O.Box 43491-63439, Zibakonar, Gilan, Iran, phys.ocean.abbasi@gmail.com*

[2*] *PhD candidate in Physical Oceanography at University of Hormozgan and Iranian National Institute of Oceanography and Atmospheric Science, Tehran, Iran, Ali.Sheykhbahaei@inio.ac.ir*

ARTICLE INFO

Article History:
Received: 5 Dec 2019
Accepted: 15 Jun 2025

Keywords:
wave
predication
swan
Hormuz Strait

ABSTRACT

Nowadays, sea operations require accurate prediction of the characteristics of the waves in the coastal and offshore areas. For modeling wave characteristics, there are various methods such as empirical methods, numerical methods and soft computing methods. In this research, the SWAN numerical model for modeling of wave characteristics in Hormuz Strait area was used. First, a global model for modeling the characteristics of the waves in the Persian Gulf domain was built. Then, the boundary condition obtained from the global model for local modeling with a larger resolution in the area of Hormuz Strait was used. The local model constructed in the Hormuz Strait area was calibrated using the recorded waveforms of the buoy deployed in that area and then was validated. Comparison of the results with the measured data of the Hormuz Strait buoy shows that the modeling has been carried out in this area has very precision results.

1. Introduction

For the design of inshore and offshore structures and for marine operations, prediction of the characteristics of the waves is required. For modeling and prediction of waves' characteristic, empirical, numerical and soft computation methods can be used.

Experimental methods base on coastal engineering manual [1], shore protection manual [2] and SMB [3] are relatively simple and low cost methods that are developed on the basis of specific conditions and in a particular region. Therefore, they are not very accurate in other areas. In comparison with experimental methods, numerical models have a much higher accuracy. Examples of numerical models are: WAVEWATCH III [4], SWAN [5], WAM [6] and Mike 21 [7].

Soft computing tools such as artificial neural network, regression decision tree, genetic algorithm and fuzzy inference system are other ways to predict the characteristics of the waves, but in a specific area.

So far, various studies have been done on the use of numerical models to predict wave characteristics. Moeini [8,9], Rogers [10], Signell [11], Caliskan [12], Rusu [13] and Bolaños-Sanchez [14] are some example of these researchers.

In this study, SWAN's numerical model was used to predict wave characteristics in Hormuz Strait. Became Considering the importance of the Hormuz Strait area, accurate and accurate modeling of wave characteristics is very important.

2. Materials and Methods

2.1. Study area

The Persian Gulf with about 900 km length and 240,000 km^2 is the third largest gulf in the world. It is one of the most important geo-economical and geo-political water body in the world. The Hormuz Strait connected the Persian Gulf to the open seas. In every one hour approximately 10 ships pass through this

narrow waterway in which this strait is a rash shipping line [15].

2.2. Required data

The data used in this modeling include the wave information recorded by the Hormuz Strait buoy. This Buoy is deployed Hormuz Strait by the consultant engineering corporation in this area and its information is available in 1-hour time series of wave information. Location of this buoy is at 55.55 degrees east and 26.31 degrees north.

Other data used which are essential as input in SWAN model are the bathymetry data and wind speed. The bathymetry data is a rectangular grid with a resolution of sixtieth degrees.

The wind speed used in this modeling has been modified by the ECMWF database, which has a magnitude of 0.2 degrees and 6 Hour interval. The correction of ECMWF wind data in coastal areas was carried out by the data measured by synoptic stations

2.3. SWAN numerical model

The SWAN model is one of the third-generation numerical models. The SWAN Cycle III version 40.72 was used in this study. It was developed by Delft University of Technology in 2009. This model is an available and freely accessible that is widely used by researchers and engineers for research and consulting.

The SWAN model solves the spectral action balance equation without any predetermined condition on the spectrum for the evolution of wave growth. In the SWAN model, waves are described by the two-dimensional spectrum of the wave-action density, in which the growth of the action density, N, is determined by the time-dependent wave action balance equation that in the Cartesian coordinates as follows:

$$\frac{\partial N}{\partial t}+(\overrightarrow{C_g}+\vec{U}).\nabla N+\frac{\partial C_\sigma N}{\partial \sigma}+\frac{\partial C_\theta N}{\partial \theta}=\frac{S_{tot}}{\sigma} \quad (1)$$

The first sentence in the equation 1 shows the rate of change in the action density. The second term indicates the wave energy propagation in a two-dimensional geographic space where C_g Wave group speed and U is the lateral limited current. This statement can be restored in the Cartesian, spherical or curvilinear coordinate. The third sentence shows the relative frequency shifting effect due to variations in depth and currents. The fourth expression reflects the refraction from the depth or current. The quantities C_σ and C_Θ are the propagation speeds in the spectral space (σ, θ), which σ shows the relative frequency and θ for propagation direction. The S_{tot} parameter is the source term in terms of energy shown in the Eq.(2):

$$S_{tot}=S_{wind}+S_{nl3}+S_{nl4}+S_{wc}+S_{bot}+S_{db} \quad (2)$$

The right parameters of the above equation are, respectively, the energy input by the wind (linear or exponential growth by wind), the nonlinear energy transfer of the wave under triple and Quadruple interactions, wave deformation due to white capping, bottom friction, and depth-induced wave breaking.

The specification of the model used includes a uniform and rectangular computational spatial grid which magnification for the overall model is 0.1 degrees (about 10 Km) and for the local model is 0.01 degrees. The grid spectrum is divided into an angular grid and a frequency grid.

An angular grid is considered as a full circle with 18 sectors, and the frequency grid is composed of a frequency of 0.8 to 1 and includes 20 parts with logarithmic distribution is divided. Figure 1 shows the position of global and local models for modeling the waves profile in the Hormuz Strait.

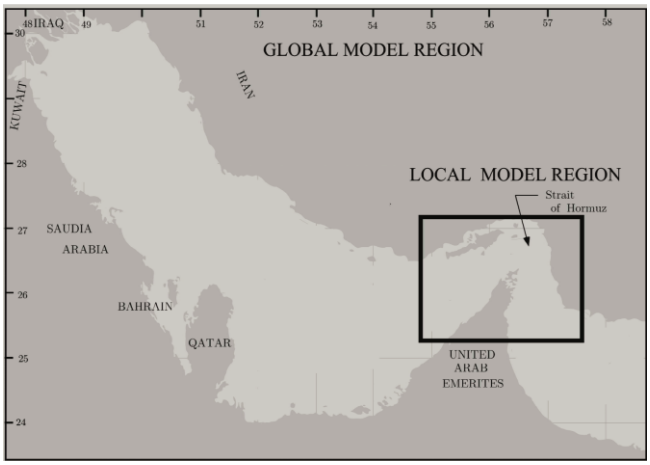

Figure 1. Global and local model domain

Local modeling was carried out after global modeling and the local model boundary conditions were extracted from global model, which was given in the next step.

3. Results and Discussion

The model should be calibrated for a period of time to reduce the difference in results with measured values. Calibration and validation durations in Hormuz Strait, from July 17 to August 17and August 20-31, 2018 was considered, respectively. The time series of wind and wave data is shown in figures 2 to 11.

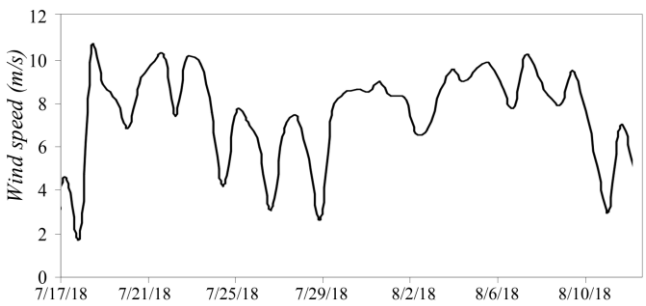

Figure 2. ECMWF wind speed time series in calibration period

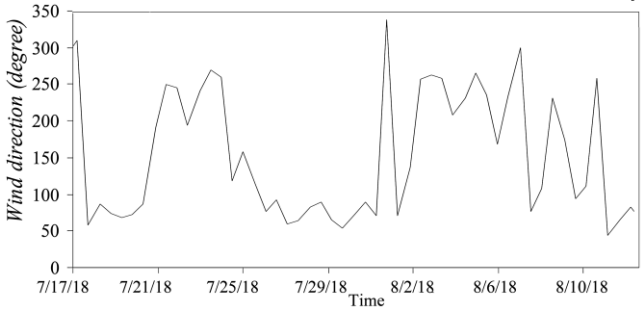

Figure 3. ECMWF wind direction time series in calibration period

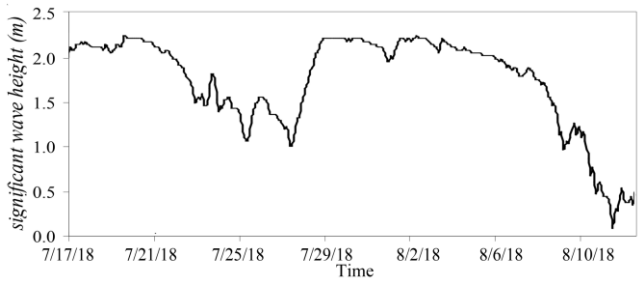

Figure 4. significant wave height time series in calibration period

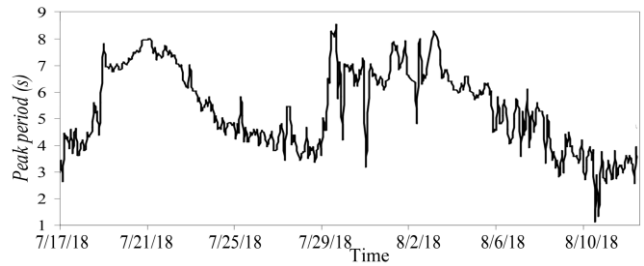

Figure 5. peak period time series in calibration period

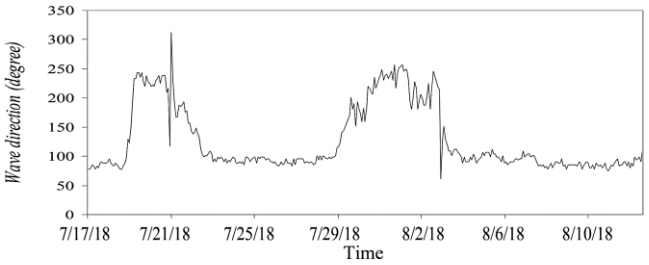

Figure 6. wave direction time series in calibration period

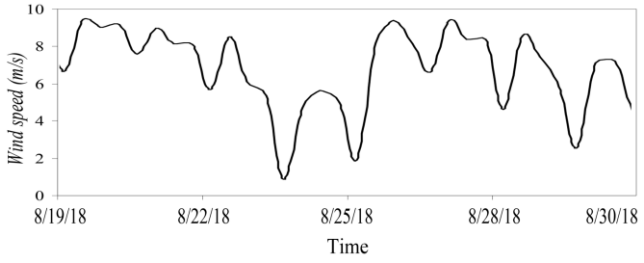

Figure 7. ECMWF wind speed time series in verification period

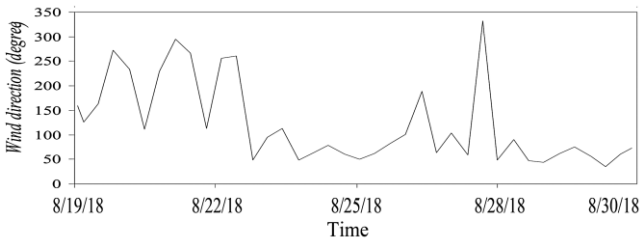

Figure 8. ECMWF wind direction time series in calibration period

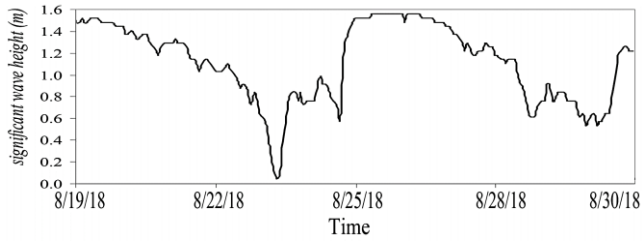

Figure 9. significant wave height time series in verification period

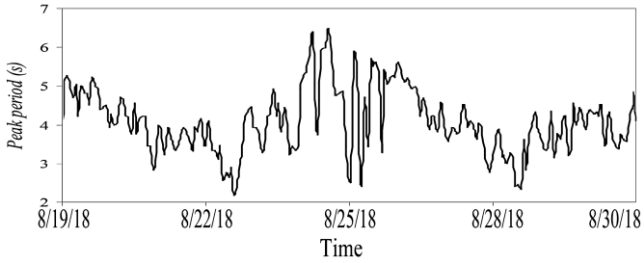

Figure 10. peak period time series in verification period

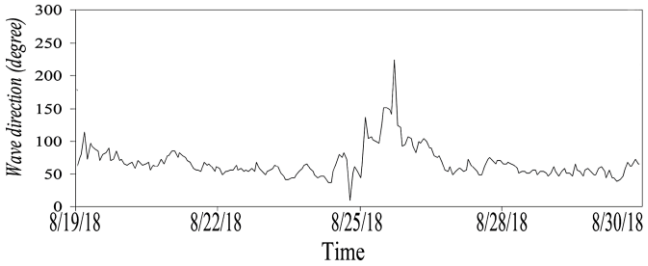

Figure 11. wave direction time series in verification period

Figures 2, 4 and 5 show that the trend of wind speed variations, significant wave height and wave peak period are roughly the same. Figure 3 shows the dominant wind direction is between 50 to 320 degrees and figure 6 shows a dominant wind of about 80 degrees.

Figures 7, 9, and 10 show similar trends for wind speed, significant wave height, and peak period. Figure 8 shows the dominant wind direction blowing is between 50 and 250 degrees and figure 11 shows a dominant wave of about 50 degrees (similar to the calibration period).

Tables 1 and 2 also show wind and wave statistics in calibration and validation periods, respectively.

Table 1. wind and wave characters in calibration period

Parameter	Min	Mean	Max	SD[1]
significant wave height	0.03	0.65	2.1	0.58
peak period	1.52	3.8	8.28	1.13
Wave direction	150	250	300	28.12
Wind speed	2	4	10	3.11
Wind direction	100	270	320	85.3

Table 1. wind and wave characters in verification period

Parameter	Min	Mean	Max	SD
significant wave height	0.03	0.45	1.8	0.49
peak period	1.62	3.2	7.88	1.01
Wave direction	200	250	300	19.23
Wind speed	2	4	10	2.57
Wind direction	50	200	300	78.9

3.1. Model Calibration

To calibrate the model, the variations of the coefficients of the whitecapping, wave breaking and sea bottom friction are used. In this modeling, sensitivity analysis indicates that the changing in whitecapping coefficient has the most effect on the accuracy of the results. Therefore, this coefficient was used for model calibration. The model was calibrated for the corresponding time period and the calibration results of the model are shown in figures 12 and 13.

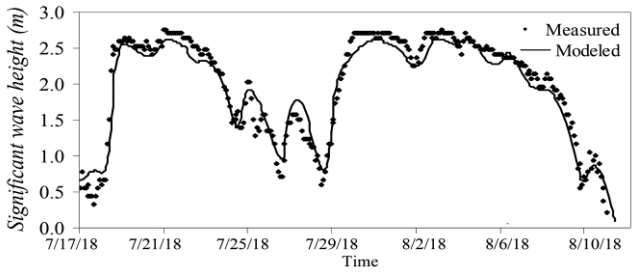

Figure 12. model and measurements significant wave height time series in calibration period

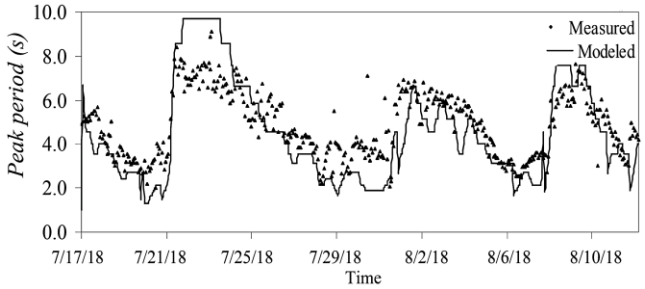

Figure 13. model and measurements peak period time series in calibration period

As shown in figures 12 and 13, the time series of the wave characteristics of the model is well suited to the time series of the measured wave specification.

To investigate the accuracy of the results, the bias, correlation coefficient(CC), root mean square error(RMSE) and the Scatter Index (SI) are calculated in accordance with relations 3 to 6 and are shown in table 3.

$$Bias = \bar{x} - \bar{y} \tag{3}$$

$$CC = \frac{\sum_i (x_i - \bar{x}) \times (y_i - \bar{y})}{\sqrt{\sum_i (x_i - \bar{x})^2 \times \sum_i (y_i - \bar{y})^2}} \tag{4}$$

$$RMSE = \sqrt{\frac{\sum_i (x_i - y_i)^2}{n}} \tag{5}$$

$$SI = \frac{\sqrt{\frac{1}{n}\sum_i (x_i - y_i)^2}}{\bar{x}} \tag{6}$$

Table 2. Error index in calibration period

Error index	Significant wave height	Peak period
Bias	-0.05	-0.26
CC	0.8	0.65
RMSE	0.13	1.10
SI	28	22

Low bias, root mean square error and dispersion index and good correlation coefficient also shows the high accuracy of modeling done in the Hormuz Strait region.

3.2. Model verification

The results of the model validation for the respective period are shown in figures 14 and 15.

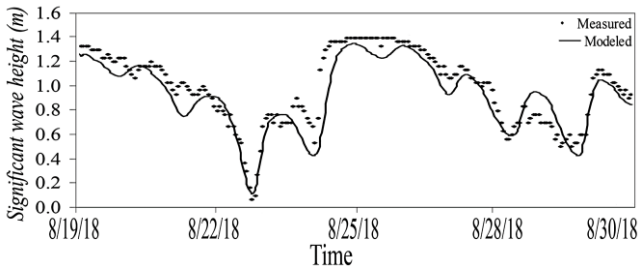

Figure 14. model and measurements significant wave height time series in verification period

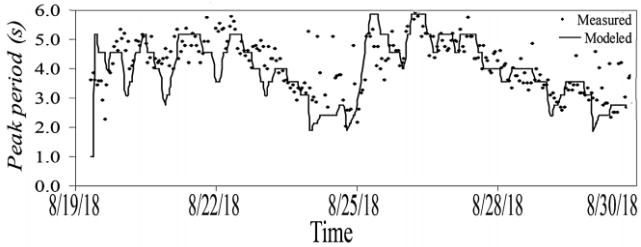

Figure 15. model and measurements peak period time series in verification period

Figures 14 and 15 show the time series matching of modeling and measured wave characteristics.

[1] Standard Deviation

Calculated error indicators for the verification period are shown in table 4.

Table 3. Error index in verification period

Error index	Significant wave height	Peak period
Bias	-0.015	-0.25
CC	0.83	0.88
RMSE	0.11	1.20
SI	18.55	25.13

The calculated error indices in the verification period also show the acceptable accuracy of modeling in the Hormuz Strait by the SWAN model.

Therefore, the constructed model can be used to predict the significant wave height and the peak period in the Hormuz Strait.

4. Conclusions

In this research, the prediction of wave characteristics in the Hormuz Strait was carried out using the SWAN numerical model. Model inputs include ECMWF wind field data and bathymetry. The model was first calibrated for a 19-day period, and then verified for the 13-day period. The verification results of the model showed that the results of the calibrated model have good precision.

5. References

1- US Army., (2003). *Coastal Engineering Manual, Chapter II-2, Meteorology and Wave Climate, Engineer Manual*. 1110-2-1100. U.S. Army Corps of Engineers, Washington, DC.

2- US Army., (1984), *Shore Protection Manual*. 4th ed. 2 vols. U.S. Army Engineer Waterways Experiment Station, U.S. Government Printing Office, Washington, DC.

3- Sverdrup, H. U., and Munk, W. H., (1947), *Wind sea and swell: theory of relations for forecasting*. Publication 601, U.S. Navy Hydrographic office, Washington, DC.

4- Tolman, H. L., (1991), *A third-generation model for wind waves on slowly varying, unsteady and inhomogeneous depths and currents*. Journal of Physical Oceanography 21,p.782-797.

5- Booij, N., Ris, R. C., and Holthuijsen, L. H., (1999), *A third-generation wave model for coastal regions. 1. Model Description and validation*. Journal of Geophysical Research 104, p.7649-7666.

6- Komen, G. J., Cavaleri, L., Donelan, M., Hasselmann, K., Hasselmann, S., and Janssen, P.A.E.M., (1994), *Dynamics and modeling of ocean waves*. Cambridge University Press.

7- DHI Water & Environment, 2004. *MIKE 21 spectral wave module*. Scientific documentation.

8- Moeini, M. H., Etemad-Shahidi, A., and Chegini, V., (2010), *Wave modeling and extreme value analysis off the northern coast of the Persian Gulf*. Applied Ocean Research 32, p.209-218.

9- Moeini, M. H., and Etemad-Shahidi, A., (2007), *Application of two numerical models for wave hindcasting in Lake Erie*. Applied Ocean Research 29, p.137-145.

10- Rogers, W. E., Kaihatu, J. M., Hsu, L., Jensen, R. E., Dykes, J. D., and Holland, K. T., (2007), *Forecasting and hindcasting waves with the SWAN model in the Southern California Bight*. Coastal Engineering 54,p.1-15.

11- Signell, R. P., Carniel, S., Cavaleri, L., Chiggiato, J., Doyle, J., Pullen, J., and Sclavo, M., (2005), *Assessment of wind quality for oceanographic modelling in semi-enclosed basins*. Journal of Marine Systems 53, p.217-33.

12- Caliskan, h., Valle-Levinson, A., (2008). *Wind-wave transformation in an elongated bay*. Continental shelf research 28,p.1702-1710.

13- Rusu, E., Pilar, P., Guedes Soares, C., (2008), *Evaluation of the wave conditions in Madeira Archipelago with spectral models*. Ocean Engineering 35, p.1357-1371.

14- Bolaños-Sanchez, R., Sanchez-Arcilla, A., Cateura, J., (2007), *Evaluation of two atmospheric models or wind–wave modeling in the NW Mediterranean*. Journal of Marine Systems 65, p.336-353.

15- Al-Hajri, K. R., Chao, S. Y. and Kao T. W., (1997), *Circulation of the Persian Gulf: A threedimensional study*. The Arabian Journal for Science and Engineering 22,1B, p. 105-128.

INTERNATIONAL JOURNAL OF
COASTAL, OFFSHORE & ENVIRONMENTAL ENGINEERING IJCOE Vol.10/No. 1/ Winter 2025 (40-49)

Available online at: www. Ijcoe.org

Zoning and Flood Management in Coastal Areas (Case Study: The Coasts of Hormozgan Province)

Parvaneh Sobhani[*1], Mahyar Majidi Nik[2]

[1*] *Corresponding author, Department of Environmental Science, Natural Resources Faculty, Lorestan University, Khorramabad, Iran. (Researcher of the Madde Danesh Studies Center); sobhani.pa@lu.ac.ir.*

[2] *Ph.D. student of oceanography, Researcher of the Department of Environmental Geography Studies, Madde Danesh Studies Center; majidynik@yahoo.com*

ARTICLE INFO

Article History:
Received: 10 July 2024
Accepted :15 Jan 2025

Keywords:
Flood, Flood zoning, Sentil-1 satellite images, Coasts, Hormozgan province

ABSTRACT

The dangers of floods worldwide have caused this environmental event to be called one of the major natural disasters. Today, remote sensing data with accuracy and low cost play a critical role in identifying flood-prone areas and flood zoning in coastal management. In the present study, the flooded and flood-prone areas on the coasts of Hormozgan province were investigated according to the intensity of the rainfall system in the last days of April 2024 by using the GRDH images of Sentinel-1 satellite and the Otsu thresholding method. The results revealed that the area and percentage of flooded zones on April 17 occupied the largest area (28.15 km2) of the coastal surface and the highest average rainfall was also related to the same date with an average of 35.05 mm. The greatest extent of changes in flood zones is also on the coastline and near the border of the region, which indicates the high sensitivity and susceptibility of the coastal areas to flooding in this region. According to the obtained results, about 1448.36 km2 of the surface area is affected by flood zones, and the largest area is assigned to the high risk category with an area of 669.30 km2. According to the obtained results, it is possible to manage and control floods spatially and temporally on the coasts and prevent the consequences. Therefore, in the field of coastal flood management, it is necessary to pay attention to flood control methods, a suitable model to improve water supply sources and improve water security for drinking and health purposes, as well as appropriate bioengineering methods to stabilize soil and control erosion.

1. Introduction

In the 21st century, due to climate change and global warming, the increased possibility of flood risk has provided major concerns. Flooding is one of the major natural hazards in the world that affects a large population every year [9], especially in coastal areas that are vulnerable to climate and human hazards [2,5,17]. According to the surveys, 80% of the casualties caused by floods occur within 100 km of the coast [8].

Among the management measures that can play an important role in reducing flood damage and coastal management is the preparation of a flood zoning map [11]. To prevent the occurrence of floods and to contain them, the areas that have a high potential for flooding must be identified and then the factors of flood occurrence should be investigated. Moreover, the study and implementation of flood control and management methods before its occurrence is very important [15]. Considering that the extent of flood damage depends on the geometric characteristics of the stream bed and also the adjacent lands, therefore, flood risk zoning for different return periods is important. For this purpose, it is necessary to predict damage levels caused by floods in different conditions and to justify the economic and social flood control and management programs [14].

Today, deltas and coastal areas have a significant share in the world population and the population density in these places is increasing day by day [26, 22]. However, the coasts are affected by the consequences of environmental hazards that are related to sea level fluctuations, and the risks of coastal flooding are more threatening. This problem has made it necessary to monitor the flood plains and each part of the basin has a certain potential to produce runoff and flood [10]. Flood potential zoning is a method that zones the basin based on flood potential by considering the amount of runoff production in each section. In addition to reducing the effects and consequences of floods, this

method provides valuable information about the surrounding environment, floods and their effects on floodplain lands and determining river boundaries [23]. Therefore, it is very important to know the flood-prone areas to control the damages caused by it, store the runoff, and increase the underground water reserves. In this regard, it is possible to identify flood-prone areas by using advanced spatial methods and use its results in coastal management planning [1]. Due to the importance of this issue and the reduction of human and financial losses caused by floods, several studies have been conducted in this field, which can be referred to the study of Doust & Shamsnia [4], in the identification and zoning of flood-prone areas using the GIS- AHP model in Bushehr province. The obtained results showed that more than 50% of the area of the region has a medium to high flood potential risk, so these areas must be the focus of urban management planning. Tabrizi et al. [23], also investigated flood zoning for use in determining the sanctuary of the Tail River. As the results indicated, the integration of HEC_RAS model and GIS geographic system is an efficient and useful tool in identifying and zoning river floods. According to the investigations and the comparison of existing maps and uses around the Tail river, in case of a flood with a return period of 25 years, there will not be much damage to these areas. In another study, Soleimani & Mohseni [20], investigated and zoned flood risk in Mazandaran province (Babelroud watershed) using GIS software. The obtained results indicate that part of the basin is affected by the risk of flooding with a very high potential, which is mainly located downstream and leading to the sea at the outlet of the basin. Sasanpour & Mohebi [16], investigated and analyzed flood risk zoning in Taleghan watershed. According to the results, 83% of the total basin area includes safe and low risk areas. While 17% of its lands have a medium and high risk of flooding, which includes areas around the main waterway and secondary waterways with residential and agricultural uses in the basin. Therefore, the need to respect the privacy of the Taleghan River in low-lying lands with a low and medium slope, in the development of urban and rural uses in the region, to reduce the damage caused by floods, should be implemented.

According to the studies, flood zoning is one of the most important management and flood control measures in flood prone areas. However, coastal areas, which are increasingly exposed to the threat of floods due to climate change, lack comprehensive studies that deal with flood control and management in these areas. Therefore, in response to this scientific limitation, in the present study, flood zoning and management were discussed in the coasts of Hormozgan province located in the south of Iran. The southern coasts of Iran on the shores of the Oman Sea and the Persian Gulf are affected by tropical storms and waves with high intensity and height. Along the coastlines, especially in the central and eastern regions, the waves caused by these storms have led to the formation of a dominant wave, which causes the coastal areas to be flooded [10]. Due to the flood on April 17, 2024, communication routes from Khamir to Lengeh port have been blocked. In addition, the consequences of the flood have blocked the road from Bashagard city to Jask and caused damage in Minab city. Therefore, flood zoning and management using remote sensing and GIS techniques is essential in these areas. Likewise, the results of this study can help to manage and control floods in coastal areas.

2. Study Area

In this study, the coastal areas of Hormozgan province along the Oman Sea and Persian Gulf were investigated and analyzed. This area is located with an area of 7,124,690 ha between the northern latitude 52 ° 44 ' 26 " to 59 ° 14 ' 27 " and the eastern longitude 25 ° 24 ' 46 " to 28 ° 53 ' 55 ". In terms of climate, it has a hot desert climate and the average annual rainfall in this area is 139.4 mm. January is the rainiest month of the year (56.8 mm) and in contrast, May is the month without rain or the least rainy month in this area. This area has an average temperature of 26.8 C0, which is the hottest and coldest months of the year, respectively, August with an average temperature of 34.21 C0 and January with an average temperature of 18.44 C0 [12]. Despite the dry weather conditions of the province, no season is without rain due to the activity of monsoon low-pressure systems and their effect on Hormozgan province in the year's hot season. As expected, the highest amount of rainfall occurs in January, February and March and the lowest amount of rainfall occurs in July, August and September [21]. Figure. 1 displays th

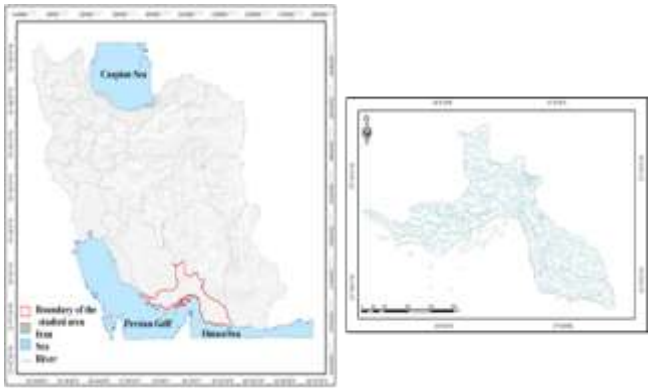

Figure. 1. Location of the studied areae location of the studied area.

3. Materials and methods

3.1 Methodology

In this study, GRDH images of Sentinel-1 satellite were used for flood zoning. The lack of need for light sources and the ability to take pictures 24 hours a day and in any weather conditions have led researchers all over the world to use these images as an efficient tool in flood

investigation [25]. The Sentinel-1 satellite belongs to the European Union Space Agency (ESA) and is placed in the Earth's orbit as part of the Copernicus program. This satellite includes two sensors, A1 and B1, which provide users with radar images in a period of 6 days [24]. Therefore, in the present study, to identify and zone the flooded areas, GRDH radar images of Sentinel-1 satellite were prepared with a spatial resolution of 10 m (Table 1). In the following, using the Otsu thresholding method, the flooded areas were separated from other complications. Data related to average daily precipitation was also obtained from the power.larc.nasa.gov website. In addition, MATLAB Otsu was used for thresholding and Arc GIS 10.8 was also used to prepare maps. Figure. 2 shows the diagram of the preparation process for the flood zoning map process in the region. Flood-prone areas in the study area were identified by determining the difference in redistribution coefficient (Gamma $\gamma 0$) between water and land and using Otsu's thresholding algorithm [13]. The limits of the determined threshold for the examined images can be seen in Table 1. In thresholding methods, the histogram of each image is divided into two parts according to the amount of gray composition. The greater the intensity of the grayness of the pixel (i.e. the pixels tend to be darker) indicates the blue area and vice versa, the pixels with a light gray tone (i.e. Pixels tend to white) indicate the land area (land). The most important feature of Otsu's method is the automatic thresholding of images. In this method, the threshold limit is determined based on the minimum intra-class variance and the maximum inter-class variance.

Table 1. Characteristics of radar images and threshold limits determined in the study

Row	Image date	Image mode	Image type	PASS	Polarization	Otsu's set threshold limit
1	2024/04/16	IW	GRDH	Ascending	VV	-16.11
2	2024/04/17	IW	GRDH	Ascending	VV	-16.36
3	2024/04/18	IW	GRDH	Descending	VV	-16.23

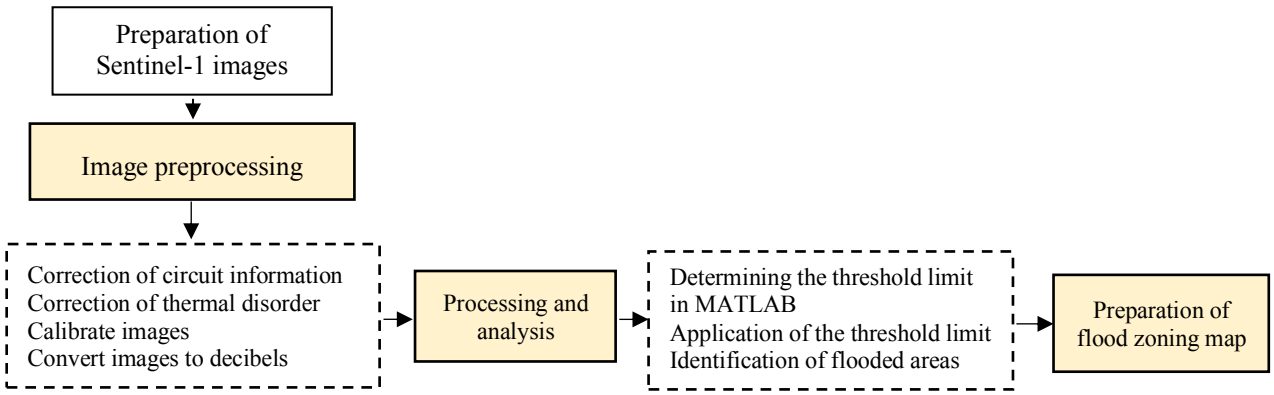

Figure 2. Diagram of the process of preparing flood zoning map in the studied area

4. Results and Discussion

4.1 Investigating flood areas and rainfall in the region

The obtained results indicate that the area and percentage of the flooded areas on April 16 occupied the largest area of the coast (28.15 km2) and the highest average rainfall was also related to the same date with an average of 35.05 mm. Table 2 displays the area and percentage of flooded areas and the amount of precipitation per day. According to the investigations, on the 16th to 18th of April 2024, the coasts of Hormozgan province were affected by a powerful rainfall system that caused torrential rain, lightning, momentary gusts and sometimes hail. In this region, Lavan, Jask, and Sardasht Bashagard synoptic weather stations have received the most rainfall from this system with total rainfall of 123.2, 121.1, and 120.5 mm, respectively. Thus, the rain gauge stations recorded more than 70 mm of rain during this rainfall system from 16 to 18 April (Figure 3). Further, to identify and zone flood areas, the map of flood areas on April 16 and 17 is shown in Figures 4 and 5, respectively. It is worth mentioning that April 18 was not included in this study due to the lack of significant changes and the limited extent of the flooded areas. As

the results show, the greatest extent of changes in floodplains is on the coastline and near the border of the region, which indicates the high sensitivity and susceptibility of coastal areas to flooding in this region (floodplains with dark gray spots in the figure). It is given that increasing darkness of pixels indicates flooded areas).

Table 2. The area and percentage of flooded areas and the amount of precipitation per day

Row	Image date	Flooded area		Average rainfall (mm)
		Area (Km2)	Percentage (%)	
1	2024/04/16	22.56	3.16	23.13
2	2024/04/17	28.15	4	35.05
3	2024/04/18	18.46	2.57	21.08

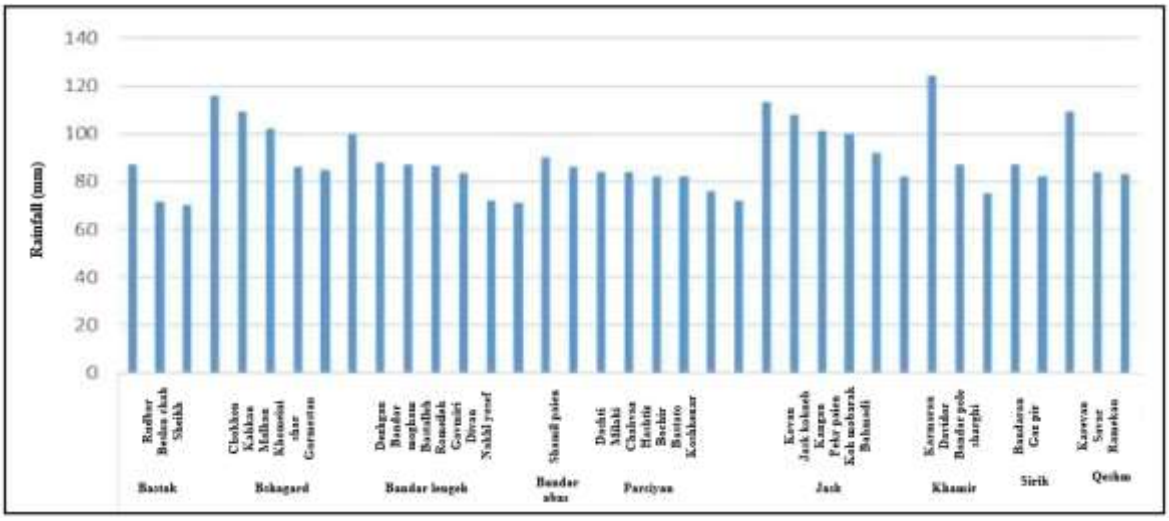

Figure 3. The graph of total rainfall of rain gauge stations in the studied area (April 16 to 18, 2024)

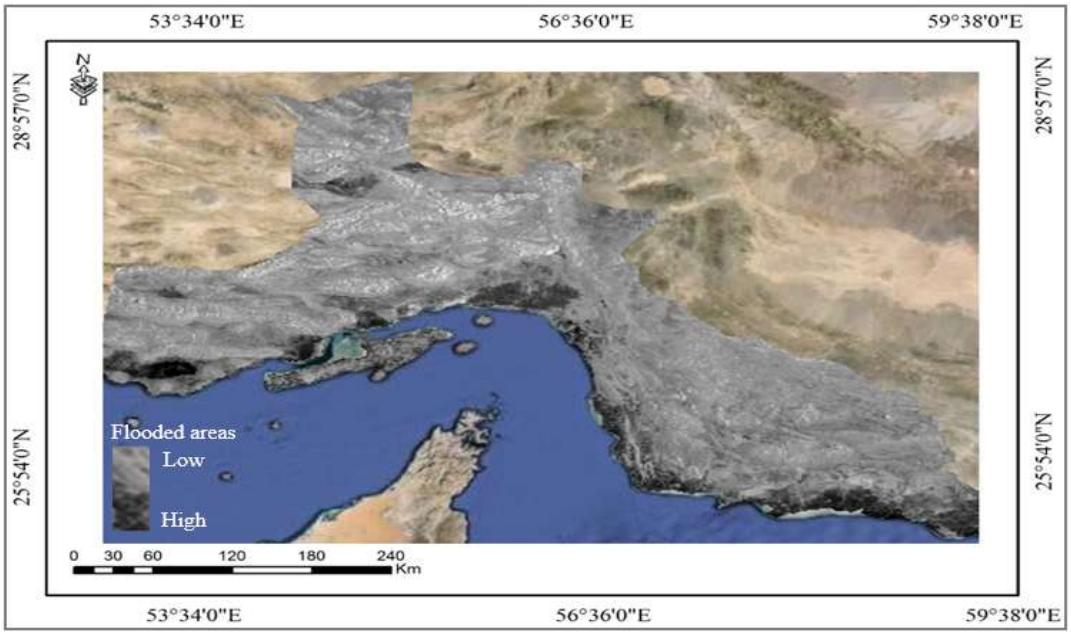

Figure 4. Map of flooded areas on April 16, 2024

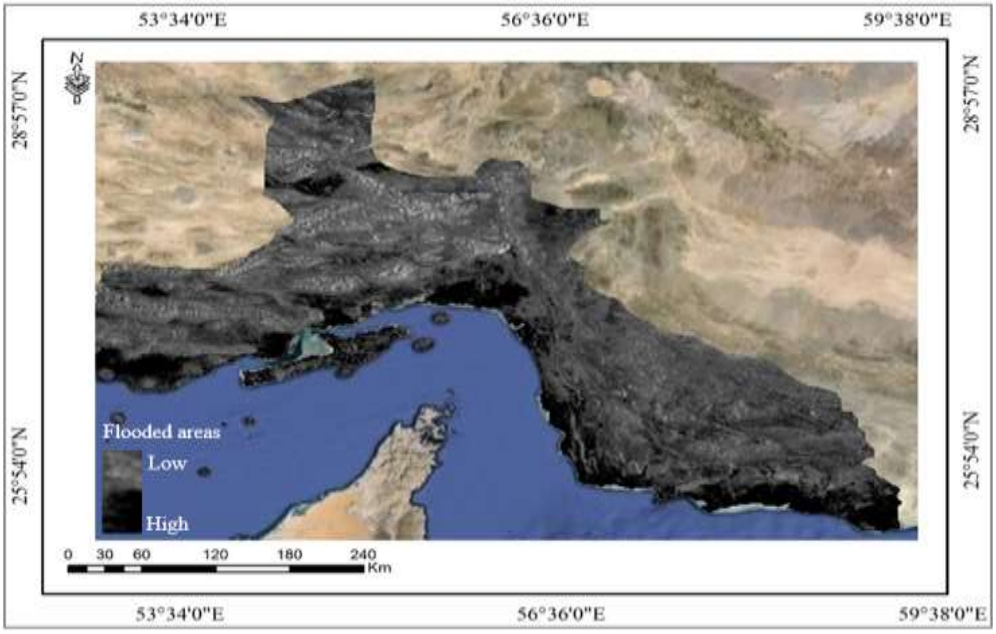

Figure 5. Map of flooded areas on April 17, 2024

4.2 Flood zoning in the area

In this study, after examining the flooded areas and the amount of rainfall that occurred in the region, the flood zoning was carried out by the spatial criteria such as the infrastructure and facilities of the region, population centers (cities and villages), communication network (main roads, railway transportation lines, airports), and rainfall distribution (maximum and average rainfall) were discussed during the studied days (Figures 6 to 10).

The map of the maximum rainfall on April 16-18, 2024, indicates that the maximum amount of rainfall was less than 20 mm in the southeast of the province, while the amount of rainfall was more than 55 mm in the eastern and western regions of the province (especially Bashagard and Persians) is considerable. Likewise, most rainfalls are related to Bashagard and Bandar-e Lengeh cities with more than 200 mm, and Bandar Abbas, Rodan and Haji Abad cities were also affected by more than 55 mm rain.

Further, due to the concentration of marine infrastructure and facilities along the coastline, the abundance of population centers, especially villages in the coastal area, and the network of roads and airports, flood zoning was analyzed in the province. As the results illustrate, 1,448.36 km^2 of the area is made up of floodplains, the largest area of which is the floodplain with an area of 669.30 km^2 (46.21 percent) along the coasts. (Table 3 and Figure 11). Since most of the cities, including Khamir, Minab, and Haji Abad, and some coastal villages are located in lowland areas and the flood plains of rivers, the occurrence of floods and river inundations in these areas is the most threatening factor.

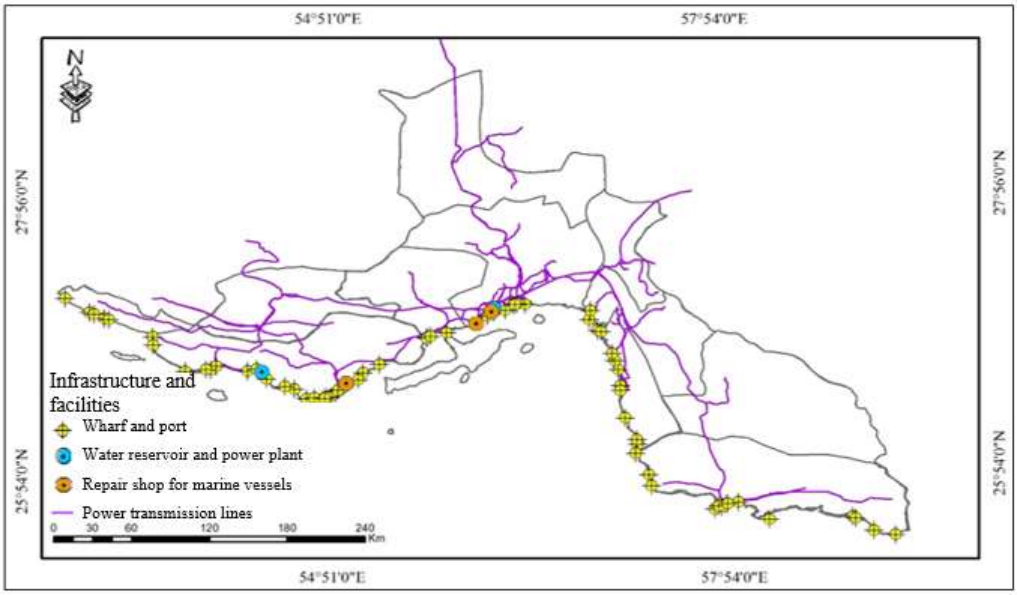

Figure 6. Map of infrastructure and facilities of the area

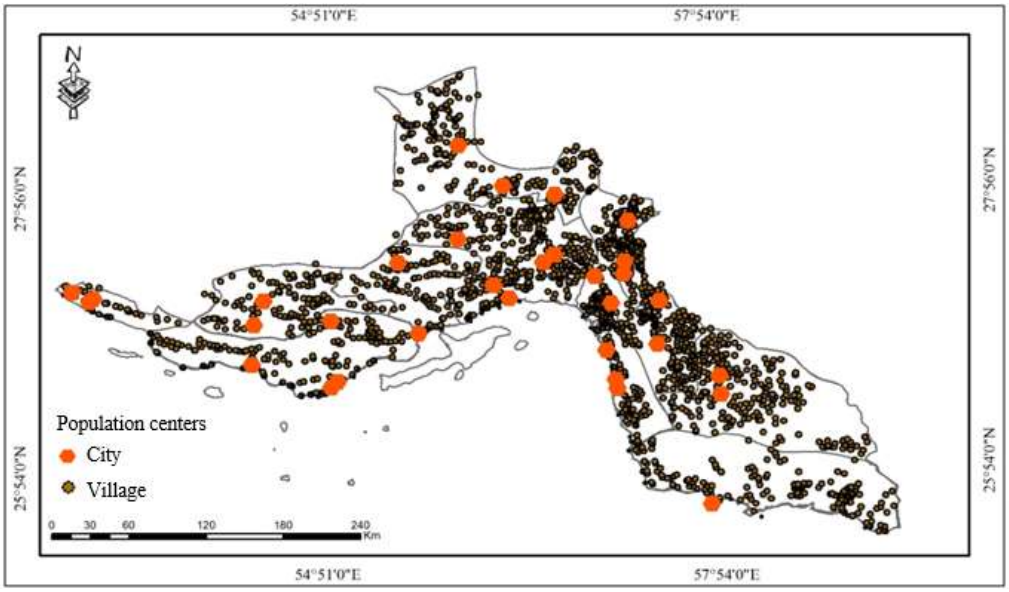

Figure 7. Map of population centers of the area

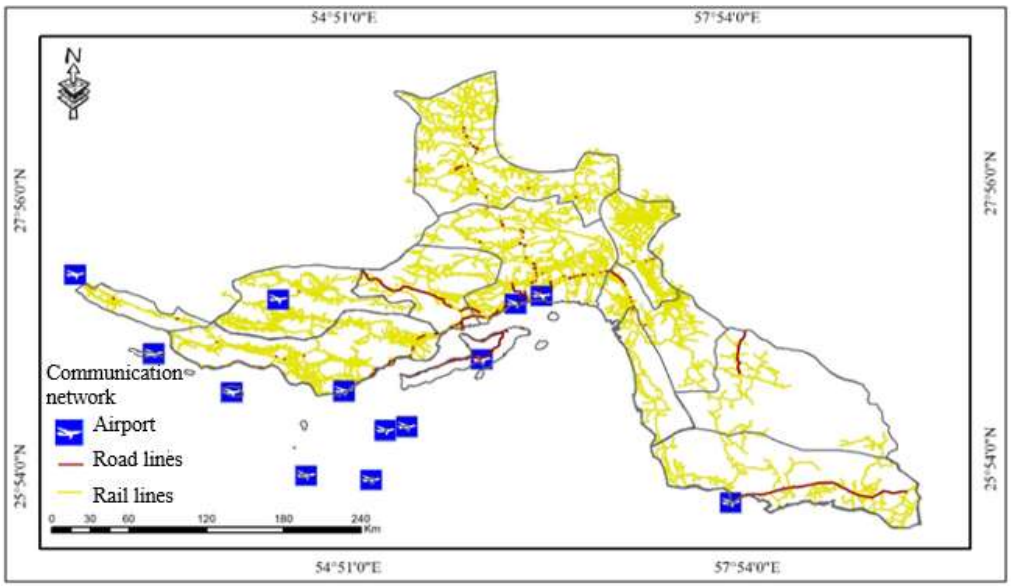

Figure 8. Map of the communication network of the area

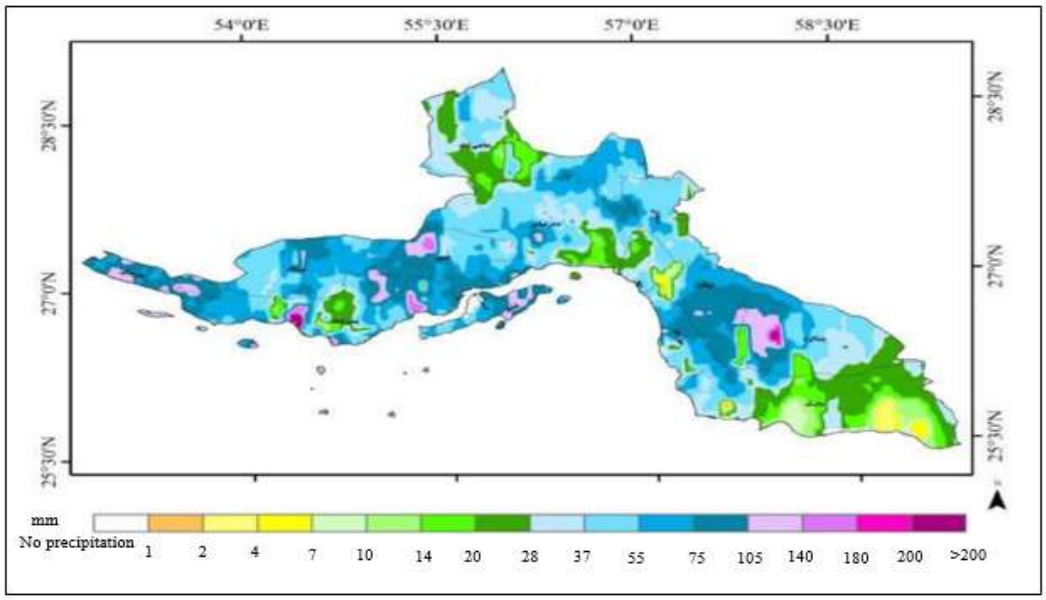

Figure 9. Map of maximum rainfall from April 16 to 18, 2024

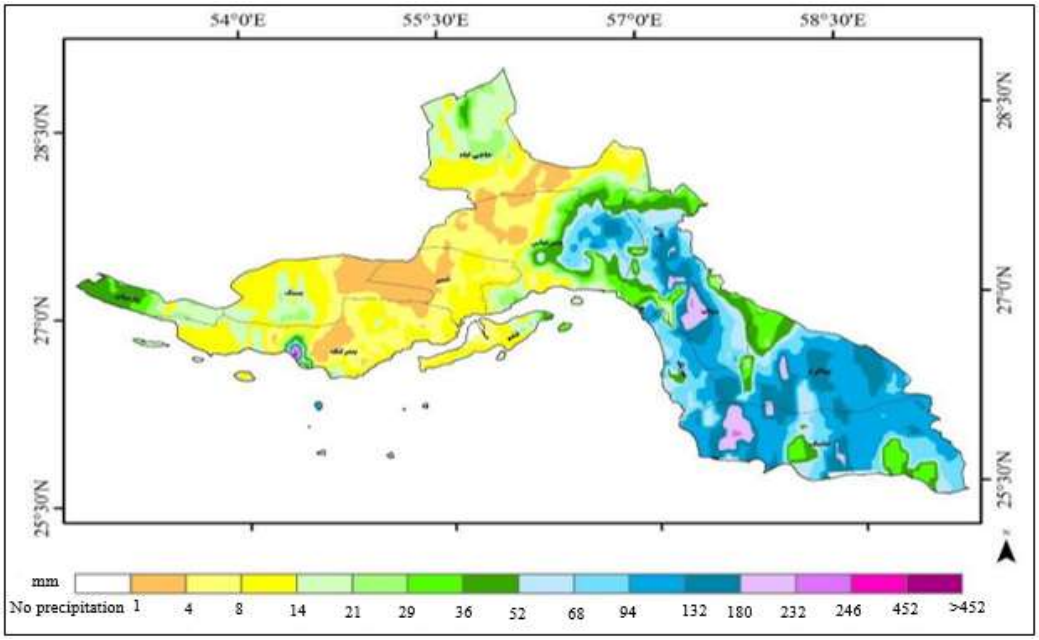

Figure 10. Map of average rainfall from April 16 to 18, 2024

Table 3. Area and percentage of flood zones in the studied area

Row	Classes	Area (Km^2)	Percentage (%)
1	Low	113.62	7.84
2	Medium	664	45.84
3	High	669.30	46.21
	Sum	1448.36	100

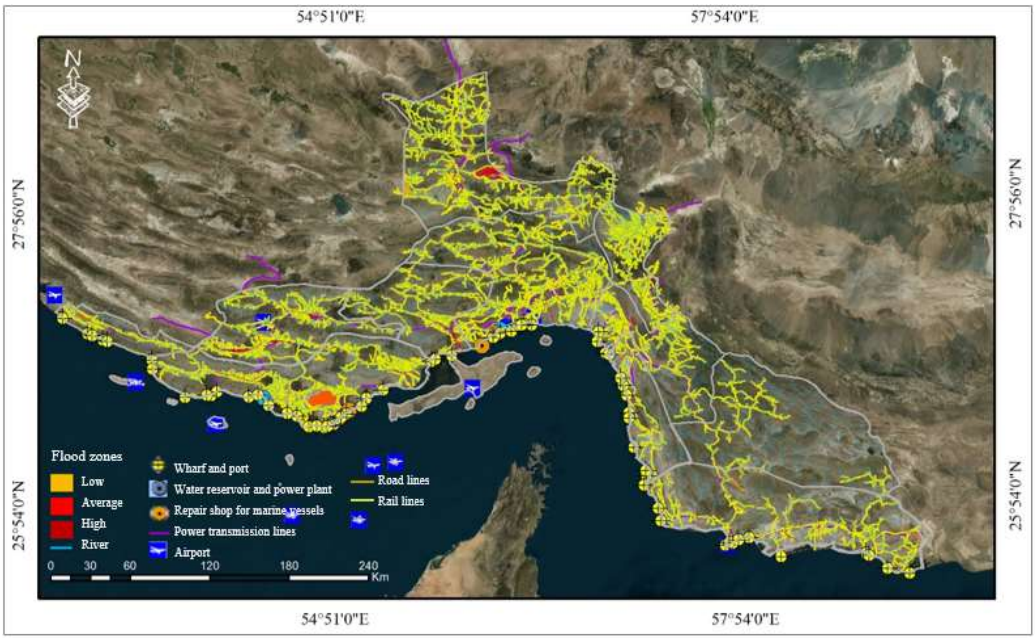

Figure 11. Flood zoning map in the studied area

The damages caused by floods worldwide have caused this environmental event to be referred to as one of the most important natural disasters. Today, along with the advancement of technology, humans can identify flood-prone areas and zoning these areas at risk [24].

In the present study, the flooded and flood-prone areas on the coasts of Hormozgan province were investigated according to the intensity of the rainfall system in the last days of April 2024 by using the GRDH images of Sentinel-1 satellite and the Otsu thresholding method.

As the results reveal, the greatest extent of changes in flood zones is in the coastline and near the border of the region, which indicates the high sensitivity and susceptibility of coastal areas to floods in this area. Therefore, controlling and managing floods in the province plays an important role in the safety of citizens, security of investment, and stability of infrastructure.

The results of studies by Carreno Conde and De Mata Munoz [3] and Gasparovic & Klobucar [6], also confirm the results obtained in this research. Their findings showed that the coastal areas are more affected by the dangers of floods due to their high sensitivity and vulnerability, as well as in the passage of the main rivers to the sea.

Likewise, according to land use planning studies of Hormozgan province [21], coastal areas are very sensitive in terms of environmental capacity and are considered as special biological areas. Therefore, in the future planning process, pay attention to the zoning of these lands in terms of the distance from the sea, determine the area of coastal, post-coastal and pre-coastal areas and functional areas.

According to the results, about 1448.36 km^2 of the area is affected by flood zones, the largest area is allocated to the high-risk category with an area of 669.30 km^2. The obtained results indicate high accuracy and its application in predicting the occurrence of floods. In this regard, Ghahreman & Zangeneh Asadi [7], also stated that radar images are a highly accurate and reliable tool in determining flooded areas, especially for quick investigations and close to the time of the flood phenomenon. In addition, the study of Sobhani & Danehkar [19], showed that remote sensing techniques are useful tools in examinations and evaluation of coastal areas.

5. Conclusion

The results obtained in this research indicate the use of new methods in a short period of time and with high

accuracy, so these results can be used for accurate flood zoning and efficient planning in the future. According to the results, it is possible to manage and control floods spatially and temporally on the coasts and prevent the consequences. Therefore, in the field of coastal flood management, it is necessary to pay attention to flood control methods, a suitable model to improve water supply sources and improve water security for drinking and health purposes, as well as appropriate bioengineering methods to stabilize soil and control erosion. Likewise, it is suggested that in addition to flood zoning, flood forecasting should also be conducted in future studies. Based on this, it is possible to manage and control flooding spatially and temporally on the coasts and prevent its consequences. The repetition of floods in the country and in the coastal areas of Hormozgan province reminds us of the necessity for zoning and forecasting against flood risks. In addition, these hazards emphasize the need to improve infrastructure and apply management strategies to control floods in the area.

Acknowledgments

This article has been completed with the cooperation and financial assistance of the Madde Danesh Studies Center.

6. References

[1] Ahmadi, Y., Bazrafshan, O., Salajeghe, A., Holisaz, A., & Azareh, A., (2021). Identifying the Factors Affecting Urban Flood Vulnerability in Bandar Abbas with Emphasis on Urban Runoff Management. Urban Economics and Planning, 2(3), 236-246.

[2] Barbaro, G., Bombino, G., Foti, G., Barillà, G. C., Puntorieri, P., & Mancuso, P., (2022). Possible increases in floodable areas due to climate change: The case study of Calabria (Italy). Water, 14 (14), 2240.

[3] Carreno Conde, F., & De Mata Munoz, M., (2019). Flood monitoring based on the study of Sentinel-1 SAR images: The Ebro River case study. Water, 11(12), 2454.

[4] Doust, A. M., Shamsnia, S. A., & Shabani, M., (2023). Spatial Analysis of Water Areas Potential for Small Water Supply Projects in the Southeast of Bushehr Province. Management, 3(4), 48-59.

[5] Garzon, J. L., Ferreira, Ó., Reis, M. T., Ferreira, A., Fortes, C. J. E. M., & Zózimo, A. C. (2023). Conceptual and quantitative categorization of wave-induced flooding impacts for pedestrians and assets in urban beaches. Scientific reports, 13(1), 7251.

[6] Gasparovic, M., & Klobucar, D., (2021). Mapping floods in lowland forest using sentinel-1 and sentinel-2 data and an object-based approach. Forests, 12(5), 553.

[7] Ghahraman, K., & Zanganeh Asadi, M., (2022). Determination of flood-prone areas using Sentinel-1 Radar images (Case study: Flood on March 2019, Kashkan River, Lorestan Province). Journal of Spatial Analysis Environmental hazarts, 9(3), 103-118.

[8] Hu, P., Zhang, Q., Shi, P., Chen, B., & Fang, J., (2018). Flood-induced mortality across the globe: Spatiotemporal pattern and influencing factors. Science of the Total Environment, 643, 171-182.

[9] Jafarzadegan, K., Moradkhani, H., Pappenberger, F., Moftakhari, H., Bates, P., Abbaszadeh, P., & Duan, Q., (2023). Recent advances and new frontiers in riverine and coastal flood modeling. Reviews of Geophysics, 61(2), e2022RG000788.

[10] Karimi, P., Safaval, P. A., Behzadi, S., Azizi, Z., Zarkash, M. M. K., & Kalashami, H. K., (2022). Flood Risk Zoning using Geographical Information System Case Study: Khorramabad Flood in April 2019. Acta hydrotechnica, 35(63), 89-100.

[11] Kautsary, J., & Rahman, B., (2024). Evaluation of Zoning Regulations in Coastal Areas for Disaster Risk Reduction of Climate Change. In IOP Conference Series: Earth and Environmental Science, 1321 (1), 012004. IOP Publishing.

[12] National Meteorological Organization., (2023). Annual climate report.

[13] Otsu, N. (1979). A threshold selection method from gray-level histograms. IEEE transactions on systems, man, and cybernetics, 9 (1), 62-66.

[14] Pornaby Darzi, S., Vafakhah, M., & Rajabi, M. R., (2021). Flood hazard zoning using HEC-RAS Hydraulic Model and ArcGIS (Case Study: CheshmehKileh River in Tonekabon County). Journal of Natural Environmental Hazards, 10(28), 15-28.

[15] Rezaee, Z., & Vahidnia, M. H., (2022). Offering flood prevention solutions using remote sensing and approaches integrating fuzzy logic and agent-based modeling. Scientific-Research Quarterly of Geographical Data (SEPEHR), 31(121), 111-125.

[16] Sasanpour, F., & Mohebbi, F., (2021). Flood risk analysis and zoning-Case study: Taleghan Watershed.

[17] Sobhani, P. & Danehkar, A., (2023). Assessment of environmental hazards and vulnerability of Hara protected area using DPSIR model. Environmental Hazards Management, 10 (3), 215-232.

[18] Sobhani, P., & Danehkar, A., (2023). Natural features and management areas of Khamir and Gheshm mangrove forests. Iran Nature, 8(4), 97-112.

[19] Sobhani, P. & Danehkar, A., (2024). Sea level changes and its impacts on Hormozgan Province mangrove forests (Case of study: Hara protected area). Journal of Oceanography, 15 (57), 115-126.

[20] Solaimani, K., & Mohseni, B., (2023). Evaluation of effective criteria on flood risk based on network analysis process and GIS in Vazroud basin of Mazandaran province. Iranian journal of Ecohydrology, 10(1), 61-75.

[21] Land use planning of Hormozgan province., (2018). Management and Planning Organization of Hormozgan Province, 1-77.

[22] Sun, H., Zhang, X., Ruan, X., Jiang, H., & Shou, W., (2024). Mapping Compound Flooding Risks for Urban Resilience in Coastal Zones: A Comprehensive Methodological Review. Remote Sensing, 16 (2), 350.[23] Tabrizi, R., Rahmati, S. H., Seyed Mohammad Shirazi, R. H., & Shahbazi Bilehsavar, M., (2023). Zoning of the 25-Year Flood for Use in Determining the Boundaries of the River's Bed and Boundaries (Til River as Case Study). Journal of Water and Soil Resources Conservation, 12(3), 111-127.

[24] Tanim, A. H., McRae, C. B., Tavakol-Davani, H., & Goharian, E., (2022). Flood detection in urban areas using satellite imagery and machine learning. Water, 14(7), 1140.

[25] Uddin, K., Matin, M., & Meyer, F., (2019). Operational flood mapping using multi-temporal sentinel-1 SAR images: a case study from Bangladesh. Remote Sensing, 11, 1581.

[26] Van de Sande, B., Lansen, J., & Hoyng, C., (2012). Sensitivity of coastal flood risk assessments to digital elevation models. Water, 4(3), 568-579

INTERNATIONAL JOURNAL OF
COASTAL, OFFSHORE & ENVIRONMENTAL ENGINEERING IJCOE Vol.10/No. 1/Winter 2025 (50-67)

Available online at: www. Ijcoe.org

Compendium of Hazards of Carbon Capture Chain

Maryam Shourideh1, Sirous Yasseri 2

1 Maryam Shourideh, Mechanical Engineering, Brunel University London, United Kingdom; maryam.shourideh@brunel.ac.uk

2 Sirous Yasseri, Mechanical Engineering, Brunel University London, United Kingdom; sirous.yasseri@brunel.ac.uk

ARTICLE INFO

Article History:
Received: 06 Feb 2024
Accepted :09 Jun 2025

Keywords:
CCS (Carbon Capture and Storage) Hazards, CCS Safety, CCS Risks, Infrastructure Integrity, Regulatory Barriers

ABSTRACT

Capturing and storing CO2 (carbon dioxide) from concentrated industrial sources (e.g., cement industries and coal power plants) is a promising technology, as part of a mix of measures, for mitigating global warming. However, the implementation of Carbon Capture and Storage (CCS) also involves potential hazards and their impacts that must be addressed to ensure its safe operation. This paper aims to produce a compendium of major hazards that a CCS operation could create. The main hazards of the CCS chain include the leakage of stored CO2, accidents during transportation, the possibility of induced seismicity, and a lot more. The hazards associated with CCS encompass not only technical aspects but also factors related to human or organizational behaviour. The hazards associated with CCS may impact humans as well as the environment and may cause economic loss associated losses CCS infrastructure and liability for potential accidents. A compendium of hazards is needed to address the hazards, risks, and safety of CCS installations is presented.

1. Introduction

Carbon Capture and Storage (CCS) is an effective technology for reducing greenhouse gas emissions (GHG) by capturing high amounts of CO2 at the source. It is a crucial technology in the effort to actively reduce industrial emissions of greenhouse gas emissions. Apart from renewable energy which can help in carbon emissions reduction, CCS or direct air capture (DAC) can also help in carbon emissions drops. CCS offers a solution for reducing emissions at the source, particularly in energy production and industrial processes, by capturing CO2 and capturing it in geological formations. This is a significant advantage compared to direct air capture (DAC), which can be costly because of the low concentration of CO2 in the atmosphere [1].

Despite the projected fast growth of renewable energy sources, the US Energy Information Administration (EIA) predicts that fossil fuels still make up to 77% of energy consumption by 2040 [2]. Large-scale CCS involves a variety of technologies, but they have three major steps in common, namely capturing carbon dioxide, compressing it for transportation, and injecting it deep underground for permanent storage [3].

At the start of a risk analysis, a list of known hazards is compiled, and the probability of occurrence for each hazard is assessed. The next step is determining the vulnerability of workers, communities, and the environment to evaluate the consequences of a hazard if it occurs. A compendium of all CCS's known hazards reported in technical literature is compiled. CCS installation is a socio-technical system, thus hazards due to human errors, weak safety culture, and poor leadership should be considered as well.

Table 1 Examples of risk review papers

Reference	Synopsis (Quoted)
[4]	Review of Factors affecting the integrity and accurate hazard assessment of CO2 pipelines, such as corrosion, hydrate formation, hydrogen embrittlement, and fast-running fractures.
[5]	Offers a sketch of how risk management is undertaken, using what is termed an "integrated risk management framework".
[6]	Discusses the usefulness of spatial planning for carbon captured, and injected for long-term, storage with minimal geo-hazards
[7]	Present a review of gas-hydrate hazards in various operational scenarios.
[8]	Presents a review of hazards posed to dense-phase CO2 pipelines in the form of internal corrosion.
[9]	Presents a review of risk, liability, and economic issues with long-term CO2 Storage

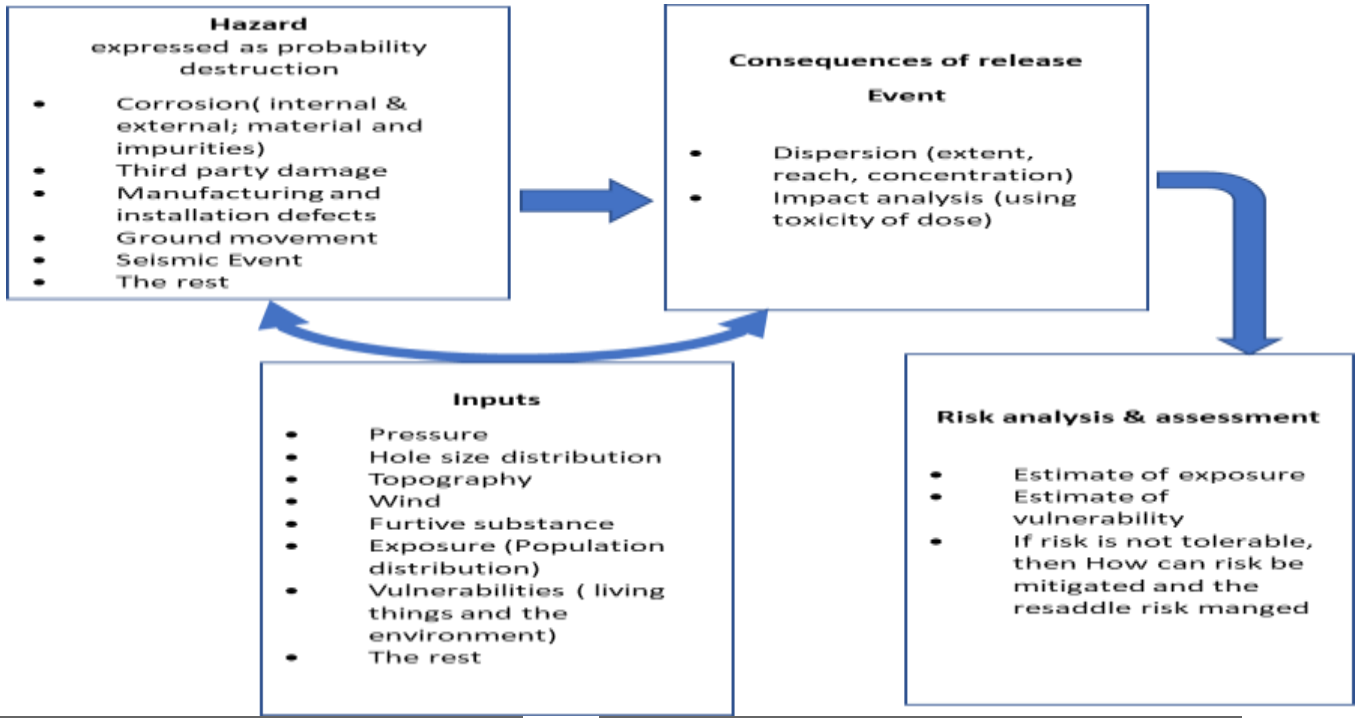

[10]	Presents a review of many challenges that delay the deployment of CO2 transport by pipelines.
[11]	Presents a review of necessary for the site selection, discussing geological, geothermal, geohazards, hydrodynamic, basin maturity, and economic, societal, and environmental factors.
[12]	The objective of the paper is to discuss corrosion inhibitors for CO2 pipelines.
[13]	Presents the design of CO2 pipelines including route selection, right of way, flow rates, and velocities, for pipelines
[14]	Presents a risk management framework for environmental and human health risks and management
[15]	Discuss the application and characteristics of three states of CO2 (i.e., gas phase, liquid phase, dense phase, and supercritical) for transmission pipelines.
[16]	Discusses developments of CO2 storage from the point of view of improving economics as well as safety.
[17]	Presents a review of various processes, technology, and materials used for the separation and capturing of CO2 from point sources.
[18]	A review of four aspects of the CO2 pipeline, i.e., design, process, safety, standard & specification
[19]	Review of storage leak risk.
[20]	An overview of common organic corrosion inhibitors commonly used for CO2 equipment.
[21]	A review of publications regarding public acceptance and social impacts of Carbon Capture projects.
[22]	A comprehensive overview of all subsystems involved in the deployment of CCS technology, encompassing both technical and non-technical aspects, such as economic, social, and technical challenges.
[23]	An overview of model-based CCS deployment pathways and the related risks financial, technical, environmental, health, and safety risks.
[24]	The focus is on carbon steel substrate behaviour as a widely used material in various industrial applications.
[25]	A review of methods used for carbon capture such as absorption-based, adsorption-based, cryogenic, and membrane-based technologies.
[26]	Geological storage reservoir integrity and leakage potential and the common monitoring methods are reviewed.

Prior case studies, (See the supplementary data Table S1), examining CCS projects hold significant importance for several key reasons, such as:

- Showing feasibility
- Learning from past incidents
- Developing business cases
- Updating policy and regulations
- Enhancing public awareness

2. Materials and Methods

2.1 Hazards and Risk

A hazard is an undesirable event, which is a source the potential harm to living beings in terms of fatality, injuries, health, financial loss, property damage, and destruction of the environment but generally a combination of them. A hazard is the chance of occurrence that could have (generally) a negative effect. The intensity of the hazard reflects:
the likelihood of a hazard occurring.
Exposure to the hazard
The vulnerability
Often, vulnerability and consequence are lumped together and termed impact.
In common usage, “hazard refers to 'the chance of danger, loss, injury or other adverse consequence” (Oxford English Dictionary) – a health hazard and so

Figure 1 Risk assessment process for a pipeline release.

on. Sometimes the word 'Hazard' is used to mean threat or the amalgamation of the probability of a hazard and the probability of its impact.

In Quantitative Risk Assessment (QRA), the risk is defined using the above factors; all expressed in probability terms. This a convenient way to combine the probability of harm due to various types of hazards with different probabilities of occurrence, consequences, and the level of exposure and vulnerability. Since harm may be a result of high-impact events but low probability (rare events) or by low-impact with high-probability events (commonplace events). Risks are ranked by the probability's presence of hazards and their impacts in the 'Risk Matix' application.

According to this definition, it is not the presence of a hazard that indicates a risk rather, a hazard becomes a menace when something or somebody is exposed to its presence and is vulnerable; thus, 'hazard is a function of circumstance. For these reasons, the notions of vulnerability and exposure must be introduced to capture these nuances – since the probability of a hazard causing harm may be mitigated by guarding against vulnerability. In QRA the following definition is adapted to determine the hazard.

Risk = Likelihood of a Hazard * Exposure * Vulnerability (1)

All the parameters on the right-hand side of this relationship are used to mitigate risks. The focus of this paper is on computing hazards. Because exposure and vulnerability are situation-dependent, the risk depends on the circumstances, i.e., it is case-specific. Figure 1 shows the above relationship for a CO2 pipeline release as shown in **Error! Reference source not found.**.

Figure 1 Shows the process of risk assessment for a pipeline release.

This definition allows adding consequences of several hazards together from various sources. However, this definition does not differentiate between hazards with high probability but low consequence (everyday common hazards) and hazards with low probability but high impact (catastrophic event).

The papers that are reviewed in this article do not differentiate between hazard and risk, and use 'hazard' to mean risks. Some attempt is made to change the original authors' use of the word 'Risk' to hazard as defined here. The above definitions of hazard and risk are adhered to in the article.

CCS poses both global and local hazards, with safety concerns dominating the last. These hazards can be divided into four categories: human health, environment, property, and financial. Government regulations play a role in each of these categories, but the extent of their involvement varies depending on the type of hazard. The CCS chain is a complex installation with many interconnections between the components requiring careful consideration [27, 28]. A primary concern in managing hazards in complex systems, especially safety systems, is to recognize and evaluate potential hazards that may compromise the system's reliability and performance [29].

2.1.1 Capture Hazards

CCS carries health hazards associated with any carbon dioxide leakage at any stage of the process which could cause asphyxiation for both humans and animals if the dosage is high as it displaces the air [30, 31]. CO2 leakage may occur suddenly or gradually, with each scenario leading to different outcomes. For instance, gradual leakage results in CO2 returning to the atmosphere, while a severe and abrupt leak can cause harm to animals and humans [14]. In severe cases where CO2 is more than 25% of the air, it may cause death if the level is maintained for some time [32, 33]- See the supplementary data Table S2. Apart from the hazard of suffocation caused by the displacement of the air due to the release of CO2, breathing in high levels of CO2 can also raise the acidity of the blood, resulting in negative consequences on the respiratory, cardiovascular, and central nervous systems [34, 35].

One of the biggest CCS hazards comes from hydrogen sulphide (H2S), which is co-generated at the same time. The high concentration of H2S can be toxic, so it is crucial to prevent gas leaks during the capture process to ensure the safety of workers [36].

In the post-combustion process, amine-based chemicals, particularly monoethanolamine (MEA), are widely utilized for absorption. It's important to note that MEA is corrosive [37]. The most common failures in the CO2 capture process are often attributed to corrosion issues [37]. In an accidental event, CO2 leakage potentially may continuously be released into the atmosphere, or it may be present in the water droplets which eventually could contaminate the lakes and nearby water supplies, thus exposing the public [38]. Amine degradation within CO2 capture installations can cause corrosion, although such a mechanism can also be reversed [39]. Three distinct types of amine degradation have been identified which are [40]:

1. carbamate polymerization, which can occur around the desorber and reboiler with the presence of CO2 and high temperatures exceeding 100 °C.

2. Oxidative degradation can appear in the absorber when the concentration of O2 in the flue gas is over 5% or because of heat-stable solids formation.

3. Thermal degradation is limited to the desorber, cross-heat exchanger, or reboiler, occurring only if the temperature exceeds 120 °C, which is the recommended maximum [37, 41].

Moreover, At the upper sections of both the absorber and regenerator, there is a significant hazard of corrosion that is caused by wet acid gases. Corrosion in the pipes can also increase the level of impurities [42]. The fire hazard can always be present due to the following three factors [43]:

- Oxygen combustion can cause an explosion.
- Amine leakage can cause a fire.
- Uncontrolled leakage of syngas can cause a fire.

Not having enough space for mixing pure oxygen with flue gas may cause an explosion [44]. During the process of separating amine, the solvent, from the gas, a fire can occur due to low water concentration and the presence of organic compounds [45]. Synthesis gas is toxic and could always cause health problems. It can also pose a fire hazard if pipework fails or due to fire.

Depending on the source of ignition, a fire may occur either immediately or after some time has passed [46]. This is due to low oxygen temperature which causes the primary flux to cool down. When liquid or dense phase CO2 is kept in pressure above the thermodynamic critical pressure, but below the critical temperature, it can diffuse in various plastics and elastomers. If the pressure is lost, the CO2 may rapidly come out of the solution, leading to explosive decompression [35]. Hazards associated with compressing CO2 include the possibility of failing to achieve the necessary pressure, consuming too much power, and operating below the intended capacity. These issues can lead to project delays, impaired functionality of facilities, and lower than anticipated return on investment [47]. The release of CO2 can cause electrostatic discharges that could ignite pyrolysis gases, leading to an explosion. Several serious accidents have been attributed to the ignition of flammable fuel/air mixtures, which was caused by the energy of electrostatic discharges resulting from the CO2 release [48]. Despite the unlikelihood of CO2 and flammable gases mixing, it may be necessary to consider this possibility during hazardous area classification studies [49, 50]. Inadequate control of the reactor temperature and impurities in the feed may have a hazard of hot spots, reduced permeance, and selectivity [51]. There will be some energy loss due to heat produced and the inability to recover this heat, makes it a lot less efficient [52]. In the case of adsorption separation, there is always a need for the gas collected from the flue treatment before the adsorption. The reason for the treatment is that impurities lower the efficiency of the adsorbent [53]. There is a hazard of amine entering into the environment, which may happen through the produced wastewater by the absorber-scrubber systems [54, 55]. In membrane separation technology, the membrane may malfunction due to various factors such as fatigue under humidity, vibrations, or shocks, which results in membrane degradation, this shows as thickness reduction, membrane delamination, pinhole formation, and membrane cracking [56]. The hazard of membrane fouling is always present; for example, when gas molecules obstruct the pores of the membrane, either partially or completely, leading to a reduction in capture efficiency [57, 58]. At the same time, the hazard of reduction in the membrane efficiency is a function of the amount of gas that passes through the membrane to accelerate the degradation process [59]. To prepare CO2 for transmission, it can be either compressed to reach its dense or supercritical phase or cooled to become a liquid. Failure or breakdowns during this stage could result in significant disruptions to the operations. The inability to transport captured CO2 may also have negative implications for meeting emissions targets and adhering to carbon credit commitments [60]. The CO2 separation process involves inherent technical risks associated with compressing and cooling gases flowing through pipes [60].

2.1.2 Transportation Hazards

Expenses involved in both building and maintaining a transportation system, and the potential dangers to life, property, and ecosystems, pipelines are deemed to be a more reliable and cost-effective option than other modes of transportation for high quantities of CO2 [61]. Accidents that might happen during truck or ship transportation can lead to CO2 escaping into the atmosphere [62]. The escape of carbon dioxide from a pipeline or intermediate storage is a risk to individuals due to its low temperature and toxicity [63]. The carbon dioxide is conveyed in a supercritical state, which means that it possesses the properties of both a gas and a liquid. In this state, CO2 has a density like that of a liquid, but its viscosity is like that of a gas which makes it more economical to transport [64]. The density of CO2 increases with decreasing temperature. The

supercritical phase is ideal for transporting to longer distances and is more cost-effective, but it is also regarded as more hazardous. Thus, pipelines are better suited for areas with lower population densities [15, 65].

There is always a pipeline leakage hazard. Faulty equipment, poor maintenance, and human error can cause overflow [41]. The process of releasing high-pressure CO2 is a multifaceted event that involves several phenomena, including the sudden discharge and expansion of CO2, the dispersion of a dense CO2 cloud, the descent of solid CO2, the sublimation of dry ice banks, and fluctuations in temperature and pressure within the pipelines [66]. Table shows that the failure of transportation pipelines can range from minor leakage through small holes to major leakage due to ruptures. The table provides rough information on the probability of such failures occurring each year. In addition to these factors, other causes of leakage include valve failure and external forces, such as accidents, support collapse, and seismic activity [67]. The leakage from a crack or pinhole has the highest frequency of 0.088 per 1000 km per year followed by hole and rupture with frequencies of 0.022 and 0.013 per 1000 km per year [68].

Table 2 Average failure rate per year per module [67]

Module		Expected failure rate (events per module per year)	Leaks every x year x=
1	CO_2 recovery at the source	1.5×10^{-1}	7
2	Converging pipelines	4.6×10^{-3}	217
3	Booster station	4.0×10^{-2}	25
4	10 km pipeline	3.4×10^{-4}	2,941
5	Injection well	1.8×10^{-1}	6

To fully comprehend the practical implications of pipeline safety requirements, especially regarding impurities, at each stage of CCS, it is essential to involve all stages, that is capture, transport, and storage site operators. This is because the transportation of CO2 cannot be viewed in isolation from the rest of the CCS chain [69]. Transportation pipelines are typically manufactured using carbon steel due to their ability to resist corrosion. The presence of free water in the pipeline promotes the formation of carbonic acid, which is highly corrosive to carbon steel [70]. Even with lower concentrations of impurities such as Sulphur dioxide (SO2), nitrogen dioxide (NO2), oxygen (O2), and water (HO2), nitric and sulfuric acid can form. This may cause the pipeline to lose its wall-thickness and eventually to failure, hence releasing CO2 into the atmosphere [71]. The presence of impurities in the CO2 stream has a notable impact on the ability to halt ductile fractures in pipelines that carry dense-phase carbon dioxide at pressures higher than 80 bar and temperatures below around 15 degrees Celsius [72]. The reason for this is believed to be the effect of impurities on the fluid bubble-point pressure and the speed at which decompression occurs [73]. The scarcity of information and regulations on the maximum level of impurities that can be present in the pipelines makes it harder to have one enveloping solution for corrosion hazards [74, 75]. Researchers reported that as the concentration of SO2 in the supercritical CO2 phase decreased, there was a corresponding decrease in the corrosion rate. Furthermore, the presence of the liquid CO2 phase resulted in notable localized corrosion [76, 77]. Pipeline blockage can decrease or stop the flow rate [41]. Assessing the detrimental effect of impurities on the operation, failure rates, and Health, Safety, and Environmental (HSE) impacts poses several challenges that need to be overcome [78].

According to studies done by EGIG from the year 1970 to 2019, it shows that pipeline failure due to the material has become a less significant cause of pipeline failure over time since material quality is continually improving. However, ground movement (landslides, unstable land, seismic shaking and displacements, debris flow, and so on), which is beyond human control, continues to affect pipeline failure [68]

The CO2 is heavier higher than air density. Releasing a large quantity of CO2 at the lower-level ground can pose a significant danger, thus it is crucial to consider the site elevation and topography [11, 79]. The dissipation of the denser-than-air vapor cloud was considerably delayed by the distinctive topographical features and atmospheric conditions present at the accident site [80]. Factors such as soil temperature, groundwater level, pipeline crossing a military-restricted area, passing through protected habitats, and heavily populated areas can all lead to health hazards depending on the rate of CO2 leakage [81]. The available information on the most suitable pipe materials is not adequate [82]. Most of the data is derived from the petroleum industry, as indicated in Table 3 which deals with the flow at a lower pressure than that of CO2. As a result, the figures may not be entirely accurate [82].

Table 3 Natural gas pipeline failure frequency [82]

Pipeline Failure	Reported Values		
Cumulative failure frequency (incidents per km per year)	6.1×10^{-4}	1.55×10^{-4}	1.1×10^{-4}

Establishing failure rates for CO2 pipelines proves to be a complex task, given the absence of uniform standards or HSE thresholds for key indicators like CO2 concentration, which adds another layer of complexity to the situation. Moreover, the absence of a universally recognized dose-response model for CO2 hinders the assessment of impact indicators, highlighting the need for prompt resolution of this issue [78]. The severity of a failure in CCS activities can be indicated by the level of CO2 leakage, which varies depending on the specific failure scenario. If the leakage is high and localized, it can pose an immediate threat to human safety. On the other hand, if the leakage is low and dispersed, it may result in long-term chronic exposure. [34].

2.1.3 Storage Hazards

Globally, geological formations have the potential to store over 12,000 Gt of CO2, with more than 300 Mt of CO2 already sequestered through various methods[83]. Inadequate storage capacity to store or inject CO2 during the assessment and injection stages at the site can lead to a risk [14]. **Error! Reference source not found.** shows the life cycle hazard profile for CO2 storage [84]. Over time, the security of the storage increases as CO2 is immobilised through capillary trapping, dissolution, and mineral trapping[85]. In the scenario of offshore storage, any unintentional discharge of carbon dioxide gas from an offshore reservoir could have a detrimental impact on the marine ecosystem. The elevated absorption of CO_2 can result in a decrease in seawater pH, leading to increased acidity. Both low pH levels and high CO_2 concentrations can have adverse effects on deep-sea organisms [86]. Although ocean currents and mixing can dilute CO2 in the water column, the extent of the impact would depend on the rate of leakage [87]. A small leakage could cause a drop in pH levels in the sediments. This reduction in pH may increase the availability of toxic substances, which could harm infauna [87].

Storing substances underground carries extra hazards, including the possibility of seepage, pollution of freshwater sources, and triggering of seismic events [88]. The potential hazards associated with CO2 leakage underground include the following [89]:

- The possibility of the substances accumulating in geological formations above the storage site, while remaining separate from other subsurface processes.
- The potential for interference with other subsurface processes, such as natural gas reserves or injection of wastewater into deep wells.
- The hazard of groundwater contamination.
- The chance that the substances could reach the surface and get back to the atmosphere.

Other potential hazards include groundwater displacement, earthquake-induced leakage, and lack of capacity [5]. The main hazard factor linked to the storage of CO2 is anticipated to be the accumulation of pressure in the storage reservoir [9, 16]. Fluid flow through fault zones in caprocks is dependent on various factors such as the internal geometry and connectivity of the fault/fracture damage zone, the local state of stress, and the level of cataclasis. These factors determine whether the fault zones control fluid flow or not. Therefore, minimizing the hazard of potential leakage rates along fault/fracture zones that are seismically invisible and may exist is crucial [61]. There are three ways that Caprock can fail [9,14].

Figure 2 Life cycle hazard profile for CO2 storage [84]

- Caprocks can fail due to hydraulic fracturing causing damage to the integrity of the caprock which has a low probability of occurring but if it happens it will have a high impact.
- The diffusive loss is very small. It takes more than 500 thousand years for CO2 to travel 700m above the reservoir.
- Capillary sealing, which is the main mechanism to stop the upward flow of CO2 might be a source of possible failure. The capillary leakage can be high and quite fast compared to diffusive failure if it is over-pressured.

Generally, most data originate from the gas industry. It is essential to keep in mind that CO2 behaves distinctively from natural gas, meaning that data on natural gas may not directly apply to CO2. Caprocks typically exhibit lower trapping efficiency for CO2 when compared to hydrocarbon gases. [90].

The

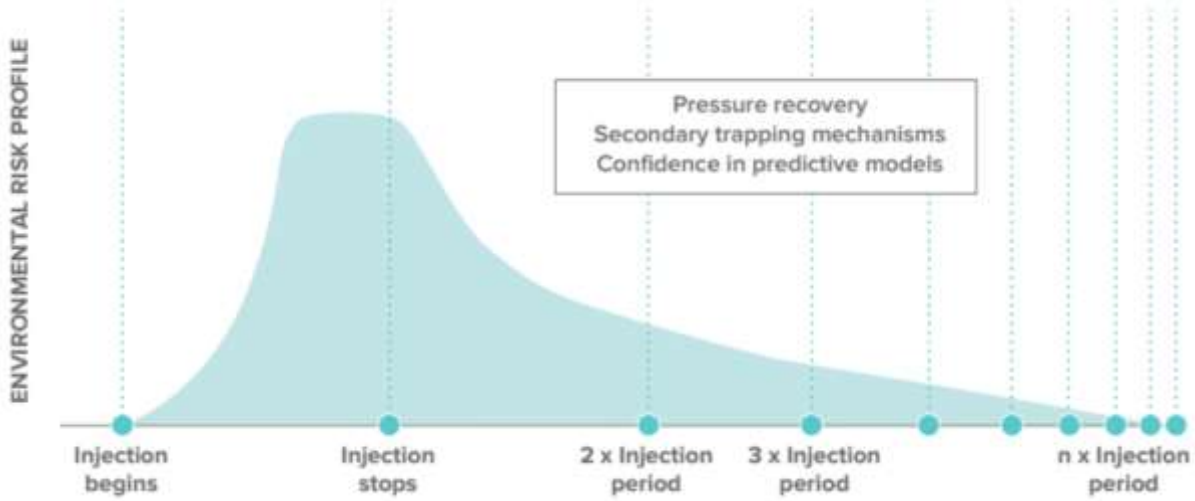

generation of a flow recirculation region around the vortex structure causes the cold fluids in the core region to be pushed toward the hot wall, causing a high-temperature gradient close to the wall. This steep temperature gradient leads to a higher heat transfer rate in that area [91]. Site characterization is very important and needs a deep study before choosing it as a storage. If any of the criteria are not met, then it may put the storage site at hazard. The criteria include the following:[19, 92].

- Adequate capacity and injectivity
- Sufficient depth of storage
- The adequate thickness of aquifers or reservoirs
- Adequate porosity
- Sufficient permeability
- Low temperature
- Optimal flow conditions
- Separated hydraulically from safeguarded underground water sources.
- Low well density in the storage's 'area of influence.'
- Multiple layers of overlying aquifers and intervening aquitards or caprocks
- Reduces the impact of leaked CO2 in the vicinity of or on the surface.
- Accessibility of the site and the facilities available
- Economics of Transportation
- Economics of storage
- Population density

1. When CO2 is injected into deep saline formations, the pressure changes are influenced by the properties of the underground formation. This displacement of saline waters and minerals by the injected carbon dioxide is dependent on the existing pressure levels [93]. Pressure buildup might cause caprock to fracture and induce seismic activity [94]. CO2 storage underground not only might cause earthquakes but also any natural ground movement can hazard leaking the stored CO2 into the atmosphere [95, 96]. Injecting CO2 into saline aquifers on a large scale will have the hazard of physical and chemical changes. These changes include the flow of fluids in multiple phases, the movement of dissolved substances, and the interaction between the fluids and minerals in the geological formation [97]. CO2 may also alter the underground pressure which can potentially lead to

leakage of brine into shallower water, resulting in contamination by lowering the PH and increasing dissolved metals and other components [89, 98, 99, 100].

2. It can be injected into deep un-mineable coal, to replace methane with CO2. The hazard of reducing the permeability of the surrounding soil causes the structure of the rocks to change. Changes in the mechanical properties of coal seams can cause difficulties in assessing the integrity and safety of CO2 storage [101]. Injecting carbon dioxide into deep coal seams can extract polycyclic aromatic hydrocarbons (PAHs) from the coal matrix and cause them to move within the coal seam. The injection of CO2 into coal seams can cause the organic constituents of the coal matrix to move, which can lead to environmental problems. When CO2 is injected and adsorbed into the coal mass, it causes the coal to expand. This expansion can result in significant changes to the internal structure of the coal mass, which can greatly affect its flow and strength properties [102]. The swelling of coal caused by CO2 adsorption significantly reduces the permeability of the coal [103]. Some concerns associated with CO2 storage in coal seams include the potential for leakage to the surface, the possibility of induced seismic activity, and the need for long-term monitoring to ensure the integrity of the storage [104,105].
3. Stored CO2 can also be reused for enhanced oil recovery (EOR). The notably low viscosity of CO2 can result in potential leakage into production wells. [106]. CO2 is commonly employed in a continuous flooding technique for EOR. Nonetheless, this method may pose challenges due to the poor mobility of CO2, issues with viscous fingering/channeling, and premature breakthrough, especially in reservoirs with varying characteristics. [107]. The term "toxic scale" refers to the formation of scales that can be harmful when CO2 is injected for enhanced oil recovery (EOR), there is a hazard that a portion of the CO2 will resurface along with the extracted oil [35]. Moreover, CO2 poor mobility control may result in large parts of the reservoir remaining unswept.

Moreover, three types of blowouts can happen with CO2-EOR activities [108]:

- Blowouts of production wells that are drilled into natural CO2 reservoirs.
- Blowouts of CO2 injection wells.
- Blowouts of active oil production wells that are part of the CO2-EOR project.

4. The captured CO2 can also be injected into the oil and gas reservoirs that are no longer in use. When CO2 in its high-density state is injected into a low-pressure reservoir, it can vaporize either in the wellbore or the subsurface reservoir formation. This vaporization process is accompanied by a temperature drop resulting from the Joule-Thomson phenomenon, abrupt changes in the thermodynamic properties of CO2 phases, and an increase in flow velocity due to CO2 expansion.

These phenomena are potentially dangerous as they can cause flow assurance problems such as hydrate formation, loss of pressure control, and compromised wellbore integrity [109].

Table 4 Leakage and blowout probability over time and their hazarded cost [113]

Scenario	Probability over 500 years including the lifetime of the project and post-closure (%)	Peak leakage rate (t/d)	Duration of leak	Total mass leaked (tones)	Risked leaked mass (tones)	Total remediation cost (including ETS cost) (€m)	Risked cost (€)
Minor leakage, fault and fracture	0.2	100	50 years	1,825,000	3,800	97	194,000
Moderate leakage, fault and fracture	0.05	700	12 years	3,066,000	1,550	178	89,000
Severe leakage, fault and fracture	0.005	5,000	4 years	7,300,000	365	589	29,450
Active well leakage	0.5	50	250 days	12,500	62.5	10.4	52,000
Active well blowout	0.15	5,000	250 days	1,250,000	1,875	93	139,500
Abandoned well blowout	0.1	3,000	1 year	1,095,000	1,100	88	88,000
Seepage in abandoned wells	0.5	7	100 years	255,500	1,250	34	170,000
Severe well problem, no repair successful	0.005	6,000	2 years	4,380,000	215	524	26,200
Leak from installation	0.25	100	5 days	500	1.25	15	37,500
Undesired plume spread	0.03	0	N/A	N/A	N/A	110	15,000
Total					10,219	1,838	840,650

Fractures and faults always present potential risks of failure, while blowouts can constitute a significant hazard. A well blowout happens when the pressure in the well is not controlled, causing fluid to flow out. The biggest hazard of CO2 injection deep underground is a well failure. This can happen because of mechanical failures or an external event that affects the well, causing a loss of control temporarily, as a result of which CO2 and other fluids would be driven out of the well [110]. Whenever there is a leakage and the pressure in the wells is not stabilized, a blowout can happen; however, CO2 is not a flammable gas and up to now there is no record of fatal accidents with CCS wells and injection processes. However, this can affect the workers' health and safety. A low level of CO2 release is not fatal, but it can be very harmful to the human body [108]. When drilling a well, one of the geotechnical problems that may arise is wellbore instability. This instability can lead to rock failure and hence movement, which can also create paths for potential leakage [111]. Moreover, the cement lining in older or abandoned wells that might have degraded over time could pose a potential issue [112].

There will be two main conclusions derived from Table 4 which were produced in the year 2019 [113].

- The likelihood of any one of these scenarios happening is remote.
- If all these unlikely scenarios happen at the same time then the total cost for one storage project would be £731.5 thousand, i.e. less than £1 million.

To ensure the success of subsea CO2 storage projects, it is crucial to include marine environment monitoring to identify any possible leaks or indications of leaks. The monitoring plan is comprised of two main components: planned and triggered monitoring. The planned component continually monitors the well and nearby areas through down-hole monitoring, as well as conducting active and passive seismic monitoring of the greater subsurface zone [114] However, creating a monitoring program that can accurately measure the likelihood of detecting the presence of a leak is a significant risk, necessitating a customized program design [114, 115].

2.1.4 Human and Organizational Hazards

These are also referred to as human and organisational factors. Human and organizational hazards must be an essential component of the overall hazard management process, [116]. Although the technical knowledge of CCS is considered to be fully developed, the cost of its implementation is a significant factor in deterring its widespread adoption [117, 118]. The total cost of building a CCS facility is 1,200 to 1,519 million pounds where 15 % of the total cost is dedicated to

hazard and contingency. This is done to protect the business from potential hazards and unexpected events; thus, it is important to develop a comprehensive contingency and hazard assessment plan for financial losses [119]. The average capital expenditure and operational cost ranged between £35-80/ tCO2 in the past (2010 prices) and it must be high enough to bring a reasonable return on investment [120]. Relying solely on public funding as the primary source of investment is not sufficient to sustain the required level of investment in CCS. CCS facilities require significant capital investments, which leads to high material costs, ultimately reducing their economic viability [84, 121, 122]. Because CCS projects often require significant infrastructure and capital investment, they typically have a long investment timeframe. This means that investors who are interested in CCS projects should be willing to commit to a long-term investment and face financial risks [123]. The absence of clearly defined regulations and scant technical knowledge could also pose financial risks and hence discourage the private sector [124, 125]. To create an adequate CO2 specification for a CCS hub network, several considerations and requirements must be taken into account throughout the CCS chain. It is crucial to balance these factors to avoid creating an overly restrictive or burdensome CO2 specification that may discourage potential users from connecting to the network, thus causing losses [126].

The process of acquiring permits for CCS projects is anticipated to be a major challenge and risk to encourage the growth of the CCS industry [127, 128]. Potential investors in CCS face uncertainties due to the legal framework, which does not provide the stability and certainty that these companies seek [129]. CCS liability is typically categorized as either operational or post-injection. Operational liability pertains to health, safety, and environmental hazards associated with capture, transportation, and injection. According to the International Hazard Governance Council (IRGC), post-injection liability covers health, safety, environmental, and climate hazards caused by CO2 that would migrate from the intended storage site to another subsurface unit or back to the atmosphere [85]. This potentially places a hazard on whoever takes the liability during different processes [9].

Public acceptance is a hazard by itself which greatly influences the development and progress of CCS [128]. Acceptance of carbon capture by the public is a major reason for discouraging CCS technology [130]. Additionally, the lack of widespread use of CCS has resulted in a scarcity of information, and an absence of knowledge management where information sharing is practiced, leading to increased hazards and barriers to CCS adoption [131, 132]. The entire technological chain is under scrutiny from a social perspective. To gain public acceptance, this new technology must prove its safety and minimal impact on the environment[28].

A significant hazard to the CCS chain is the uncertainty surrounding policies [128]. This may implement local or regional hazards [125]. Investors' reaction to the apparent level of policy commitment of the chain is substantial, since they are liable to policy hazards, especially in the case of long-lived assets like CCS, which rely heavily on government support. The absence of incentives, political will, and public support are among the primary hazard factors [133]. Regulators expect investors to exhibit their commitment to mitigating potential incidents and hazards by producing an environmental impact study proving the collective hazards are below a tolerable level. This expectation is placed on the investors not only by the public, customers, and governments but also by plant personnel [134]. With numerous projects involving collaboration between the government and the industry, it can be difficult to determine the appropriate party to lead the communication plan. This is because the duty holder is tasked with developing a safety case for the installation, rather than the design team. [135, 136]. A CCS project must deal with numerous knowledge-related hazards that can be broadly categorized into three groups: human hazards, operational hazards, and technological hazards [137].

3. Results and Discussions

Although CCS is a proven technology for controlling CO2 emissions, its adoption is not yet widespread. The lack of widespread adaptation of CCS has affected knowledge generation, which potentially can lead to enhanced hazards, which in turn affects its adoption. There is a possibility that CO2 leakage to occur at any point along the chain and at any time [23]. The accidental release of CO2 poses a threat to living organisms and marine ecosystems and harms the environment. This paper summarizes hazards associated with the CCS chain by categorizing them into four distinct classes, which are described separately. The four categories are related to the capture process, transmission process, storage process, and non-technical factors (soft issues). Each of these categories is studied separately to understand the

associated hazards. The non-technical category includes human and organizational behavior and culture (corporate and operation management) within the system, which adds to the overall hazard of implementing the technology. Tables 5, 6,7, and 8 show a summary of major hazards in each of the subsystems.

Table 5 A summary of major capture hazards

Capture	
Hazards	**References**
Health	[14, 30, 31, 32, 33, 34, 35]
Energy consumption	[52, 138]
Amine degradation	[39, 40, 53]
Explosion due to oxygen combustion	[43,44]
Fire due to amine leakage can cause fire	[43, 45]
Fire due to uncontrolled leakage of syngas	[43, 46]
Pressure and phase change	[35, 60]
Flammable air mixtures	[48, 49, 50]
Amine leakage	[54, 55]
CO2 compression	[47]

Table 6 A summary of major Transportation hazards

Transportation	
Hazards	**References**
Corrosion (In all stages of CCS)	[37, 42, 71, 74, 75],). ,
Hydrate formation	[139, 140]
Population density consideration	[15, 65]
Carbonic acid formation	[70]
Impurities	[71, 72, 73, 78
Pipeline blockage	[41]
Site elevation and topography	[11, 79]
Site conditions	[81]
Lack of information on pipelines' characteristics	[78, 82]
Ship or truck tank leakage	[62]

Table 7 A summary of major storage hazards

Storage	
Hazards	**References**
Leakage (In all stages of CCS)	[38, 41, 63, 67]
Contamination of water due to acid formation	[139, 141, 142]
Hydrate formation during storage	[143]
Inadequate storage capacity	[5, 14]
Threat to marine living creatures	[87, 142]
Groundwater Contamination	[88, 89, 98, 99, 100, 144]
Triggering seismic activity	[11, 88, 89, 94]
Interference with other subsurface activity	[89]
Pressure accumulation	[9, 16, 145]
Caprock fail	[9, 14]
Site characterization	[19, 92]
Natural groundwater movement	[95, 96]
Changing soil characteristics	[101]
Toxic scale	[35]
Blowouts	[108]
Well Integrity	[106, 109, 110, 111, 112]
Monitoring	[114, 115]

Table 8 A summary of major non-technical hazards

Non- Technical (Human elements, legal, financial)	
Hazards	**References**
Investment hazard	[84, 121, 122, 134, 147]
Public acceptance	[21, 28, 128, 130, 146]
Liability	([9, 85, 93]
Regulations	[27, 28 63]
Environmental	[148]
Lack of political support	[133]
Project Permitting	[127, 128]
Lack of technical knowledge	[124, 125]
Legal uncertainties	[129, 147]
High facility cost	[120]
Restrictive CO2 specification	[126]
Knowledge Management	([131, 132, 137, 149]
Absence of Incentives	[133]
Communication hazards	[135, 136]

4. Conclusion

In conclusion, the compendium of hazards associated with carbon capture and storage (CCS) technology assists in understanding and mitigating risks throughout the entire CCS chain. The potential for CO2 leakage and associated environmental, health, and safety risks requires addressing all hazards listed in this

paper and hazards that are specific to the installation. By categorizing hazards into capture, transmission, storage processes, and non-technical factors, this paper aims to provide a comprehensive examination of the various hazards associated with CCS technology. Moving forward, continued research, constant monitoring, and strict regulatory standards are essential to ensure the safe and effective deployment of CCS technology as a vital tool in mitigating climate change.

5.References

[1] Fasihi, M., Efimova, O., & Breyer, C. (2019). Techno-Economic Assessment of CO2 Direct Air Capture Plants. Journal of Cleaner Production, 224, 957–980. https://doi.org/10.1016/j.jclepro.2019.03.086

[2] Jezard, A. (2017, October 16). Fossil fuels will still dominate energy in 20 years despite Green Power rising. World Economic Forum. https://www.weforum.org/agenda/2017/10/fossil-fuels-will-dominate-energy-in-2040/

[3] International CCS Knowledge Centre, "What Is CCS." 2023, ccsknowledge.com/what-is-ccs. Accessed 1 May 2023.

[4] Bilio, M., Brown, S., Fairweather, M., & Mahgerefteh, H. (2009). CO_2 Pipelines Material and Safety Considerations. IChemE Symposium, 423–429. https://doi.org/https://www.icheme.org/media/9558/xxi-paper-061.pdf

[5] Leiss, W., & Krewski, D. (2019). Environmental scan and issue awareness: Risk management challenges for CCS. International Journal of Risk Assessment and Management, 22(3/4), 234. https://doi.org/10.1504/ijram.2019.103340

[6] Ghalehteimouri, K. J., & Eskandarian, I. (2012). Spatial Planning for Underground Carbon Storage and Relative Geo-hazards Assessment. International Journal of Bio-Resource and Stress Management, 3(1).

[7] Nazeri, M., Tohidi, B., & Chapoy, A. (2014). An evaluation of the risk of hydrate formation at the top of a pipeline. All Days. https://doi.org/10.2118/160404-ms

[8] Barker, R., Hua, Y., & Neville, A. (2016). Internal Corrosion of carbon steel pipelines for dense-phase co2transport in carbon capture and storage (CCS) – A Review. International Materials Reviews, 62(1), 1–31. https://doi.org/10.1080/09506608.2016.1176306

[9] Anderson, S. T. (2016). Risk, liability, and economic issues with long-term CO_2 storage—a review. Natural Resources Research, 26(1), 89–112. https://doi.org/10.1007/s11053-016-9303-6

[10] Onyebuchi, V. E., Kolios, A., Hanak, D. P., Biliyok, C., & Manovic, V. (2018). A systematic review of key challenges of CO_2 Transport via pipelines. Renewable and Sustainable Energy Reviews, 81, 2563–2583. https://doi.org/10.1016/j.rser.2017.06.064

[11] Aminu, M. D., Nabavi, S. A., Rochelle, C. A., & Manovic, V. (2017). A review of developments in carbon dioxide storage. Applied Energy, 208, 1389–1419. https://doi.org/https://doi.org/10.1016/j.apenergy.2017.09.015

[12] Usman, B. J., & Ali, S. A. (2017). Carbon Dioxide Corrosion Inhibitors: A review. Arabian Journal for Science and Engineering, 43, 1–22. https://doi.org/10.1007/s13369-017-2949-5

[13] Peletiri, S., Rahmanian, N., & Mujtaba, I. (2018). CO_2 Pipeline Design: A Review. Energies, 11(9), 2184. https://doi.org/10.3390/en11092184

[14] Larkin, P., Gracie, R., Shafiei, A., Dusseault, M., Sarkarfarshi, M., Aspinall, W., & Krewski, D. (2019). Uncertainty in risk issues for carbon capture and geological storage: Findings from structured expert elicitation. International Journal of Risk Assessment and Management, 22(3/4), 429–463. https://doi.org/10.1504/ijram.2019.103335

[15] Wang, H., Chen, J., & Li, Q. (2019). IOP Conference Series: Earth and Environmental Science. In A Review of Pipeline Transportation Technology of Carbon Dioxide (Vol. 310).

[16] Cao, C., Liu, H., Hou, Z., Mehmood, F., Liao, J., & Feng, W. (2020). A review of CO2 Storage in view of safety and cost-effectiveness. Energies, 13(3), 600. https://doi.org/10.3390/en13030600

[17] Maniarasu, R., Rathore, S. K., & Murugan, S. (2021). A review of materials and processes for carbon dioxide separation and capture. Energy; Environment, 34(1), 3–57. https://doi.org/10.1177/0958305x211050984

[18] Lu, H., Ma, X., Huang, K., Fu, L., & Azimi, M. (2020). Carbon Dioxide Transport via pipelines: A systematic review. Journal of Cleaner Production, 266, 121994. https://doi.org/10.1016/j.jclepro.2020.121994

[19] Gholami, R., Raza, A., & Iglauer, S. (2021). Leakage risk assessment of a CO_2 storage site: A Review. Earth-Science Reviews, 223, 103849. https://doi.org/10.1016/j.earscirev.2021.103849

[20] Chauhan, D. S., Quraishi, M. A., Sorour, A. A., & Verma, C. (2022). A review on corrosion inhibitors for high-pressure supercritical CO $CO_2$2 Environment: Challenges and Opportunities. Journal of Petroleum Science and Engineering, 215, 110695. https://doi.org/10.1016/j.petrol.2022.110695

[21] Nielsen, J. A., Stavrianakis, K., & Morrison, Z. (2022). Community acceptance and social impacts

of carbon capture, utilization, and storage projects: A systematic meta-narrative literature review. PLOS ONE, 17(8). https://doi.org/10.1371/journal.pone.0272409

[22] Shourideh, M., & Yasseri, S. (2023). Uncertainties and Barriers to Carbon Capture and Storage Acceptance & Implementation. IJCOE, 8(4), 18–30. https://doi.org/https://www.researchgate.net/publication/377964737_Uncertainties_and_Barriers_to_CCS_Acceptance_Implementation

[23] deployment planning and risk analysis of carbon capture, utilization, and storage (CCUS) toward carbon neutrality. Renewable and Sustainable Energy Reviews, 167, 112537. https://doi.org/10.1016/j.rser.2022.112537

[24] Desai, P. D., Pawar, C. B., Avhad, M. S., & P., A. (2022). Corrosion inhibitors for carbon steel: A review. Vietnam Journal of Chemistry, 61(1), 15–42. https://doi.org/10.1002/vjch.202200111

[25] Sahu, T., Ghuman, K., & O'Brien, P. G. (2023). Chapter 7 - A review of materials used for carbon dioxide capture. In Progress in Sustainable Development (pp. 205–232). essay, Sustainable Engineering Practices.

[26] Liu, E., Lu, X., & Wang, D. (2023). A systematic review of carbon capture, utilization, and storage: Status, progress, and challenges. Energies, 16(6), 2865. https://doi.org/10.3390/en16062865

[27] Groš, S. (2011). Complex systems and risk management. In Proceedings of the 34th International Convention MIPRO (pp. 1522–1527). Opatija; IEEE.

[28] Paltrinieri, N., Breedveld, L., Wilday, J., & Cozzani, V. (2013). Identification of hazards and environmental impact assessment for an integrated approach to emerging risks of CO_2 Capture installations. Energy Procedia, 37, 2811–2818. https://doi.org/10.1016/j.egypro.2013.06.166

[29] Selvik, J. T., & Signoret, J.-P. (2020). Risk management of complex systems: Understanding the difference between systematic and systemic failures. Engineering Assets and Public Infrastructures in the Age of Digitalization, 128–136. https://doi.org/10.1007/978-3-030-48021-9_15

[30] Fogarty, J., & McCally, M. (2010). Health and safety risks of carbon capture and storage. JAMA, 303(1), 67. https://doi.org/10.1001/jama.2009.1951

[31] Engebø, A., Ahmed, N., Garstad, J. J., & Holt, H. (2013). Risk assessment and management for CO_2 Capture and Transport Facilities. Energy Procedia, 37, 2783–2793. https://doi.org/10.1016/j.egypro.2013.06.163

[32] Harper, P., Wilday, J., & Bilio, M. (2011). Assessment of the major hazard potential of carbon dioxide (CO2). Health and Safety Executive, 1–28.

[33] Pothumsetty, R., Viswam, N., & Thomas, M. R. (2021). Health benefits of shifting from Bharat Stage Four to Bharat Stage Six. International Journal of Behavioural and Healthcare Research, 7(2), 77. https://doi.org/10.1504/ijbhr.2020.112147

[34] Wilday, J., McGillivray, A., Harper, P., & Wardman, M. (2009). A Comparison of Hazard and Risks for Carbon Dioxide and Natural Gas Pipelines. Hazards, (155), 392–398.

[35] Wilday, J., Wardman, M., Johnson, M., & Haines, M. (2011). Hazards from carbon dioxide capture, transport, and storage. Process Safety and Environmental Protection, 89(6), 482–491. https://doi.org/10.1016/j.psep.2011.09.002

[36] O'callaghan, J. (2018, November 27). Storing CO2 underground can curb carbon emissions, but is it safe? European Commission. https://ec.europa.eu/research-and-innovation/en/horizon-magazine/storing-co2-underground-can-curb-carbon-emissions-it-safe

[37] Krzemień, A., Więckol-Ryk, A., Smoliński, A., Koteras, A., & Więcław-Solny, L. (2016). Assessing the risk of corrosion in amine-based CO_2 Capture Process. Journal of Loss Prevention in the Process Industries, 43, 189–197. https://doi.org/10.1016/j.jlp.2016.05.020

[3838 CO 2 capture and Storage Technology. International Journal of Greenhouse Gas Control, 55, 118–143. https://doi.org/10.1016/j.ijggc.2016.10.014

[39] Davoudi, M., Safadoust, A. R., Akbar Mansoori, S. A., & Mottaghi, H. R. (2014). The impurities effect on thermal degradation and corrosivity of amine solution in south pars gas sweetening plants. Journal of Natural Gas Science and Engineering, 19, 116–124. https://doi.org/10.1016/j.jngse.2014.05.001

[40] Vega, F., Sanna, A., Navarrete, B., Maroto-Valer, M. M., & Cortés, V. J. (2014). Degradation of amine-based solvents in CO_2 capture process by chemical absorption. Greenhouse Gases: Science and Technology, 4(6), 707–733. https://doi.org/10.1002/ghg.1446

[41] Notz, R., Mangalapally, H. P., & Hasse, H. (2011). Post-combustion CO_2 capture by reactive absorption: Pilot plant description and results of systematic studies with mea. International Journal of Greenhouse Gas Control, 6, 84–112. https://doi.org/10.1016/j.ijggc.2011.11.004

[42] Sotoodeh, K. (2020). Requirement and calculation of corrosion allowance for piping and valves in the oil and gas industry. Journal of Bio- and Tribo-Corrosion, 6(1). https://doi.org/10.1007/s40735-019-0319-4

[43] Rusin, A., & Stolecka, K. (2013). Environmental Hazards Caused by Carbon Capture and Storage (CCS) Technologies. Polish Journal of Environmental Studies, 22(1), 205–211.

[44] Raho, B., Colangelo, G., Milanese, M., & de Risi, A. (2022). A critical analysis of the oxy-combustion process: From mathematical models to combustion product analysis. Energies, 15(18), 6514. https://doi.org/10.3390/en15186514

[45] Maeda, N., Kishimoto, A., Machida, H., Yamaguchi, T., Yanase, K., & Norinaga, K. (2021). Durability and fire-hazardous-risk evaluation of unique phase separation solvent using high-boiling amine and ether. International Journal of Greenhouse Gas Control, 114. https://doi.org/10.2139/ssrn.3821366

[46] Stolecka, K., Rusin, A. (2019). Hazards associated with Syngas Storage. E3S Web of Conferences, 137, 01022. https://doi.org/10.1051/e3sconf/201913701022

[47] Lepinski, J. A. (2013). (rep.). Comprehensive, Quantitative Risk Assessment of CO_2 Geologic Sequestration. U.S. Department of Energy Office of Scientific and Technical Information.

[48] Hedlund, F. H. (2018). Carbon dioxide is not suitable for the extinguishment of smouldering silo fires: Static electricity may cause silo explosions. Biomass and Bioenergy, 108, 113–119. https://doi.org/10.1016/j.biombioe.2017.11.009

[49] Santon, R., Mat., Ivings, M., Webber, D., & Kelsey, A. (2012). New Methods for Hazardous Area Classification for Explosive Gas Atmospheres. Institution of Chemical Engineers Symposium Series, 339–346.

[50] Meyers, R. A. (Ed.). (2001). Encyclopedia of Physical Science and Technology. Academic Press.

[51] Koc, R., Kazantzis, N. K., & Ma, Y. H. (2011). Process safety aspects in water-gas-shift (WGS) membrane reactors used for pure hydrogen production. Journal of Loss Prevention in the Process Industries, 24(6), 852–869. https://doi.org/10.1016/j.jlp.2011.06.012

[52] IEAGHG. (2012). (rep.). CO_2 CAPTURE AT GAS FIRE POWER PLANTS.

[53] Kothandaraman, A. (2010). Carbon dioxide capture by chemical absorption: A solvent comparison study (thesis). Massachusetts Institute of Technology.

[54] Scottish Environment Protection Agency. (2015). (rep.). Emissions from amine-based post-combustion CO_2 capture plants.

[55] Spigarelli, B. P., Kawatra, S. K. (2013). Opportunities and challenges in carbon dioxide capture. Journal of CO_2 Utilization, 1, 69–87. https://doi.org/10.1016/j.jcou.2013.03.002

[56] Dafalla, A. M., Wei, L., Habte, B. T., Guo, J., & Jiang, F. (2022). Membrane electrode assembly degradation modelling of proton exchange membrane fuel cells: A Review. Energies, 15(23), 9247. https://doi.org/10.3390/en15239247

[57] Bravo, J. A. (2018). CCS membrane development at CIUDEN's Technology Development Centre for CO_2 Capture. Journal of Power and Energy Engineering, 06(12), 1–16. https://doi.org/10.4236/jpee.2018.612001

[58] Liu, L., Luo, X.-B., Ding, L., & Luo, S.-L. (2019). Application of nanotechnology in the removal of heavy metal from water. Nanomaterials for the Removal of Pollutants and Resource Reutilization, 83–147. https://doi.org/10.1016/b978-0-12-814837-2.00004-4

[59] Chuang, S. S., Soong, Y., & Gray, M. (2006). Thermal and Chemical Stability of Regenerable Solid Amine Sorbent for CO_2 Capture. Energy Fuels, 20(4), 1514–1520. https://doi.org/10.1021/ef050402y

[60] Herring, A., Smith, T. R. D., & Vorobet, V. (2021, November 11). Carbon capture in the UK: risk considerations. Marsh. https://www.marsh.com/uk/industries/energy-and-power/insights/carbon-capture-in-uk-risk-considerations.html

[61] Energy, Equipment, and Infrastructure alliance. (2019). (rep.). Meeting the Dual Challenge: A Roadmap to At-Scale Deployment of Carbon Capture, Use, and Storage.

[62] Sarkarfarshi, M., Ladubec, C., Gracie, R., Dusseault, M. B., Leiss, W., & Krewski, D. (2019). Potential technical hazards associated with four North American Carbon Capture and sequestration projects. International Journal of Risk Assessment and Management, 22(3/4), 359. https://doi.org/10.1504/ijram.2019.103341

[63] Shuter, D., Bilio, M., Wilday, J., Murray, L., & Whitbread, R. (2011). Safety issues and research priorities for CCS Systems and Infrastructure. Energy Procedia, 4, 2261–2268. https://doi.org/10.1016/j.egypro.2011.02.115

[64] Uwineza, P. A., & Waśkiewicz, A. (2020). Recent advances in supercritical fluid extraction of natural bioactive compounds from natural plant materials. Molecules, 25(17), 3847. https://doi.org/10.3390/molecules25173847

[65] Vitali, M., Zuliani, C., Corvaro, F., Marchetti, B., Terenzi, A., & Tallone, F. (2021). Risks and safety of CO_2 Transport Via Pipeline: A review of risk analysis and modelling approaches for accidental releases. Energies, 14(15), 4601. https://doi.org/10.3390/en14154601

[66] Xie, Q., Tu, R., Jiang, X., Li, K., & Zhou, X. (2014). The leakage behaviour of Supercritical CO_2 flow in an experimental pipeline system. Applied Energy, 130, 574–580. https://doi.org/10.1016/j.apenergy.2014.01.088

[67] Mazzoldi, A., & Oldenburg, C. M. (2014). Leakage risk assessment of CO_2 Transportation by pipeline at the Illinois Basin Decatur Project, Decatur, Illinois. Lawrence Berkeley National Laboratory. https://doi.org/10.2172/1164904

[68] EGIG. (2020). (rep.). 11th Report of the European Gas Pipeline Incident Data Group (period 1970 - 2019).

[69] Chrysostomidis, I., Geyer, T. A. W., Smith, A., Fedorowick, J., Bohm, M., Beynon, E., Little, C. T., & Lee, A. (2010). CO_2 Pipeline Systems: Assessment of the Risks And Health & Safety Regulations. Institution of Chemical Engineers Symposium Series.

[70] Clarkson, K. (2022). (rep.). CO_2 Pipelines – Dangerous and Under-Regulated. Pipeline Safety Trust.

[71] Quynh Hoa, L., Baessler, R., & Bettge, D. (2019). On the corrosion mechanism of CO_2 Transport Pipeline Steel caused by condensate: Synergistic effects of no2 and SO2. Materials, 12(3), 364. https://doi.org/10.3390/ma12030364

[72] Curson, N. (2021, August 3). Assessing safety risks for CO_2 pipelines. Penspen. https://www.penspen.com/insights/assessing-safety-risks-for-co2-pipelines/

[73] Martynov, S. B., Talemi, R. H., Brown, S., & Mahgerefteh, H. (2017). Assessment of fracture propagation in pipelines transporting impure CO_2 streams. Energy Procedia, 114, 6685–6697. https://doi.org/10.1016/j.egypro.2017.03.1797

[74] Cole, I. S., Corrigan, P., Sim, S., & Birbilis, N. (2011). Corrosion of pipelines used for CO_2Transport in CCS: Is it a real problem? International Journal of Greenhouse Gas Control, 5(4), 749–756. https://doi.org/10.1016/j.ijggc.2011.05.010

[75] Jacobson, G. A. (2020, April 5). Pipeline corrosion issues related to carbon capture, and transportation. Materials Performance. https://www.materialsperformance.com/articles/material-selection-design/2015/08/pipeline-corrosion-issues-related-to-carbon-capture-transportation-and-storage

[76] Patchigolla, K., Oakey, J. E., & Anthony, E. J. (2014). Understanding dense phase CO_2 corrosion problems. Energy Procedia, 63, 2493–2499. https://doi.org/10.1016/j.egypro.2014.11.272

[77] Farelas, F., Choi, Y. S., & Nesic, S. (2012). CORROSION 2012. In Effects of CO_2 Phase Change, SO2 Content And Flow On the Corrosion of CO_2 Transmission Pipeline Steel. Utah; OnePetro.

[78] Koornneef, J., Ramírez, A., Turkenburg, W., & Faaij, A. (2011). The Environmental Impact and risk assessment of CO_2 Capture, transport, and storage- an evaluation of the knowledge base using the DPSIR framework. Energy Procedia, 4, 2293–2300. https://doi.org/10.1016/j.egypro.2011.02.119

[79] Global CCS Institute. (2013). (rep.). Hazard analysis for offshore carbon capture platforms and offshore pipelines. London.

[80] Pipeline and Hazardous Materials Safety Administration. (2022). (rep.). Failure Investigation Report - Denbury Gulf Coast Pipelines, LLC – Pipeline Rupture/ Natural Force Damage. US Department of Transportation.

[81] Metz, B., Davidson, O., Coninck, H. de, Loos, M., & Meyer, L. (Eds.). (2005). (rep.). Carbon Dioxide Capture and Storage (p. 431). Cambridge: Cambridge University Press.

[82] Vianello, C., Machietto, S., & Maschio, G. (2012). Conceptual models for CO_2 release and risk assessment: a review. Chemical Engineering Transactions, 26, 573–578. https://doi.org/doi

[83] Vishal, V., Verma, Y., Chandra, D., & Ashok, D. (2021). A systematic capacity assessment and classification of geologic CO_2Storage Systems in India. International Journal of Greenhouse Gas Control, 111, 103458. https://doi.org/10.1016/j.ijggc.2021.103458

[84] Global CCS Institute. (2019). (rep.). Carbon Neutrality: Scenarios for & Deep Decarbonization

[85] International Hazard Governance Council. (2023). (rep.). policy brief regulation of carbon capture and storage. Geneva.

[86] Tamburri, M. N., Peltzer, E. T., Friederich, G. E., Aya, I., Yamane, K., & Brewer, P. G. (2000b). A field study of the effects of CO2 Ocean Disposal on mobile deep-sea animals. Marine Chemistry, 72(2–4), 95–101. https://doi.org/10.1016/s0304-4203(00)00075-x

[87] Lichtschlag, A., Haeckel, M., Olierook, D., Peel, K., Flohr, A., Pearce, C. R., Marieni, C., James, R. H., & Connelly, D. P. (2021). Impact of CO_2 leakage from sub-seabed carbon dioxide storage on sediment and Porewater geochemistry. International Journal of Greenhouse Gas Control, 109, 103352. https://doi.org/10.1016/j.ijggc.2021.103352

[88] Center for International Environmental Law. (2021, July 19). Carbon capture and storage. CIEL. https://www.ciel.org/issue/carbon-capture-and-storage/

[89] Deng, H., Bielicki, J. M., Oppenheimer, M., Fitts, J. P., & Peters, C. A. (2017). Leakage risks of geologic CO_2storage and the impacts on the global energy system and climate change mitigation. Climatic Change, 144(2), 151–163. https://doi.org/10.1007/s10584-017-2035-8

[90] Bonto, M., Welch, M. J., Lüthje, M., Andersen, S. I., Veshareh, M. J., Amour, F., Afrough, A., Mokhtari, R., Hajiabadi, M. R., Alizadeh, M. R., Larsen, C. N., & Nick, H. M. (2021). Challenges and enablers for large-scale CO_2 storage in Chalk

Formations. Earth-Science Reviews, 222, 103826. https://doi.org/10.1016/j.earscirev.2021.103826

[91] Choi, H. S., Park, H. C., Huh, C., & Kang, S.-G. (2011). Numerical simulation of fluid flow and heat transfer of Supercritical CO2 in micro-porous media. Energy Procedia, 4, 3786–3793. https://doi.org/10.1016/j.egypro.2011.02.313

[92] Global CCS Institute. (2009). (rep.). CCS Site Characterization Criteria.

[93] Eames, F. R., & Fewell, B. (2008, October). Carbon Capture and Storage Risks and Liabilities. Hunton Andrews Kurth LLP. https://www.huntonak.com/images/content/3/6/v3/3632/Capturing-and-Storing-Carbon.pdf

[94] Kelemen, P., Benson, S. M., Pilorgé, H., Psarras, P., & Wilcox, J. (2019). An overview of the status and challenges of CO_2 Storage in Minerals and Geological Formations. Frontiers in Climate, 1. https://doi.org/10.3389/fclim.2019.00009

[95] British Geological Survey. (2011). (rep.). Kingsnorth E.ON UK Carbon Capture & Storage Front End Engineering and Design (FEED) - Chapter 04: Project Design.

[96] Verdon, J. P., & Stork, A. L. (2016). Carbon capture and storage, geomechanics, and induced seismic activity. Journal of Rock Mechanics and Geotechnical Engineering, 8(6), 928–935. https://doi.org/10.1016/j.jrmge.2016.06.004

[97] Ji, X., & Zhu, C. (2015). CO_2 storage in deep saline aquifers. Novel Materials for Carbon Dioxide Mitigation Technology, 299–332. https://doi.org/10.1016/b978-0-444-63259-3.00010-0

[98] Birkholzer, J., Zhou, Q., & Tsang, C. F. (2008). Large-scale impact of CO_2 storage in deep saline aquifers: A sensitivity study on pressure response in Stratified Systems. International Journal of Greenhouse Gas Control, 3(2), 181–194. https://doi.org/10.1016/j.ijggc.2008.08.002

[99] Hu, L., Pan, L., & Zhang, K. (2012). Modelling brine leakage to the shallow aquifer through an open wellbore using T2WELL/ECO2N. International Journal of Greenhouse Gas Control, 9, 393–401. https://doi.org/10.1016/j.ijggc.2012.05.010

[100] Leung, D. Y. C., Caramanna, G., & Maroto-Valer, M. M. (2014). An overview of the current status of carbon dioxide capture and Storage Technologies. Renewable and Sustainable Energy Reviews, 39, 426–443. https://doi.org/10.1016/j.rser.2014.07.093

[101] Talapatra, A. (2020). A study on the carbon dioxide injection into coal seam aiming at enhancing coal bed methane (ECBM) recovery. Journal of Petroleum Exploration and Production Technology, 10(5), 1965–1981. https://doi.org/10.1007/s13202-020-00847-y

[102] Perera, M. S. (2017). Influences of CO_2 injection into deep coal seams: A Review. Energy & Fuels, 31(10), 10324–10334. https://doi.org/10.1021/acs.energyfuels.7b01740

[103] Jiang, L., Chen, Z., Farouq Ali, S. M., Zhang, J., Chen, Y., & Chen, S. (2022). Storing carbon dioxide in deep unmineable coal seams for centuries following underground coal gasification. Journal of Cleaner Production, 378, 134565. https://doi.org/10.1016/j.jclepro.2022.134565

[104] White, C. M., Smith, D. H., Jones, K. L., Goodman, A. L., Jikich, S. A., LaCount, R. B., DuBose, S. B., Ozdemir, E., Morsi, B. I., & Schroeder, K. T. (2005). Sequestration of carbon dioxide in coal with enhanced Coalbed Methane Recovery A Review. Energy Fuels, 19(3), 659–724. https://doi.org/10.1021/ef040047w

[105] Vora, M., Sanni, S., & Flage, R. (2021). An environmental risk assessment framework for enhanced oil recovery solutions from the offshore oil and Gas Industry. Environmental Impact Assessment Review, 88, 106512. https://doi.org/10.1016/j.eiar.2020.106512

[106] Los Alamos National Laboratory. (2017, April 3). Risk analysis for CO_22 sequestration at Enhanced Oil Recovery Sites. Phys.org. https://phys.org/news/2017-04-analysis-co2-sequestration-oil-recovery.html

[107] Massarweh, O., & Abushaikha, A. S. (2022). A review of recent developments in CO_2 Mobility Control in enhanced oil recovery. Petroleum, 8(3), 291–317. https://doi.org/10.1016/j.petlm.2021.05.002

[108] Duncan, I. J., Nicot, J.-P., & Choi, J.-W. (2009). Risk assessment for future CO_2 sequestration projects-based CO_2 Enhanced Oil Recovery in the U.S. Energy Procedia, 1(1), 2037–2042. https://doi.org/10.1016/j.egypro.2009.01.265

[109] Hoteit, H., Fahs, M., & Soltanian, M. R. (2019). Assessment of CO_2 injectivity during sequestration in depleted Gas Reservoirs. Geosciences, 9(5), 199. https://doi.org/10.3390/geosciences9050199

[110] Duguid, A., Glier, J., Heinrichs, M., Hawkins, J., Peterson, R., & Mishra, S. (2021). Practical leakage risk assessment for CO_2 Assisted Enhanced Oil Recovery and geologic storage in Ohio's depleted oil fields. International Journal of Greenhouse Gas Control, 109, 103338. https://doi.org/https://doi.org/10.1016/j.ijggc.2021.103338

[111] He, M., Luis, S., Rita, S., Ana, G., Euripedes, V., & Zhang, N. (2011). Risk assessment of CO_2 injection processes and storage in Carboniferous Formations: A Review. Journal of Rock Mechanics and Geotechnical Engineering, 3(1), 39–56. https://doi.org/10.3724/sp.j.1235.2011.00039

[112] Morton, L. (2013, March 5). Effect of CO_2 on the integrity of well cement examined. Phys.org.

https://phys.org/news/2013-03-effect-co2-cement.html

[113] Zero Emissions Platform. (2019). (rep.). CO_2 Storage Safety in the North Sea: Implications of the CO_2 Storage.

[114] Furre, A.-K., Meneguolo, R., Pinturier, L., & Bakke, K. (2020). Planning deep subsurface CO_2 storage monitoring for the Norwegian full-scale CCS Project. First Break, 38(10), 55–60. https://doi.org/10.3997/1365-2397.fb2020074

[115] Hvidevold, H. K., Alendal, G., Johannessen, T., Ali, A., Mannseth, T., & Avlesen, H. (2015). The layout of CCS monitoring infrastructure with the highest probability of detecting a footprint of a CO_2 leak in a varying marine environment. International Journal of Greenhouse Gas Control, 37, 274–279. https://doi.org/10.1016/j.ijggc.2015.03.013

[116] Gerstenbergera, M. C., Christophersen, A., Buxton, R., Allinson, G., Hou, W., Leamon, G., & Nicol, A. (2013). Integrated Risk Assessment for CCS. Energy Procedia, 37, 2775–2782. https://doi.org/https://doi.org/10.1016/j.egypro.2013.06.162

[117] Miranda-Barbosa, E., Sigfússon, B., Carlsson, J., & Tzimas, E. (2017). Advantages of combining CCS with geothermal energy. Energy Procedia, 114, 6666–6676. https://doi.org/10.1016/j.egypro.2017.03.1794

[118] Dapeng, L., & Weiwei, W. (2009). Barriers and incentives of CCS deployment in China: Results from semi-structured interviews. Energy Policy, 37(6), 2421–2432. https://doi.org/10.1016/j.enpol.2009.02.032

[119] Garnham, P. J., & Tucker, O. D. (2012). The Longannet to Goldeneye project: Challenges in developing an end-to-end CCS scheme. Carbon Management Technology Conference. https://doi.org/10.7122/151716-ms

[120] Stigson, P., Hansson, A., & Lind, M. (2012). Obstacles for CCS deployment: An analysis of discrepancies of perceptions. Mitigation and Adaptation Strategies for Global Change, 17(6), 601–619. https://doi.org/10.1007/s11027-011-9353-3

[121] Bergstrom, J. C., & Ty, D. (2017). Economics of Carbon Capture and Storage. In Y. Yun (Ed.), Recent Advances in Carbon Capture and Storage. essay, IntechOpen

[123] Department for Business Energy and Industrial Strategy. (2020). (rep.). CCS deployment at dispersed industrial sites.

[124] Zapantis, A., Townsend, A., & Rassool, D. (2019). (rep.). Policy Priorities to Incentivise Large-Scale Deployment of CCS. Global CCS Institute.

[125] Oraee-Mirzamani, B., Cockerill, T., & Makuch, Z. (2013). Risk assessment and management associated with CCS. Energy Procedia, 37, 4757–4764. https://doi.org/10.1016/j.egypro.2013.06.385

[126] Harkin, T., Filby, I., Sick, H., Manderson, D., & Ashton, R. (2017). Development of a CO_2 specification for a CCS Hub Network. Energy Procedia, 114, 6708–6720. https://doi.org/10.1016/j.egypro.2017.03.1801

[127] Esau, I. (2022, August 30). US: Permitting is a key challenge for the nation's fledgling Carbon Capture Sector. Upstream Online | Latest oil and gas news. https://www.upstreamonline.com/energy-transition/us-permitting-is-key-challenge-for-nation-s-fledgling-carbon-capture-sector/2-1-1287189

[128] Samadi, J., & Garbolino, E. (2012). Development of a Systemic Risk Management Approach for CO_2 Capture, Transport, and Storage Projects (thesis).

[129] Haan-Kamminga, A., Roggenkamp, M., & Woerdman, E. (2010). Legal uncertainties of carbon capture and storage in the EU: The Netherlands as an example. Carbon Climate Law Review, 4(3), 240–249. https://doi.org/10.21552/cclr/2010/3/140

[130] Terwel, B. W., Harinck, F., Ellemers, N., & Daamen, D. D. L. (2011). Going beyond the properties of CO_2 Capture and Storage (CCS) technology: How trust in stakeholders affects public acceptance of CCS. International Journal of Greenhouse Gas Control, 5(2), 181–188. https://doi.org/10.1016/j.ijggc.2010.10.001

[131] Budinis, S., Krevor, S., Dowell, N. M., Brandon, N., & Hawkes, A. (2018). An assessment of CCS costs, barriers, and potential. Energy Strategy Reviews, 22, 61–81. https://doi.org/10.1016/j.esr.2018.08.003

[132] Takase, H., McKinley, I. G., West, J. M., Kumagai, T., & Akai, M. (2011). Advanced KMS for knowledge sharing and building confidence in CCS. Energy Procedia, 4, 6202–6209. https://doi.org/10.1016/j.egypro.2011.02.632

[133] Janipour, Z., Swennenhuis, F., de Gooyert, V., & de Coninck, H. (2021). Understanding contrasting narratives on carbon dioxide capture and storage for Dutch industry using system dynamics. International Journal of Greenhouse Gas Control, 105, 103235. https://doi.org/10.1016/j.ijggc.2020.103235

[134] Romasheva, N., & Ilinova, A. (2019). CCS Projects: How Regulatory Framework Influences their Deployment. Resources, 8(4), 181. https://doi.org/10.3390/resources8040181

[135] Ashworth, P. (2010). (rep.). Communication of carbon capture and storage: Outcomes from an international workshop to summarise the current global position. Global CCS Institute.

[136] Bradbury, J., W., Greenberg, S., & Wade, S. (2011). (rep.). Communicating the Risks of CCS. Global CCS Institute.

[137] Durst, S., & Zieba, M. (2018). Mapping knowledge risks: Towards a better understanding of knowledge management. Knowledge Management Research Practice, 17(1), 1–13. https://doi.org/10.1080/14778238.2018.1538603

[138] Rackley, S. A. (2017). carbon capture and storage. Butterworth-Heinemann.

[139] Uilhoorn, F. E. (2013). Evaluating the risk of hydrate formation in CO_2 Pipelines Under Transient Operation. International Journal of Greenhouse Gas Control, 14, 177–182. https://doi.org/10.1016/j.ijggc.2013.01.021

[140] Chapoy, A., Burgass, R., Tohidi, B., & Alsiyabi, I. (2014). Hydrate and phase behaviour modelling in CO2-rich pipelines. Journal of Chemical Engineering Data, 60(2), 447–453. https://doi.org/10.1021/je500834t

[141] Solomon Aforkoghene, A. (2022). Hydrate Phase Transition-Hazard, Energy Potential, and CO_2 Storage Possibilities. (thesis). Bergen Open Research Archive, Bergen

[142] U.S. Environmental Protection Agency. (2008). (rep.). Vulnerability Evaluation Framework for Geologic Sequestration of Carbon Dioxide. U.S. Environmental Protection Agency.

[143] Gauteplass, J., Almenningen, S., Barth, T., & Ersland, G. (2020). Hydrate plugging and flow remediation during CO_2 Injection in sediments. Energies, 13(17), 4511. https://doi.org/10.3390/en13174511

[144] Eldardiry, H., & Habib, E. (2018). Carbon capture and sequestration in power generation: Review of impacts and opportunities for water sustainability. Energy, Sustainability and Society, 8(1). https://doi.org/10.1186/s13705-018-0146-3

[145] Busch, A., Hangx, S. J. T., Marshall, J. D., & Wentinck, H. M. (2019). Swelling clay minerals and containment risk assessment for the storage seal of the Peterhead CCS Project. International Journal of Greenhouse Gas Control, 94, 102924. https://doi.org/10.1016/j.ijggc.2019.102924

[146] Gelderen, L. van. (2013). Improving a risk assessment method for CCS (thesis). National Institute for Public Health and the Environment.

[147] Pihkola, H., Tsupari, E., Kojo, M., Kujanpää, L., Nissilä, M., Sokka, L., & Behm, K. (2017). Integrated Sustainability Assessment of CCS – identifying non-technical barriers and drivers for CCS implementation in Finland. Energy Procedia, 114, 7625–7637. https://doi.org/10.1016/j.egypro.2017.03.1895

[148] Aker Carbon Capture. (2022). (rep.). Climate risk review. The Governance Group.

[149] L'Orange Seigo, S., Arvai, J., Dohle, S., & Siegrist, M. (2014). Predictors of risk and benefit perception of carbon capture and storage (CCS) in regions with different stages of deployment. International Journal of Greenhouse Gas Control, 25, 23–32. https://doi.org/10.1016/j.ijggc.2014.03.007

INTERNATIONAL JOURNAL OF
COASTAL, OFFSHORE & ENVIRONMENTAL ENGINEERING IJCOE Vol.10/No. 1/Winter 2025 (68-74)

Available online at: www. Ijcoe.org

Estimation of suspended sediment concentration based on water samples' turbidity in aquatic environments

Saeed Shabani [1], Amir Ashtari Larki [2], Mohammad Akbarinasab [3,*], Mohammad Fayaz Mohammadi [4]

[1] PHD Candidate, Department of Physical Oceanography, Faculty of Marine Science and Oceanography, University of Marine Science and Technology, Khorramshahr, Iran, shsaeed2024@gmail.com

[2] Associate Professor, Department of Physical Oceanography, Faculty of Marine Science and Oceanography, University of Marine Science and Technology, Khorramshahr, Iran, ashtari@kmsu.ac.ir

[3,] Associate Professor, Department of Marine Physics, Faculty of Marine and Environmental Sciences, University of Mazandaran, Babolsar, Iran, m.akbarinasab@umz.ac.ir*

[4] Assistant Professor, Department of Physical Oceanography, Faculty of Marine Science and Oceanography, University of Marine Science and Technology, Khorramshahr, Iran, m.fayaz@kmsu.ac.ir

ARTICLE INFO

Article History:
Received : 22 July 2024
Accepted : 02 Feb 2025

Keywords:
Suspended sediment
Water turbidity
In-lab calibration
Pierson correlation coefficients
Surrogate data

ABSTRACT

The primary method for measuring suspended sediment concentration (SSC) is the gravimetric analysis of water–sediment samples collected using grab or bottle samplers from the sea or rivers at regular or irregular intervals. Although this method is reliable, it requires substantial effort and cost for sampling, transportation to the laboratory, and long processing times for sample analysis. This study aims to introduce an alternative method for estimating SSC based on measuring the water turbidity (WT) of water–sediment samples. A case study was conducted in the coastal waters of the Caspian Sea to determine the Pearson correlation coefficients between these two parameters.

In-lab calibration between SSC and WT data using site-specific sampling is essential, as the mean particle size and particle size distribution (PSD) can vary considerably in space and time. Therefore, several water–sediment samples were collected from inside and outside the basins of Amirabad and Anzali ports, and grain-size analyses were performed. Subsequently, sediment–seawater mixtures (50 L) were prepared stepwise at eleven concentrations: 125, 250, 500 mg/L and 1, 2, 3, 4, 5, 6, 7, and 8 g/L. For each concentration, WT was measured using a HATCH 2100N turbidimeter and an auxiliary TSW-20 turbidity sensor.

Sieve and hydrometer analyses were conducted, and particle size distribution curves for two water–sediment samples from inside the basins of Amirabad and Anzali ports were plotted. The D_{10}, D_{30}, D_{50}, D_{60}, and D_{90} statistics were extracted and compared. WT values for the eleven sediment mixtures were measured using the HATCH 2100N turbidimeter. Pearson correlation coefficients between SSC and WT were calculated for linear, second-order polynomial, third-order polynomial, and power regression fittings, and SSC–WT correlation curves were drawn.

A step-by-step alternative method for estimating SSC based on WT measurements using a laboratory turbidimeter was designed. Applying this method to the case study yielded Pearson correlation coefficients between SSC and WT for water–sediment samples from Amirabad Port. The proposed approach is suitable for use in a real-time and continuous sediment monitoring network, enabling the integration of WT as a surrogate parameter for SSC in the national sediment monitoring database.

1. Introduction

Understanding the sedimentation regime in an aquatic basin is essential not only for comprehending the gradual transformation of the shoreline and for the optimal design of ports and coastal structures, but also for effective operational management, improving efficiency and performance, and reducing maintenance costs throughout the service life of the port.

The suspended sediment concentration (SSC), expressed in grams per litre (g/L), is an essential physical indicator for better understanding the sedimentation regime, including bed erosion, deposition, accumulation, and sediment transport in lakes, river deltas, estuaries, and the coastal waters of seas and oceans. The mechanism of formation and transport of sediments and suspended sediment load includes cohesive particles (clay minerals and organic matter) and non-cohesive particles (silt, sand, and gravel), as shown in Figure 1. In Figure 1(A), the seabed is dense (rocky or coral), while in Figure 1(B) the seabed is non-dense (muddy), each having a different effect on the amount of SSC [1–3].

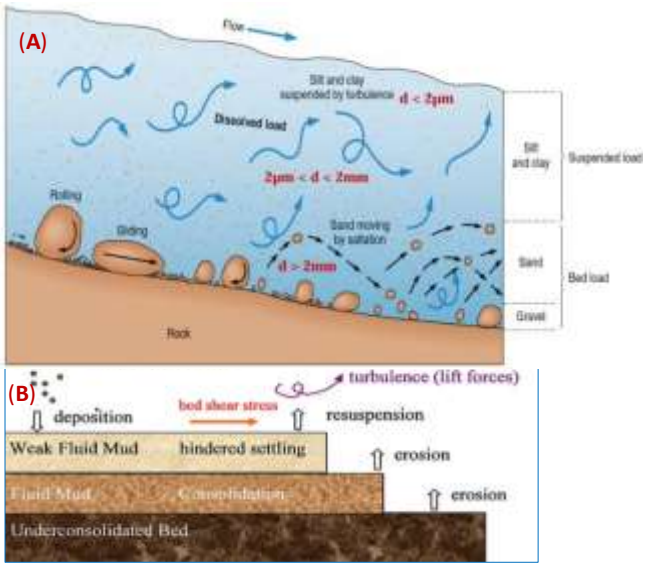

Figure 1. (A) Cohesive and non-cohesive sediments and mechanism of sediment transport in water; (B) The transport of mud model and the interaction between mud and the bed [1, 2, 3]

If the flow velocity is sufficiently strong, some of the smaller and lighter particles deposited at the bottom of a river can be lifted into the water column and remain suspended. The size of particles that can be carried as suspended load depends on the flow velocity: the higher the velocity, the greater the suspension force acting on sediment particles. Larger and heavier particles are more likely to settle out during upward–downward current motion unless the velocity increases to generate greater turbulence along the bed. Conversely, a reduction in flow velocity can cause suspended sediment to settle.

Suspended sediment can also behave differently at various depths within the water column. In river mouths and coastal areas, sediment dynamics are influenced not only by downstream flow velocity but also by marine currents, tides, waves, diverse geological settings of the watershed, seasonal and climatic effects, storms, pollution, and other environmental processes. For these reasons, understanding sedimentary processes and developing predictive models are challenging tasks [4–6].

The first step toward overcoming this challenge is to establish a sufficiently dense sediment database covering the study area. Due to the diversity and complexity of sedimentary processes, spatial variation in hydrodynamic conditions, and the lack of consistent time-series observations, continuous SSC monitoring within a measurement network with adequate spatial and temporal resolution is necessary.

Traditionally, SSC has been measured gravimetrically by collecting samples from specific locations in waterways or port basins, transporting them to a laboratory, and determining the water volume and sediment mass using oceanographic and river engineering laboratory equipment. In recent years, some portable particle size analysers (PSA) have been developed for in situ sediment analysis, as shown in Figure 2 [7].

However, SSC data obtained through either traditional sampling and laboratory analysis or portable advanced equipment cannot be collected easily, continuously, and in sufficient quantity over the entire study area.

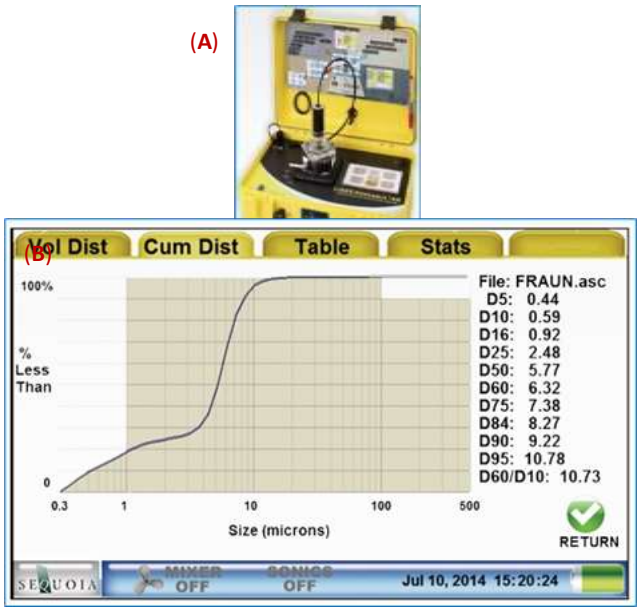

Figure 2. (A) LISST-Portable Low-Cost Particle Size Analyser (PSA); (B) Touch panel screenshot of size distribution [7]

An alternative approach is to measure a physical parameter that is strongly correlated with SSC and then estimate SSC from it by deriving correlation coefficients. A suitable physical parameter with simple measurement technology and cost-effectiveness is water turbidity (WT). WT can be measured in situ by installing an automated sensor at the desired location, with real-time data recorded in nephelometric turbidity units (NTU) [8, 9].

For better illustration, Figure 3 shows a satellite image of turbidity variation in the coastal waters of Nowshahr Port and at the mouths of the Mashalak and Moghadam Rivers. As can be seen, turbidity is highest at the river mouths and disperses into the surrounding coastal waters depending on the direction and magnitude of the current velocity vectors [10].

Figure 3. Satellite image of water turbidity variation due to suspended sediment concentration (SSC) in the coastal waters of Nowshahr Port

Accordingly, the higher the SSC in the water, the greater the WT, and vice versa. Thus, by measuring WT across a sufficiently dense monitoring network, the SSC distribution can be estimated.

This paper presents the research steps taken to determine the correlation coefficients between WT and SSC for water–sediment samples from coastal areas near Amirabad and Anzali ports, located on the eastern and western coasts of the Caspian Sea. The research approach is designed so that the results can be applied as a reference model for other northern and southern ports of the country, ultimately contributing to the creation of a comprehensive sediment monitoring database.

2. Materials and Methods

2.1. Water-sediment samples

As mentioned earlier, before measuring SSC in an aquatic basin, it is necessary to understand the spatial variation of sediment texture within the basin as well as its seasonal changes. The NTU unit, as the measurement unit for WT, is not directly comparable across all aquatic basins and sensors. In other words, it cannot be assumed that a WT of 1000 NTU at two different ports (or at the same port with two different sensors) corresponds to the same SSC value in g/L. This is because turbidity depends not only on SSC but also on the particle size distribution (PSD), shape and physical properties of the particles—such as colour (reflectivity), density, refractive index, and surface roughness [11, 12].

Therefore, understanding the sediment texture of each aquatic environment and performing a calibration between WT and SSC using water–sediment samples collected from the same study site is of utmost importance.

In this study, the coastal waters of the Caspian Sea were selected as the research area, specifically Amirabad Port in the east and Anzali Port in the west. These sites were chosen based on the following:

The southern Caspian Sea, from a sedimentological perspective, shows variations in sediment composition and grain size from west to east. The southern shores (land area) are very gently sloped, which prevents large waves from reaching the coast. As a result, the coastal sediments are fine-grained and marshy, with indistinct shorelines in some areas [13].

The coastal sediments range mainly from sandy to muddy. The eastern part of Gorgan Bay toward the north is muddy, with local sandy deposits only at the mouth of the Gorgan River. Moving westward across the southern bay, sediments transition from muddy to sandy. The Miankaleh Peninsula coast is predominantly sandy [14, 15].

Based on this, two water–sediment samples were collected from inside the basins of Amirabad and Anzali Ports with geographical coordinates shown in Table 1 and red markers and yellow ovals in Figure 4 from the dredging contractor of the Ports and Maritime Organisation (PMO). Additionally, 100 litres of seawater were collected from the same sampling sites to ensure laboratory calibration conditions closely matched the field environment.

2.2. Laboratory Devices and Equipment

The required devices and equipment for this study included:

Standard sieves and a hydrometer for generating grain-size distribution curves.

HATCH 2100N turbidimeter for measuring turbidity of sediment–water mixtures.

Magnetic stirrer for homogenizing sediment mixtures.

Auxiliary TSW-20 turbidity sensor for measuring turbidity of sediment samples in a 250 mL beaker.

The lab instruments and equipment mentioned above are shown in Figure 5.

Table 1. Geographical coordinates of sediment sampling locations (inside and outside basins)

Row	Location	Latitude	Longitude
A	**Port Amirabad**		
2	AMA-1-In	36 º 51 ' 41.01 " N	53 º 22 ' 23.91 " E
3	AMA-2-In	36 º 51 ' 29.61 " N	53 º 22 ' 28.78 " E
4	AMA-2	36 º 51 ' 28.44 " N	53 º 21 ' 07.20 " E
5	AMA-5	36 º 51 ' 45.60 " N	53 º 23 ' 10.68 " E
B	**Port Anzali**		
1	ANZ-1-In	37 º 28 ' 45.60 " N	49 º 27 ' 37.24 " E
2	ANZ-2	37 º 29 ' 00.96 " N	49 º 26 ' 55.68 " E
3	ANZ-8	37 º 28 ' 35.04 " N	49 º 27 00.72 " E

Figure 4. (A) Satellite image of Amirabad Port sampling locations (outside basin – PMO project, inside basin – this study); (B) Satellite image of Anzali Port sampling locations (outside basin – PMO project, inside basin – this study)

2.3. Measurement data

National project reports from the Water Research Institute (WRI) in collaboration with PMO on Caspian Sea sediment field studies were used, containing sediment data from 12 sampling points in Amirabad and 8 points in Anzali. [16].

In Amirabad port, six points are adjacent to the eastern and western arms of the pond; two points, 2 and 5, are adjacent to the coastal waters. In Bandar Anzali, five points are adjacent to the eastern and western arms of

Figure 5. (A) HATCH 2100N turbidimeter; (B) Magnetic stirrer; (C) TSW-20 water turbidity sensor; (D) Data reading from TSW-20 sensor

in the pond, of which two points 2 and 8 are adjacent to the coastal waters. The geographical coordinates of two points 2 and 5 of Amirabad port and two points 2 and 8 of Anzali port are also shown in Table 1. They are shown in Figure 4 with a yellow indicator for the points outside the pond and a red indicator for the points inside the pond. In this study, the data of the points outside the pond from the WRI-PMO project and the results of the gradation test of the samples have been precisely investigated.

2.4. Laboratory Calibration Method

2.4.1. Laboratory Main Tests

Two main tests were performed: (1) grain-size analysis to determine sediment texture, and (2) turbidity measurements for prepared sediment–water mixtures. Grain-size analysis followed ASTM D422-63 (Reapproved 2002), combining standard sieve analysis for particles >75 µm and hydrometer analysis for particles <75 µm.

2.4.2. Proposed Six-step Calibration Method

When a certified reference turbidity sensor is available, placing it in the sediment–water mixture allows direct calibration of other sensors. In this study, due to the unavailability of an affordable certified reference, an alternative six-step calibration method was used:

Step-1: Collect fine sediment (<75 µm) from the target site and prepare in 25 g and 50 g portions.

Step-2: Place 50 litres of seawater from the same site into an 80 L container, install a magnetic stirrer and the target turbidity sensor.

Step-3: Prepare sediment mixtures with concentrations from 0.25 g/L to 8 g/L, keeping the stirrer running at optimal speed.

Step-4: At each step, take a 10 mL sample, place it in the HATCH 2100N turbidimeter cell, and record WT in NTU.

Step-5: Simultaneously record WT from the TSW-20 sensor in the stirred mixture.

Step-6: Plot SSC–Turbidity curves based on HATCH 2100N measurements.

3. Results and Discussion

3.1. Grain-Size Analysis and Coastal Sediment Texture

Grain-size distribution curves for samples taken from Points 1 and 2 inside the Amirabad Port basin and Points 2 and 5 outside the basin (adjacent coastal waters) are shown in Figures 6 and 7. These data were extracted from the PMO–WRI sediment study report.

From these curves, the grain-size percentiles D_{10}, D_{30}, D_{50}, D_{60}, and D_{90} were calculated for each sample and are presented in Table 2.

Analysis of these values shows that more than 90% of the sediment inside the basin at points AMA-1-In and AMA-2-In consists of silt and silty sand, with only about 10% clay-silt at AMA-1-In. In contrast, more than 98% of the coastal sediment at AMA-2 consists of sand (with <2% silt), and the AMA-5 sample is nearly 100% sand.

Thus, the southern Caspian coast in the Amirabad study area consists mainly (up to 90%) of non-cohesive silty-sand sediments, with particle sizes ranging from 63 to 285 µm inside the basin and 70 to 290 µm outside the basin. These ranges can be divided into two subranges—63–150 µm and 150–290 µm—for further calibration analysis.

Grain-size curves for one sample inside Anzali Port (ANZ-1-In) and two samples from coastal waters outside the basin (ANZ-2 and ANZ-8) are shown in Table 3 and Figure 8.

Row	Sample	D_{10} (µm)	D_{30}	D_{50}	D_{60}	D_{90}
1	AMA-1-In	10	69	105	129	236
2	AMA-2-In	18	137	207	229	285
3	AMA-2	90	140	180	290	290
4	AMA-5	70	90	100	170	170

Results show that over 90% of the sediment inside Anzali basin at ANZ-1-In is silt and silty sand, with ~10% clay-silt. Coastal sediment at ANZ-2 is >98% sand, while ANZ-8 is almost 100% sand.

Table 2. D_{10}, D_{30}, D_{50}, D_{60}, and D_{90} of Amirabad sediment samples

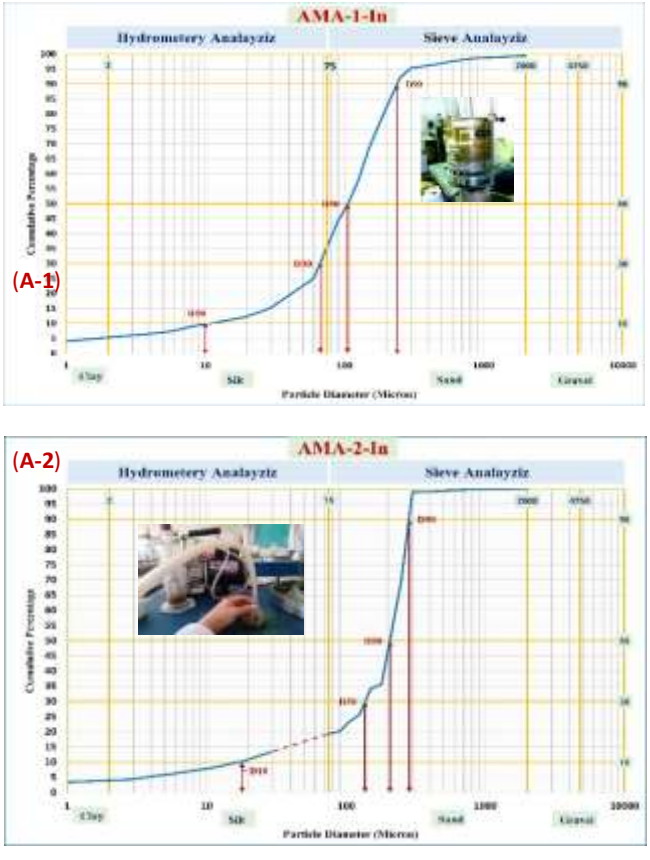

Figure 6. Grain-size distribution curves of two sediment samples inside the Amirabad Port basin

3.2. Calibration of WT and SSC

3.2.1 Selection of Regression Relationship

For estimating SSC from WT, various empirical relationships have been used in previous studies. The SSC–WT relationship varies with particle size, PSD,

and site-specific water properties. An example of this dependency on mean grain size (D_{50}) is shown in Figure 9 [17, 18].

Sometimes, a single regression equation is insufficient for the full WT range, requiring separate fits for different WT or SSC intervals, as shown in Table 4.

Figure 8. (A) Grain-size distribution curve of the sample inside the Anzali Port basin (this study)

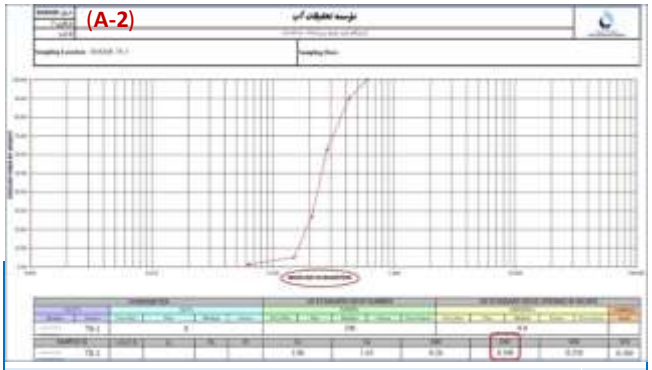

2	ANZ-2	80	100	140	160	270
3	ANZ-8	170	200	280	300	380

Figure 7. Grain-size distribution curves of two sediment samples outside the Amirabad Port basin (from PMO sediment project – WRI [16])

Table 3. D_{10}, D_{30}, D_{50}, D_{60}, and D_{90} of Anzali sediment samples

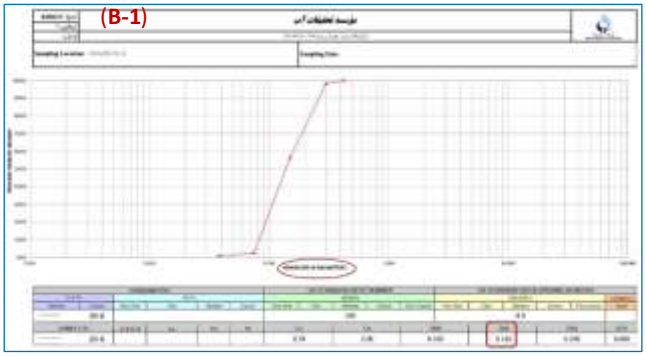

Figure 8. (B)-Outside the Anzali basin (from PMO sediment project – WRI [16])

Although there is still no uniform proposed method for a formal and specific relationship for SSC-WT, nevertheless, in a number of recent studies, the relationships presented in Table 5 have been more sought after [17, 18, 19, 20, 21, 22, 23].

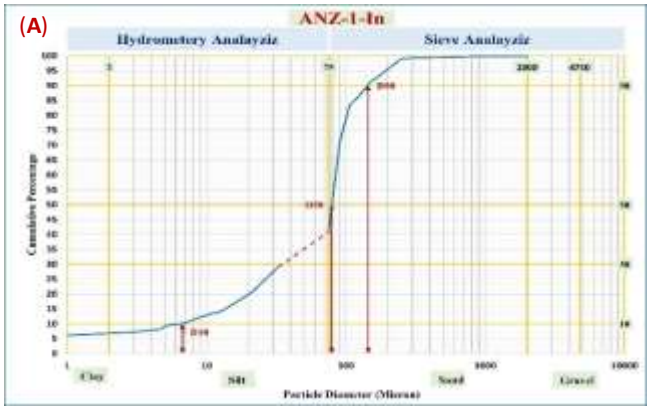

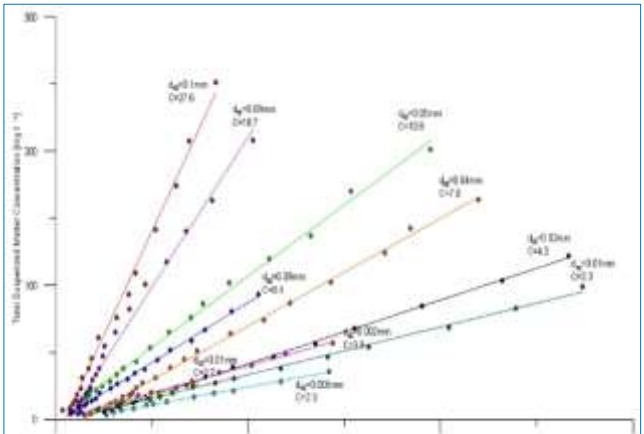

Figure 9. Increase in regression slope with increasing mean grain size (D_{50}) [18]

Table 4. WT and SSC intervals for SSC–WT regression

Row	SSC intervals (grm/L)	WT intervals (NTU)
1	1 < SSC < 5	0 < WT < 10
2	5 < SSC < 10	10 < WT < 100
3	10 < SSC < 30	100 < WT < 1000
4	SSC > 30	1000 < WT < 4000

Table 5. Several regression equations for SSC-WT

(1)	*SSC = f (WT)*	One variable
Linear	$SSC = a \cdot (WT) + b$	
Polynomial	$SSC = a \cdot (WT)^2 + b.\ (WT) + c$	
Polynomial	$SSC = a \cdot (WT)^3 + b \cdot (WT)^2 + c.\ (WT) + d$	
Power	$SSC = a \cdot (WT)^b$	
(2)	More than one variable	
	SSC = f (WT, Color, D_{50})	
	Note: SSC in ppm, WT in NTU, D_{50} in micron	

3.2.2 Calibration and Pearson Correlation Coefficients

Following the proposed six-step method, sediment–water mixtures for samples from Amirabad and Anzali were prepared at concentrations of 250 mg/L, 500 mg/L, and 1–8 g/L. WT was measured with both the HATCH 2100N turbidimeter and the auxiliary TSW-20 sensor.

Pearson correlation coefficients for linear, quadratic, cubic, and power-law regressions were calculated using relationship (1):

$$PCC = \frac{\sum_{i=1}^{n}(xi - x)(yi - \bar{y})}{\sqrt{\sum_{i=1}^{n} sqr.(xi - x)\ \sum_{i=1}^{n} sqr.(yi - \bar{y})}} \quad (1)$$

for SSC–WT relationships (see Table 6). Calibration curves are shown in Figure 10.

4. Conclusion

A step-by-step laboratory method was developed for estimating SSC based on WT measurements using a turbidimeter and an auxiliary sensor. Applying this method to samples from Amirabad and Anzali ports produced high Pearson correlation coefficients for linear, quadratic, cubic, and power-law regressions.

The proposed approach is suitable for integration into a real-time and continuous sediment monitoring network, where WT serves as a surrogate parameter for SSC in national monitoring programs.

Table 6. Pearson correlation coefficients for SSC–WT regressions

Sample	SSC-WT Pierson correlation coefficients			
	Linear	Polynomial -Order2	Polynomial-Order3	Power
AMA-1-In	0.966	0.984	0.986	0.980
AMA-2-In	0.972	0.995	0.995	0.984
ANZ-1-In	0.959	0.998	0.998	0.964

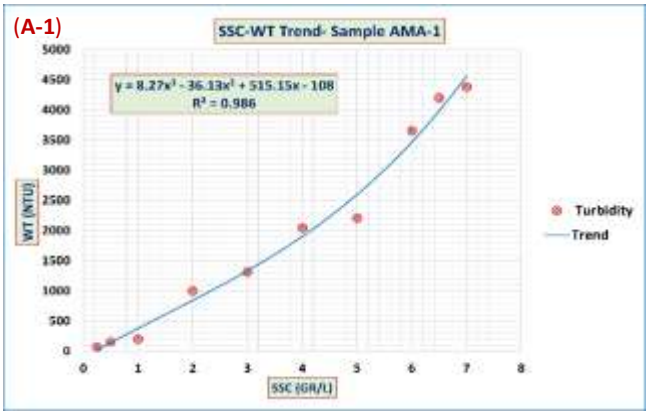

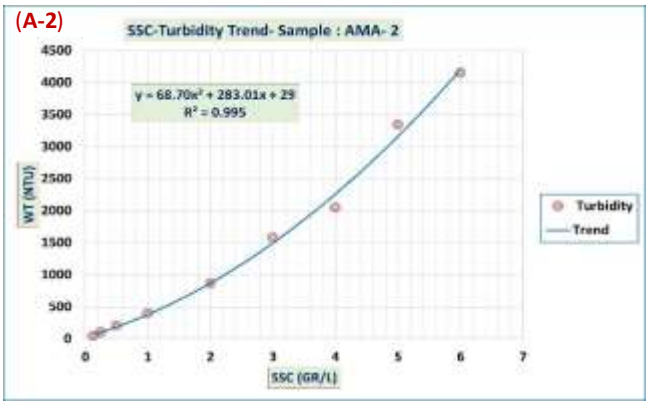

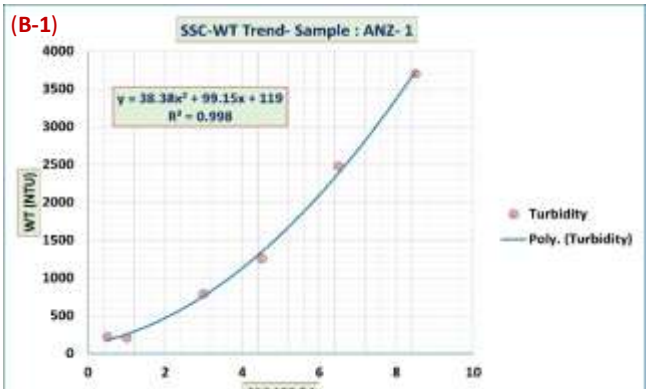

Figure 10. (A) Calibration curves for AMA-1-In and AMA-2-In and (B) ANZ-1-In samples

4. References

[1] Zhang, W. (2012). *Sediment transport models, Encyclopedia of Marine Geosciences*, 1-7 https://doi.org/10.1007/978-94-6644-0 176-1

[2] DHI group, (2024). (1)-MIKE 21_3 Sand Transport-ModellingSoftware. https://www.dhigroup.com/technologies/mikepoweredbydhi/mike-21-3-sand-transport

[3] DHI group, (2024). (2)- R.7.1. MIKE 21_3 Mud Transport-ModellingSoftware. https://www.dhigroup.com/technologies/mikepoweredbydhi/mike-21-3-mud-transport

[4] Shao, Y.; P.-Y Maa, J., (2018). Comparison of different instruments for measuring suspended cohesive sediment concentrations, Water MDPI, 9(968):1-8. https://mdpi.com/journal/water/doi.org/10.3390/w9120968

[5] Matos, T.; Faria, C.L.; Martins, M.S; Henriques, R.; Gomes, P.A.; Goncalves, L.M. (2020). Design of a multipoint cost-effective optical instrument for continuous in-situ monitoring of turbidity and sediment. Sensors MDPI: 20(3194): 1-16. https://mdpi.com/journal/sensors/doi.org/10.3390/s20113194

[6] Matos, T.; Faria, C.L.; Martins, M.S; Henriques, R.; Gomes, P.A.; Goncalves, L.M. (2019). Development of a cost-effective optical sensor for continuous monitoring of turbidity and suspended particulate matter in marine environment. Sensors MDPI:19(4439):1-21. https://mdpi.com/journal/sensors/doi.org/10.3390/s19204439

[7] SEQUIA, LISST Instruments, (2020), Tools and research for particle intelligence, Product catalogue,1-32 https://mdpi.com/journal/sensors/doi.org/10.3390/s19204439

[8] Davies-Colley, R.J.; Smith, D.G., (2001). Turbidity, suspended sediment, and water clarity: A review. J. Am. Water Resour. Assoc. 2001, 37, 1085–1101

[9] Measuring turbidity |Turbidity measurement methods (2025). https://in-situ.com/en/parameters/turbidity

[10] Ross, M., (2019)., Aqua Sat: Studying water quality with satellites and public data, 55(11): 1-8 https://warnercnr.source.colostate.edu/studying-water-quality-with-satellites-and-public-data/

[11] Droujko, J.; Molnar, P. (2022). Open-source, low cost, in-situ turbidity sensor for river network monitoring. Nature portfolio, 12(10341): 1-13., https://nature.com/scientificreport/doi.org/10.1038/s41598-022-14228-4

[12] Kim, J.; Mmjjh, Kwon S.; Chung, S.; Do Kim, Y. (2025) Turbidity and suspended sediment relationship based on sediment composition and particle size distribution. Nature portfolio, 12(10341):1-11. https://nature.com/scientificreport/doi.org/10.1038/ s41598-025-004352

[13] Moafi Madani, S.A.; Mosavi harami, S.R.; Naji, A.; Rezaee, P. (2023). Sedimentology, petrography, mineralogy and geochemistry of deposits off the coast of the Caspian Sea in Babolsar City. J. Oceanography (JOC). Vol.14 (54):122-138. (Persian) https://joc.inio.ac.ir/article 1-1730-fa.pdf

[14] Lahiji, H.; Haeri, O.; Sharifi, A.; Naderi, A.m., (2012). Sedimentological and geochemical indexs of sediments in the Gorgan bay. J. Oceanography (JOC). Vol. 1(1): 45-55 (Persian), http://joc.inio.ac.ir/article-1-6-fa.pdf

[15] Kiani, S.; Lak, R.; Haftani, Z.; Najafiha, B.; Ahmadabadi, A., (2023). Sedimentological and geochemical characterization of the sediments in the south of Gorgan bay. (Persian), https://doi.org/10.21203/rs.3.rs-2968043/v1

[16] PMO, PMO-WRI, (2014), Field and environmental studies for sediment in Caspian Sea ports, (Persian)

[17] Bundgaard, K.; Lumborg, U.; Nyborg, L.; Jakobsen, B.H., (2019). Challenges of optical backscatter monitoring in mixed sediment environment, DHI, 22-29

[18] Wang, Y.; Peng, Y.; Du, Z.; Lin, H.; Yu, Q., (2020). Calibrations of Suspended Sediment Concentrations in high turbidity waters using different in-situ optical instruments, Water MDPI,

12(3296):1-13. https://mdpi.com/journal/water/doi.org/10.3390/w12113296

[19] De Meo, O.A.; Bales, R.D.; Ganju, N.K.; Marsjanik, E.D; Sattles, S.E, (2024), Calculation of a Suspended-Sediment Concentration-Turbidity Regression Model and Flood-Ebb Suspended-Sediment Concentration Differentials from Marshes Near Stone Harbor and Thompsons Beach, New Jersey, 2018–19 and 2022–23, Coastal/Marine Hazards and Resources Program, Data Report 1193, U.S. Geological Survey, Reston, Virginia:1–20. https://doi.org/10.3133/dr1193

[20] Kang, W.; Lee, K.; Kim, J., (2022), Prediction of suspended sediment concentration based on turbidity- concentration relationship determined via underwater image analysis, Appl. Sci. 2022, 12, 6125.: 1–18. https://doi.org/10.3133/dr1193

[21] Minella, P.G.; Merten, G.; Reichert, J.; Clarke, R., (2008), Estimating suspended sediment concentrations from turbidity measurements and calibration problem, Hydrol. Process. 22, 1819–1830.

[22] Matos, T.; Martins, M.S.; Henriques, R.; Goncalves, M.S., (2024), A review of methods and instruments to monitor turbidity and suspended sediment concentration, Journal of Water Process Engineering, 64(2024) 105624;

https://doi.org/10.1016/j.jwpe.2024.105624

[23] Whinney, J. (2018). Theme 4 Development of an optical backscatter sensor for continuous in situ monitoring of sediment deposition. 1-18